2007

Modeling three-dimensional shape of sand grains using Discrete Element Method

Nivedita Das
University of South Florida

Modeling Three-Dimensional Shape of Sand Grains Using Discrete Element Method

by

Nivedita Das

A dissertation submitted in partial fulfillment
of the requirements for the degree of
Doctor of Philosophy
Department of Civil and Environmental Engineering
College of Engineering
University of South Florida

Co-Major Professor: Alaa K. Ashmawy, Ph.D.
Co-Major Professor: Sudeep Sarkar, Ph.D.
Manjriker Gunaratne, Ph.D.
Beena Sukumaran, Ph.D.
Abla M. Zayed, Ph.D.

Date of Approval:
May 4, 2007

Keywords: Fourier transform, spherical harmonics, shape descriptors, skeletonization, angularity, roundness, liquefaction, overlapping discrete element cluster

DEDICATION

To my parents.....

ACKNOWLEDGEMENTS

First of all, I would like to thank my doctoral committee members – Dr. Alaa Ashmawy, Dr. Sudeep Sarkar, Dr. Manjriker Gunaratne, Dr. Abla Zayed and Dr. Beena Sukumaran for their insights and suggestions that have immensely contributed in improving the quality of this dissertation. I would also like to thank Dr. Chris Ferekides for serving as the chair for my doctoral dissertation defense.

In particular, I wish to express my sincere gratitude to my advisor, Dr. Alaa Ashmawy and co-advisor, Dr. Sudeep Sarkar for their invaluable guidance and continued support for this research work. Without their generous help and support, successful completion of this dissertation would not have been possible.

Sincere thanks to Dr. Beena Sukumaran, Dr. Shreekanth Mandayam and the graduate students at the Rowan University for making three-dimensional particle database available online.

I am also very thankful to my colleagues, in particular, former USF graduate students Mr. Delfin Carreon and Mr. Jorge Rivas for helping me greatly in characterizing two-dimensional particle shapes.

I am indebted to the Department of Civil and Environmental Engineering at USF for providing excellent research environment and facilities.

Finally, I would like to extend my heartfelt thanks to my parents and my husband, Amlan for their unconditional sacrifice and inspiration during the completion of this dissertation.

TABLE OF CONTENTS

LIST OF TABLES

LIST OF FIGURES

MODELING THREE-DIMENSIONAL SHAPE OF SAND GRAINS USING DISCRETE ELEMENT METHOD

Nivedita Das

ABSTRACT

The study of particle morphology plays an important role in understanding the micromechanical behavior of cohesionless soil. Shear strength and liquefaction characteristics of granular soil depend on various morphological characteristics of soil grains such as their particle size, shape and surface texture. Therefore, accurate characterization and quantification of particle shape is necessary to study the effect of grain shape on mechanical behavior of granular assembly. However, the theoretical and practical developments of quantification of particle morphology and its influence on the mechanical response of granular assemblies has been very limited due to the lack of quantitative information about particle geometries, the experimental and numerical difficulties in characterizing and modeling irregular particle morphology. Motivated by the practical relevance of these challenges, this research presents a comprehensive approach to model irregular particle shape accurately both in two and three dimensions. To facilitate the research goal, a variety of natural and processed sand samples is collected from various locations around the world. A series of experimental and analytical studies are performed following the sample collection effort to characterize and quantify particle shapes of various sand samples by using Fourier shape descriptors. As part of the particle shape quantification and modeling, a methodology is developed to determine an optimum sample size for each sand sample used in the analysis. Recently, Discrete Element Method (DEM) has gained attention to model irregular particle morphology in two and three dimensions. In order to generate and reconstruct particle

assemblies of highly irregular geometric shapes of a particular sand sample in the DEM environment, the relationship between grain size and shape is explored and no relationship is found between grain size and shape for the sand samples analyzed. A skeletonization algorithm is developed in this study in order to automate the Overlapping Discrete Element Cluster (ODEC) technique for modeling irregular particle shape in two and three dimensions. Finally, the two-dimensional and three-dimensional particle shapes are implemented within discrete element modeling software, PFC^{2D} and PFC^{3D}, to evaluate the influence of grain shape on shear strength behavior of granular soil by using discrete simulation of direct shear test.

CHAPTER 1
INTRODUCTION

1.1 Problem Statement

Particle morphology is an important parameter to study the micromechanical behavior of granular media. Accurate modeling of particle shape is necessary to study the effect of grain shape on mechanical behavior of granular soil such as inter-particle contacts, dilation and liquefaction. The shear strength of granular soil is greatly influenced by its dilative and contractive behavior which in turn depends on various intrinsic soil properties such as grain size, size distribution, shape (angularity or roundness) and surface roughness of soil grains.

Substantial research on particle morphology has been conducted to evaluate the effect of grain shape on the mechanical response of granular soil by theoretical and experimental investigation and numerical modeling. However, in spite of significant progress in particle shape characterization and reconstruction through digital imaging, majority of the available resources describing the particle shape modeling technique remains limited to two-dimensional modeling and characterization, with minimal progress in three-dimensional domain due to lack of quantitative information about particle geometries, and the experimental and numerical difficulties associated with characterizing and modeling irregular particle shape. However, the microstructural phenomena (soil fabric, particle to particle interaction) in granular assemblies cannot be represented by two-dimensional simulation where the degrees of freedom are limited by enforcing restrictions in the third dimensions. These limitations warrant accurate modeling and quantitative characterization of three-dimensional particle shape to better understand the mechanical processes that control natural phenomena such as liquefaction susceptibility and shear flow. Proper characterization of particle shape is also

relevant to several other geotechnical applications such as studying soil-structure interaction, strength and deformation characteristics of pavement, soil erosion, and geotechnical interface design.

In the recent past, Discrete Element Method (DEM) has gained momentum in the field of micromechanical modeling. With the advancement of DEM, characterization of particle morphology in two and three dimensions has become increasingly relevant. Discrete element method is a numerical technique which allows modeling of a system of discontinuous material as an assembly of discrete elements interacting with each other. The main advantage of DEM lies in its ability to capture the mechanical interaction between different discrete bodies that cannot be solved by traditional continuum-based techniques such as the Finite Element Method. Although the two-dimensional DEM framework has seen considerable development in the area of particle shape characterization, however, three dimensional characterization and modeling of non-spherical particles is still in the early stage of development. Considering the current need to advance the existing research methodologies, the current research aims to model irregular particle geometries to evaluate the influence of three-dimensional particle shape on the shear strength behavior of granular soil using DEM.

1.2 Particle Shape Modeling in Two and Three Dimensions

Traditional approaches in DEM have modeled soil samples as an assembly of two-dimensional discs or three-dimensional spheres. But considering each particle as a disc or sphere would be too idealized and it does not capture the real behavior of the system as the shapes of soil grains are highly irregular in reality. Moreover, the circular or spherical particles have a higher tendency to rotate compared to the actual particle. Hence the angle of internal shearing resistance of the material comprising of circular or spherical particles would be much less than that of actual material. To overcome the limitation of this methodology, various formulations have been suggested in the literature to model non-circular particle outline such as approximating the particle shape by ellipse, polygon and combining several circular outlines into a cluster. However, the irregular particle shape could not be simulated accurately using these approaches. Notably, Ashmawy et al.

(2003) proposed a more accurate clumping technique (ODEC) in two dimensions to model angular particle shapes using real sand particles. In the ODEC (Overlapping Discrete Element Cluster) method, two-dimensional particle shape was modeled by clumping a number of overlapping disc elements within the particle boundary so that the resulting outline resembles the outline of the actual particle. The advantage of the ODEC method is that the built-in clump logic allows bonding between several disc elements without detecting contacts between disc elements belonging to the same clump (Ashmawy et al., 2003). The ability of the ODEC technique to model the behavior of irregular particle shape was verified numerically and experimentally by Sallam (2004). Good agreement was observed between experimental results and numerical simulations. However, the procedure primarily relied on several manual operations which necessarily warranted the development of a computer-based technique. The current research intends to take the next step to automate the ODEC technique in two dimensions by developing an algorithm (ODEC2D). In this method, overlapping disc elements are inscribed within the particle outline until a reasonable percentage of the grain area is covered. The ODEC2D algorithm is found to be capable of capturing angular particle shape accurately in two dimensions. As it can be conceivable that two-dimensional simulation limits the accuracy of modeling soil behavior from quantitative standpoint, which further necessitates extension of the ODEC technique in three dimensions to better understand the mechanical response of granular media in its entirety.

Literature describing particle shape modeling technique in three dimensions is scarce due to many research constraints such as difficulties in image capturing, three-dimensional reconstruction and handling large volume of data sets. However, some of the studies which are worth mentioning include ellipsoid-based three-dimensional DEM code, ELLIPSE3D (Lin and Ng, 1997), polyhedron-based approach (Ghaboussi and Barbosa, 1990) and three-dimensional image-based discrete element modeling procedure considering a virtual attraction between the grain surface and a number of primitive elements (Matsushima, 2004). The current study suggests another sphere-based approach by developing an algorithm (ODEC3D) to model three-dimensional irregular particle shape. Skeletonization is an efficient technique to inscribe sphere within a particle

boundary because skeleton of a region is the locus of centers of all maximally inscribed spheres. After generating skeleton of a given shape of sand particle, the volume is covered by clumping a number of overlapping spheres within the particle surface until the desired level of accuracy is achieved.

In order to generate and reconstruct particle assemblies for discrete element modeling simulation, relationship between grain size and shape needs to be explored. Therefore, this research conducts a detailed statistical analysis to explore the existence of any relationship between grain size and shape using different natural and processed sand samples. If no relationship exists between grain size and shape, then shapes belonging to a particular sand sample can be selected randomly from the particle shape library irrespective of sizes, for discrete element modeling simulation. However, if any particular sand sample is found to exhibit such relationship, then it would be necessary to separate the particles into different groups or bins based on their size.

Optimum sample size selection is considered as an important aspect of any experimental design. In the context of this study, it is hypothesized that the model behavior would be highly sensitive to the variability of size and shape of particles within a particular sand sample. Therefore, this study offers a statistical procedure to determine the optimum sample size for different materials used in the analysis. These tasks render proper characterization and quantification of particle morphology. In the current study, the grain shapes are quantified using Fourier shape descriptors and the first four Fourier descriptors are used to investigate the relationship between grain size and shape.

1.3 Research Objectives

Considering the emerging need of evaluating micromechanical behavior of granular soil, it is important to accurately model highly irregular particle shape in two and three dimensions and incorporate those shapes within discrete element modeling simulation. To fulfill these research goals, the main objectives of this research can be broadly classified into the following categories:

- Compilation of particle morphology data for sand samples collected from locations around the world and additional information obtained from various sources in the literature.
- Characterization of two-dimensional and three-dimensional shapes of granular materials.
- Quantification of particle shape using Fourier Shape Descriptors in two dimensions.
- Verification of any existing relationship between grain size and grain shape.
- Development of an algorithm for skeletonization of irregular particle shapes in two and three dimensions.
- Automation of the ODEC (Overlapping Discrete Element Cluster) method in two and three dimensions.
- Implementation of two-dimensional and three-dimensional particle shapes within DEM simulations to study of influence of particle shapes on the shear strength behavior of soil.
- Development of an online database for particle morphology.

1.4 Outline of the Dissertation

The state-of-the-art practices in quantifying and modeling angular particle shape are discussed in the next chapter. The third chapter describes the properties of various materials collected from different locations around the world. Particle shape characterization and quantification technique will be presented in the fourth chapter. The fifth chapter offers a methodology to determine the sample size for sand samples and explores relationship between grain size and grain shape. A detailed skeletonization algorithm and a procedure of automating the ODEC technique in two and three dimensions will be discussed in the sixth chapter. Chapter 7 describes the implementation of particle shape within DEM simulation and influence of particle shape on shear strength behavior of granular soil. Information about particle shape library will also be documented in chapter 7. Finally, a concluding discussion, research summary and future recommendation will be included in the eighth chapter.

CHAPTER 2

STATE OF THE ART IN PARTICLE SHAPE QUANTIFICATION AND MODELING

The previous chapter has introduced the importance of modeling particle shape in two and three dimensions. Having the research problem stated, the need for accurate particle shape modeling approaches is acknowledged and then research objectives are outlined. The current chapter discusses about the past and recent developments in particle shape quantification and modeling.

2.1 Existing Methods of Quantifying Particle Shape

Many research studies have been conducted to characterize and quantify the particle shape in two and three dimensions. Conventional methods available to quantify particle shape do not provide any quantitative information. For example, the comparison charts developed by Krumbein (1941) and the verbal descriptors assigned by Powers (1953), are based on qualitative visual assessment. The shape descriptors commonly used in the literature to quantify particle morphology are described next.

2.1.1 Shape Descriptors in Two Dimensions

A shape can be quantitatively described by a set of numbers which are often called descriptors. The three main features used to describe a shape are *form*, *roundness* and *surface texture* (Barrett, 1980). *Form* is the first order morphological descriptor, used to describe the gross shape of a particle. *Form* is related to the three principal axes, usually quantified in terms of sphericity (Diepenbroek, et al, 1992) and is independent of *angularity* and *surface roughness* (Sukumaran & Ashmawy, 2001).

Roundness and *angularity*, the second order descriptors, reflect the variations in corners, edges and faces and are related to *surface texture*. *Roundness* was defined as the

ratio of the curvature of corners and edges of the particle to that of the overall particle (Wadell, 1932). The defining equation is as follows:

Degree of *Roundness* of a particle in one plane = arithmetic mean of the roundness of individual corners in that plane $= \frac{\sum\left(\frac{r}{R}\right)}{N}$, r is the radius of curvature of a corner and R is the radius of the largest inscribed circle within the shape, $\sum\left(\frac{r}{R}\right)$ is the sum of the roundness values of the corners, N is the number of corners of the particle in the given plane (Wadell, 1932). *Roundness* is sensitive to abrasion during transportation and can be used as a measure of distance of transport.

Surface texture, the third order descriptor, reflects the roughness along the particle surface and on corners (Sukumaran & Ashmawy, 2001). This property is usually used to describe the small-scale details along the particle surface.

Other two-dimensional shape descriptors include *Aspect ratio*, *elongation*, *circularity*, *shape factor* and *angularity factor*. *Aspect ratio* is the ratio between major axis and minor axis of ellipse equivalent to the shape. *Elongation* is defined as the ratio of the length of the longest chord of the shape to the longest chord perpendicular to it. Wadell (1933) described *circularity* as the ratio of circumference of a circle of the same area as the shape, to the actual circumference of the shape. The standard equation to calculate circularity is:

$$Circularity = \frac{(4\pi)area}{perimeter^2} \tag{2.1}$$

Sukumaran & Ashmawy (2001) proposed a *shape factor* which is defined as the sum of the deviation of global particle outline from a circle and an *angularity factor* which is defined in terms of the number and sharpness of corners. In this method the particle shape was approximated by an equivalent polygon and compared to an ideal shape (circle) as shown in Figure 2.1.

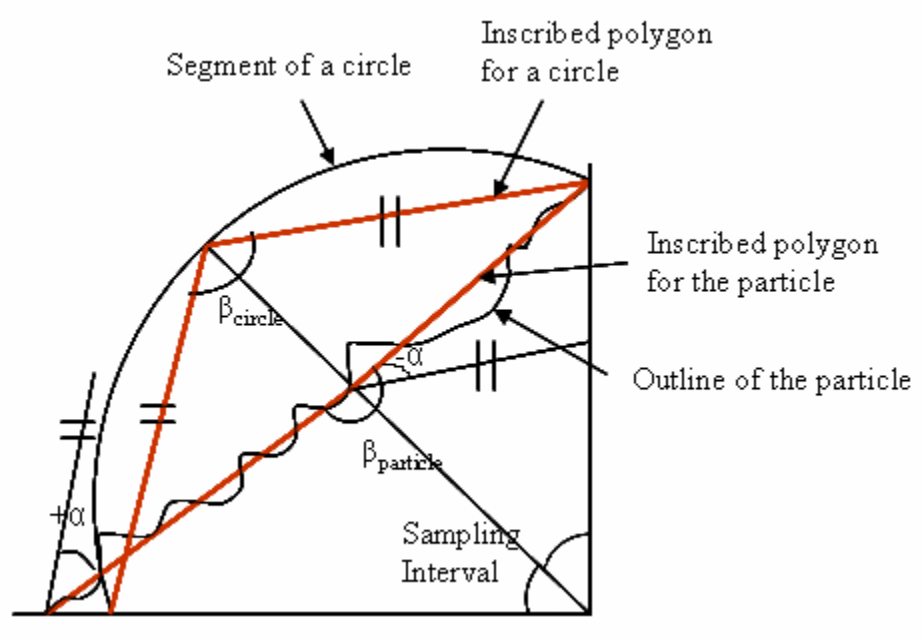

Figure 2.1 Ideal Geometric Shape Used to Define the Shape and Angularity Factors
[Source: Sukumaran (1996)]

2.1.1.1 Shape Factor (SF)

Sukumaran and Ashmawy (2001) defined the particle shape in terms of the deviation of the particle outline from a circle and distortion diagram was used to determine the shape factor. Distortion diagram (Sukumaran, 1996) is a plot of distortion angles (α_i) against the cumulative sampling interval. The distortion diagram is a mapping technique from which the particle shape can be fully reconstructed (Sukumaran and Ashmawy, 2001).

The normalized shape factor was obtained by using equation 2.2.

$$SF = \frac{\sum_{i=1}^{N} \alpha_{iParticle}}{N \times 45^0} \times 100\% \qquad (2.2)$$

Where, the numerator is the sum of the absolute values of α_i for a given shape and the denominator represents the sum of the distortion angles for a flat particle. The shape factor is zero for a circle and one for a flat particle.

2.1.1.2 Angularity Factor (AF)

Sukumaran and Ashmawy (2001) defined the angularity of a particle in terms of the number and sharpness of the corners and the angularity factor was estimated by using the following equation:

$$AF = \frac{\sum_{i=1}^{N}(\beta_{iParticle} - 180)^2 - (360^2 / N)}{3 \times (180)^2 - (360^2 / N)} \times 100\% \quad (2.3)$$

Based on the above equation, the angularity factor of a sphere will be zero. Though reliable, the method is difficult to implement for three-dimensional shapes.

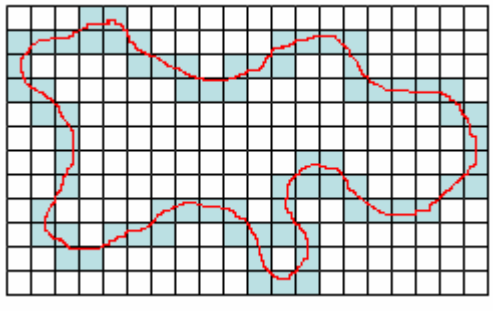

Figure 2.2 Perimeter of an Aggregate

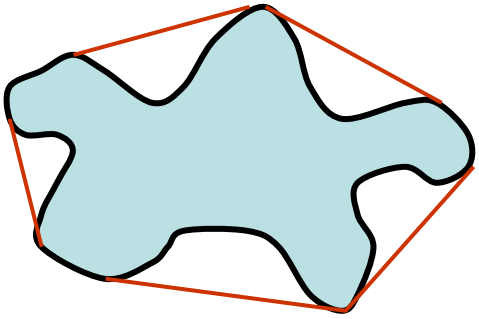

Figure 2.3 Convex Perimeter

[Source: Janoo, 1998]

Janoo (1998) proposed a roundness/angularity index and roughness of particles. The angularity index was obtained by using equation 2.4:

$$R_n = \frac{4\pi A}{p^2} \quad (2.4)$$

where, R_n is the roundness index, A is the area of aggregate and p is the perimeter of aggregate (Figure 2.2). An object with irregular surface will have a smaller value than the circular one.

The roughness of a grain was defined as the ratio of perimeter to the convex perimeter (Figure 2.3) and it was calculated using equation 2.5.

$$r = \frac{p}{p_c} \quad (2.5)$$

Where, r is the roughness, p is the perimeter of aggregate and p_C is the convex perimeter of aggregate (Janoo, 1998). For a smooth particle, the roughness factor is 1.00 and the roughness factor increases with the roughness of the particle (Uthus et al.,2005).

2.1.1.3 Fractal Based Shape Measures

Fractal Analysis is another approach to quantify particle shape. The 20th century mathematician, Benoit Mandelbrot (1977) first developed the concept of *fractal dimension* in order to quantify the complexity of nature in relatively simplistic ways. A point is a dimensionless object, a line has one dimension, a plane has two dimensions and space has three dimensions. Fractals can have fractional dimensions.

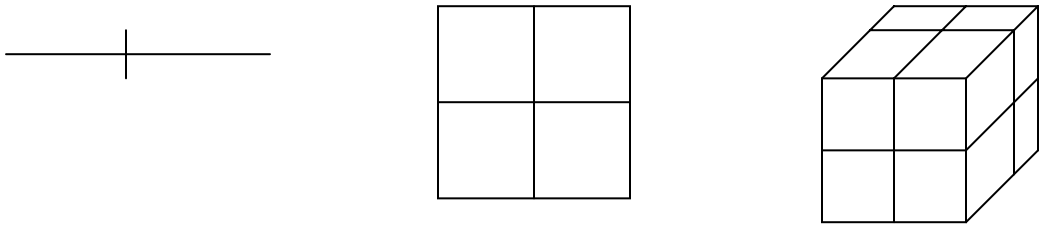

(A) (B) (C)

Figure 2.4 Self-Similar Figures: (A) Line Segments, (B) Square, (C) Cube

All of the above figures are self-similar. In figure 2.4 (A) the line is divided into two similar pieces. When magnified by a factor of 2, each of the two pieces will look exactly like the original line. In figure 2.4 (B) each of the four small squares will be identical to the original large square when magnified by a factor of 2. Similarly, in figure 2.4 (C) each of the eight small cubes needs to be magnified by a factor of 2 to generate the original large cube.

Table 2.1 Relationship Between Number of Miniature Pieces and Fractal Dimensions

Figure	Dimension	No. of miniature pieces
Line	1	2
Square	2	4
Cube	3	8

So, there exists a relationship between number of miniature pieces (N) and the dimension (D) of the object which is as follows:

$$N = M^{D} \tag{2.6}$$

where, M is the scaling factor/magnification factor.

Sierpinski Triangle (Figure 2.5) is another self-similar figure. Doubling the sides generates three similar copies. So, considering the above relationship, $3 = 2^{D}$; $\ln(3) = D \times \ln(2)$; $D = \ln(3) / \ln(2) = 1.585$, so fractal is a geometric figure that can have fractional dimension. This relationship [$D = \ln(N) / \ln(M)$] is used to compute the *fractal dimension* (D) of any self-similar fractals.

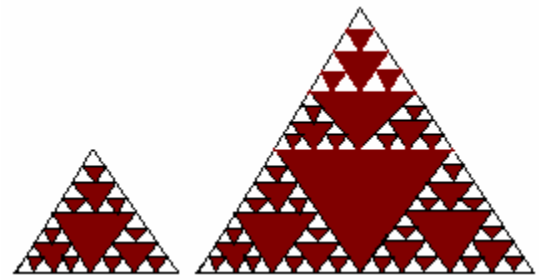

Figure 2.5 Sierpinski Triangle
[Source: http://math.rice.edu/~lanius/fractals]

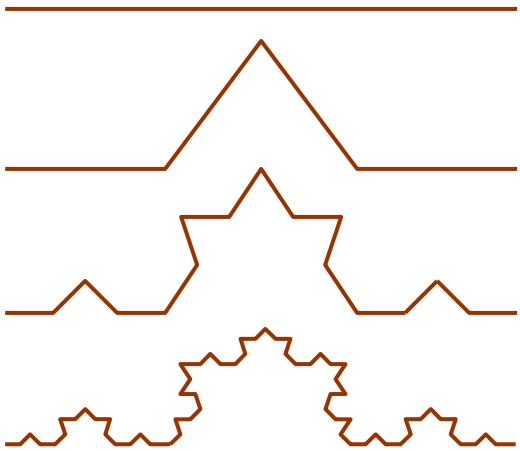

Figure 2.6 The Koch Curve
[Source: www.jimloy.com/fractals/koch.html]

One example of such fractal is Van-Koch snowflake (Figure 2.6). The Van-Koch curve starts with a straight line and replaces it with four lines; each of those is one-third the length of the original line. From Figure 2.7, N = 4, M = 3, D = ln (4) / ln (3) = 1.262. So, a fractal can be defined as an irregular geometric object with an infinite nesting of structure. Fractals are self-similar copies of themselves.

In the existing literatures there are some examples of using fractal technique for particle shape analysis. In fractal based shape measurement, the shape was approximated by a series of equilateral polygons (Kennedy & Lin, 1992). With the increase in number of polygon sides, there was a resulting increase in polygon perimeter and decrease in step length (length of each polygon side), so irregularities in the original shape were more closely observed. A relationship was developed by Mandelbrot (1967) between the perimeter estimate (P) and the step length (S). A series of log P versus log S pairs yielded a line (M-R plot) as shown in Figure 2.7, and the slope of the line was used as a measure of the irregularity of the shape. The information about the shape of the particle can be obtained from the slope of the line, greater slope indicates more irregularity in the shape. The relationship between the slope of the line (b) and the fractal dimension (FD) is as follows:

$$FD = 1 - b \tag{2.7}$$

This relationship is valid for self-similar (same degree of irregularity at all scales, Kennedy & Lin, 1992). The shapes which are not self-similar (sedimentary particles) can not be represented by a single fractal dimension since the M-R plot for these particles is not a single straight line. In case of non self-similar particles, two linear elements can appear in the M-R plot. These two linear elements represent two separate fractal dimensions, D_1 and D_2 (Figure 2.8). D_1 is related to the smallest step length and referred to as the textural fractal (Kaye, 1978; Flook, 1979) and the second element (D_2) is defined as the structural fractal (Flook, 1979) which represents the gross shape features of the particle. T_r marks the boundary between the textural and the structural fractal. Two different fractal elements represent two separate self-similar scales of particle geometry (Orford and Whalley, 1983). The occasional existence of the third element was considered as an artifact of the algorithm proposed by Schwarz and Exner (1980).

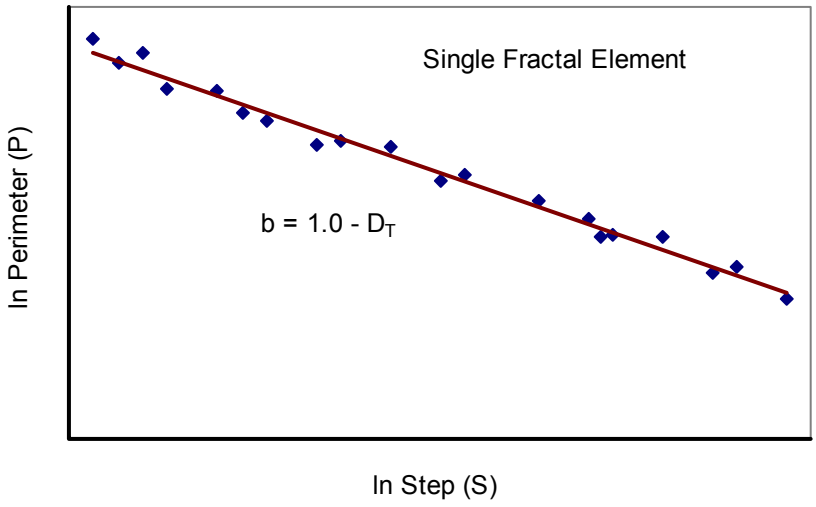

Figure 2.7 Single Fractal Element Overall Represented by D_T
[Source: Orford and Whalley (1983)]

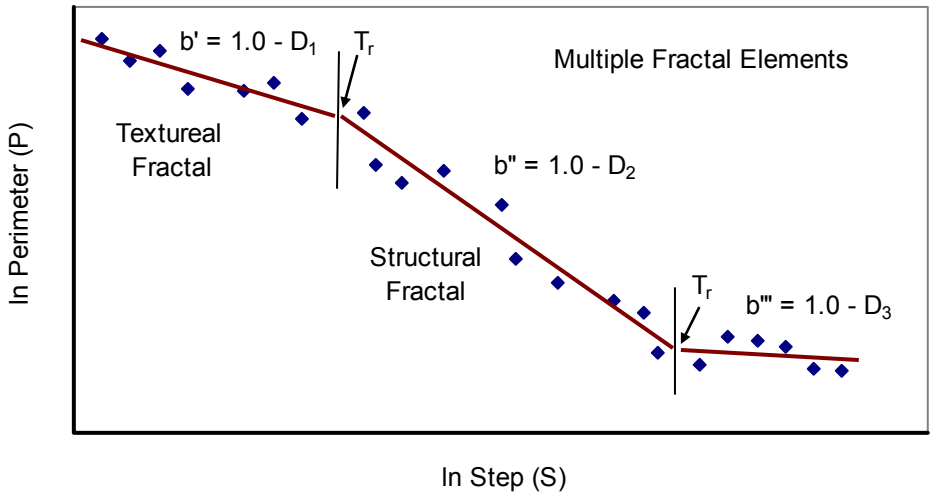

Figure 2.8 Multiple Fractal Elements Represented by D1 and D2
[Source: Orford and Whalley (1983)]

Orford & Whalley (1983) used fractal dimension to quantify the morphology of irregular-shape particles. They defined the boundary of the two fractal models as T_r (where $T_r=S/H_{max}$, S is the step length at the boundary and H_{max} is the particle's A-axis length). Three types of fractal combination were observed from the relative steepness of fractal element slopes. Type I was the standard single fractal element which usually refers to the gross shape of particle outline. Type II exhibited more irregular fractal structure and no prominent edge texture was observed in type II. Type III showed a concave fractal assemblage with marked irregular edge texture.

According to many researchers, the problem of having two different fractal elements in the M-R plot can be solved by segmenting the M-R plot into two components, one of them represents represent the gross shape of the particle and the other represents small scale details or surface texture. Kennedy & Lin (1992) mentioned that there are two problems with this approach, first is to identify the hinge point separating the two components. The inflection point occurs at different step lengths for each object. Therefore, selection of a single hinge point cannot represent some fractal components properly. The second problem is that it may be necessary to consider more than two fractal components in case of complex plot.

These problems can be overcome by segmenting the M-R plot into a larger number of fractal components, each of which is associated with the information about particle shape at a specific scale (Figure 2.9). The plot was divided into 10 straight line segments, the first representing the gross shape of the particle and the last representing finer scale features and the fractal dimension of each line segment was calculated. So each grain in a sample was represented by 10 fractal components that are analogous to the 24 Fourier harmonics and the dimension of each fractal component was analogous to the amplitude of the Fourier series (Kennedy & Lin, 1986). From their study, it was concluded that the fractal-based approach can be considered for the shape characterization of sedimentary particles. At the same time, research needs to be done to better understand the usefulness of this technique in discriminating the particles of vastly different shapes.

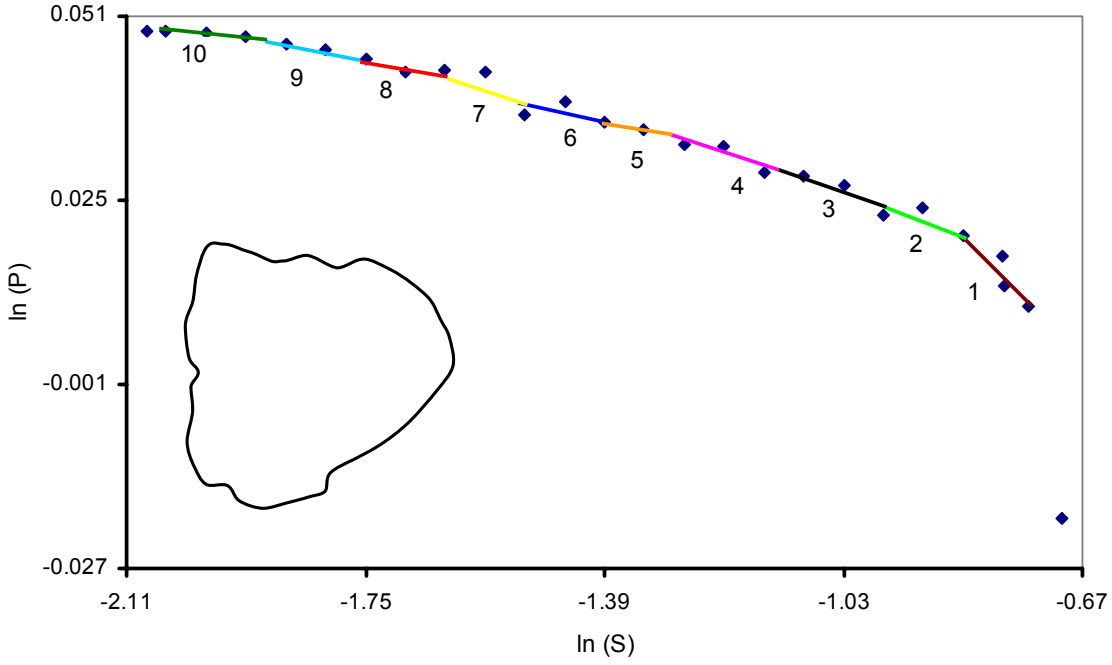

Figure 2.9 M-R Plot for a Sedimentary Particle
[Source: Kennedy and Lin (1992)]

The studies suggest that the irregular particle shape can be characterized by the use of *fractal analysis* and the power of this technique improves as the particle outline becomes more complex and irregular (Orford and Whalley, 1983). However, *Fractal dimension* is a measure of surface texture rather than the overall particle morphology, hence, the large scale surface features (gross shape) cannot be quantified by the use of *Fractal dimension* only. Another limitation of this approach is the difficulty in defining the range of fractal length (Dodds, J., 2003).

2.1.1.4 Fourier Shape Descriptors

Fourier transform is a mathematical technique that provides an alternative approach to characterize two-dimensional particle shape by fitting a *Fourier* series on the unrolled particle outline. The grain shape can be analyzed by (R, θ) Fourier method in closed form (Ehrlich & Weinberg, 1970), where the outline of a two-dimensional soil particle is traced out as shown in Figure 2.10.

The equation of the profile is:

$$R(\theta) = R_0 + \sum_{n=1}^{N} [A_n \cos(n\theta) + B_n \sin(n\theta)] \tag{2.8}$$

where, $R(\theta)$ is the radius at angle θ, N is the total number of harmonics, n is the harmonic number, A_n and B_n are the coefficient, giving the magnitude for each harmonic (Bowman et al., 2001). One drawback with this approach is the possibility of re-entrant angles where the radius intersects the particle outline twice resulting in two possible values of radius R at a particular angle θ (Figure 2.10).

Fourier descriptor method (Clark, 1981) is a possible alternative to the above method. In this method the particle outline is traversed in the complex plane at constant speed. The complex function used in the analysis is:

$$x_m + iy_m = \sum_{n=-N/2+1}^{N/2} (a_n + ib_n)\left[\cos\left(\frac{2\pi nm}{M}\right) + i\sin\left(\frac{2\pi nm}{M}\right)\right] \tag{2.9}$$

where, (x, y) are the coordinates of the particle outline; N is the total number of descriptors; n is the descriptor number; M is the total number of points describing the particle; m is the index number of a point on the particle; a and b are the coefficients for

each descriptor; and *i* is the imaginary unit number (Bowman et al., 2001). This method doesn't suffer from the re-entrant angle problem. In this research, particle shape is characterized by the *Fourier* mathematical technique.

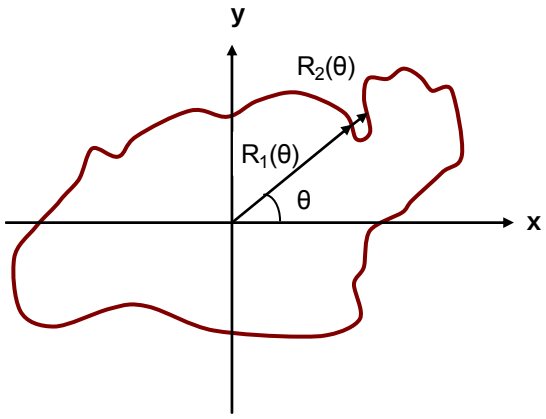

Figure 2.10 Fourier Analysis in Closed Form
[Source: Bowman et al., 2001]

2.1.2 Shape Descriptors in Three Dimensions

Three-dimensional descriptors commonly used to characterize particle shape include the length ratios of orthogonal axes (Krumbein, 1941; Yudhbir & Abedinzadeh, 1991), *sphericity* (Wadell, 1932; Krumbein, 1941). S*phericity* is the ratio of surface area of a sphere of the same volume as the shape, to actual surface area of the shape (Wadell, 1932). Krumbein (1941) defined the sphericity as the ratio of particle volume to that of the smallest circumscribing sphere.

Sphericity and roundness are two different morphological properties. Sphericity is related to the form and elongation, while roundness is related to angularity and surface roughness. Therefore, a spherical particle may have low roundness value if the surface is rough (Bowman et al., 2001). Conversely, a non-spherical particle can be perfectly round in shape (ellipse-shaped particle) and equidimensional particles (cube or hexahedron) can be very angular (Cho et al., 2006).

Lees (1964) described the shape of the aggregates by a shape factor (F) and the sphericity (ψ) and these descriptors were defined in terms of the flatness and elongation ratio. The flatness ratio (p) is the ratio of the short length (thickness) to the intermediate

length (width) and the elongation ratio (q) is the ratio of the intermediate length to the longest length (length). The shape factor was defined by equation 2.10 which is the ratio of the elongation ratio and the flatness ratio (Uthus et al.,2005).

$$F = p/q \tag{2.10}$$

The sphericity of a particle was also expressed by the flatness and elongation ratios as shown in Equation 2.11.

$$\psi = \frac{12.8(\sqrt[3]{p^2 q})}{1 + p(1+q) + 6\sqrt{1 + p^2(1+q^2)}} \tag{2.11}$$

Rao et al. (2002) described a three-dimensional descriptor, called Angularity Index by obtaining an angularity value for each of the three 2-D images acquired from the three views using the image analysis procedure. Then the angularity was calculated as a weighted average of all three views.

$$AI_{Particle} = \frac{\text{Ang. (front). Area (front) + Ang. (top). Area (top) + Ang. (side).Area(side)}}{\text{Area(front) + Area(top) + Area(side)}} \tag{2.12}$$

Where, $AI_{Particle}$ is the Angularity Index of the particle. The unit for AI is degree.

Masad et al. (1999) determined the Surface Texture (ST) by fine aggregates by erosion-dilation technique. Erosion is a morphological operation which causes an object shrink by one pixel along the boundary. Dilation is the reverse of erosion, where the boundary of an object is dilated or grown by a layer of pixels. ST is defined by the area lost due to the erosion-dilation operation as a percentage of the total area of the original image.

$$ST = [(A_1 - A_2) * 100] / A_1 \tag{2.13}$$

Where, A_1 and A_2 are the areas of the two-dimensional image before and after erosion-dilation respectively. The surface texture of an object was calculated as a weighted average of all three views.

$$ST_{Particle} = \frac{\text{ST (front) . Area (front) + ST (top) . Area (top) + ST (side) . Area(side)}}{\text{Area (front) + Area (top) + Area (side)}} \quad (2.14)$$

Where, $ST_{Particle}$ is the Surface Texture of the particle, ST is the Surface Texture for one view and Area is the area for one view.

2.1.2.1 Representing Grain Shape in Spherical Coordinates

Three-dimensional surface of any particle can be characterized by $R = R(\theta, \phi)$ in closed form (Schwarcz & Shane, 1969) where θ, ϕ are angles measured from two perpendicular axes intersecting at the centroid of the particle ($0 \le \theta \le 2\pi$; $0 \le \phi \le \pi$) and R is the radial distance from the centroid to a point on the surface. For such surfaces $R(\theta, \phi)$ can be represented by a set of *spherical harmonics* of the form:

$$R(\theta, \phi) = \sum_{m,l} [A_{ml} Y^{e}_{ml}(\theta, \phi) + B_{ml} Y^{0}_{ml}(\theta, \phi)] \quad (2.15)$$

where $Y^{e}_{ml} = \cos(m\phi) P^{m}_{l}(\cos\theta)$ and $Y^{0}_{ml} = \sin(m\phi) P^{m}_{l}(\cos\theta)$ are the *spherical harmonics* based on the Legendre function P^{m}_{l} (Morse & Feschbach, 1953). The coefficients A_{ml} and B_{ml} are obtained as follows:

$$\frac{(2n+1)\varepsilon_m}{4\pi}\left[\frac{(l-m)!}{(l+m)!}\right] \int_0^{2\pi} d\phi \int_0^{\pi} R(\phi, \theta) Y_{ml} \sin\theta d\theta \quad \begin{Bmatrix} = A_{ml} \text{ for } Y^{\varepsilon}_{ml} \\ = B_{ml} \text{ for } Y^{0}_{ml} \end{Bmatrix} \quad (2.16)$$

$\varepsilon_0 = 1$, $\varepsilon_n = 2$ (n=1, 2, ……)

The *spherical harmonics* are the angular portion of the solution to Laplace's equation in spherical coordinates. Spherical coordinates are a system of curvilinear coordinates, describing positions on a sphere (Figure 2.11).

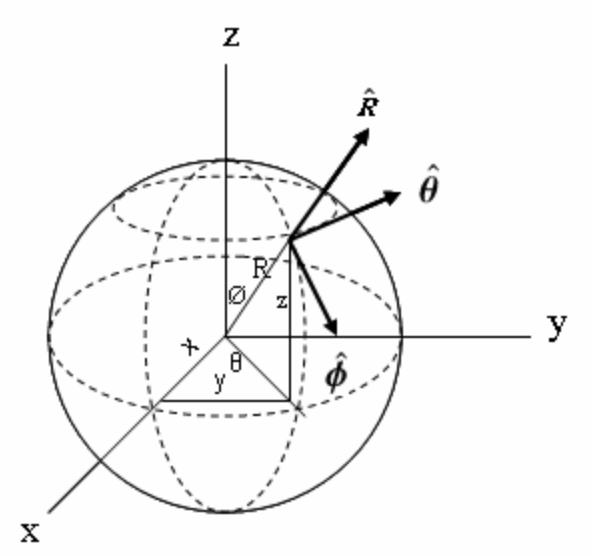

Figure 2.11 Spherical Harmonic Transform
[Source: http://mathworld.wolfram.com/SphericalCoordinates]

The equations of transformation between Cartesian and spherical coordinates are as follows:

$$x = R\sin\phi\cos\theta \qquad R = (x^2 + y^2 + z^2)^{1/2} \tag{2.17-a}$$

$$y = R\sin\phi\sin\theta \qquad \phi = \cos^{-1}\left[\frac{z}{(x^2 + y^2 + z^2)^{1/2}}\right] \tag{2.17-b}$$

$$z = R\cos\phi \qquad \theta = \sin^{-1}\left[\frac{y}{(x^2 + y^2)^{1/2}}\right] = \cos^{-1}\left[\frac{x}{(x^2 + y^2)^{1/2}}\right] \tag{2.17-c}$$

Three-dimensional particle surface can be quantified using Spherical Harmonic Transform (3-D equivalent of 2-D Fourier transform). Cartesian coordinates (x, y, z) of the each voxel are transformed into spherical coordinates (R, ϕ, θ) using equations (2.17-a) to (2.17-c). In this case the object surface is scanned by the variation of two parameters (θ and ϕ) where $0 \le \phi \le \pi$ and $0 \le \theta \le 2\pi$. A suitable sampling interval should be chosen for proper characterization of the particle shape. An efficient algorithm of spherical harmonic series has been developed by Garboczi (2002) and implemented by Masad et al. (2005) on various three-dimensional particle shapes.

2.2 Relationship Between Grain Size and Shape

Particle morphology plays a very important role in understanding the micromechanical behavior of cohesionless soils. Grain shape depends on various factors such as source of material, mineralogical composition, distance of transport and environmental conditions affecting formation of deposit. In order to generate and reconstruct particle assemblies of highly irregular geometric shapes of a particular sand sample, the relationship between grain size and shape needs to be evaluated. For example, size-shape relationships are necessary to generate representative assemblies of angular particles for discrete element modeling simulations.

Various research studies have been documented in the literature describing the relationship between particle size and particle shape. The dependence of particle shape on particle size was investigated by Russell and Taylor (1937), Pollack (1961), Ramez and Mosalamy (1969), Wadell (1935), Pettijohn and Lundahl (1934), McCarthy (1933), Inman (1953), Inman et al. (1966) and Conolly (1965) and these studies demonstrated a decrease in roundness with a decrease in particle size for intertidal sands (Balazs, 1972).

Banerjee (1964) conducted a study to evaluate size-shape relation and observed that the finer grains are more rounded than the coarser ones (Figure 2.12) and it was concluded that the negative correlation between grain size and roundness of the grains is due to two different sources of sands (Pettijohn, 1957). The study also suggested that the finer rounded particles were generated from a mature pre-existing sedimentary rock whereas the coarser angular particles were originated from nearby freshly-weathered igneous and metamorphic rocks (Banerjee, 1964).

A reverse relationship was found in a study (Yudhbir and Abedinzadeh, 1991) where a relationship was established between average value of particle angularity and the grain size for each sieve fraction (Figure 2.13). The study proposed that the particle angularity decreases (or roundness increases) with size which was also suggested by Twenhofell (1950), Folk (1978), Khalaf and Gharib (1985).

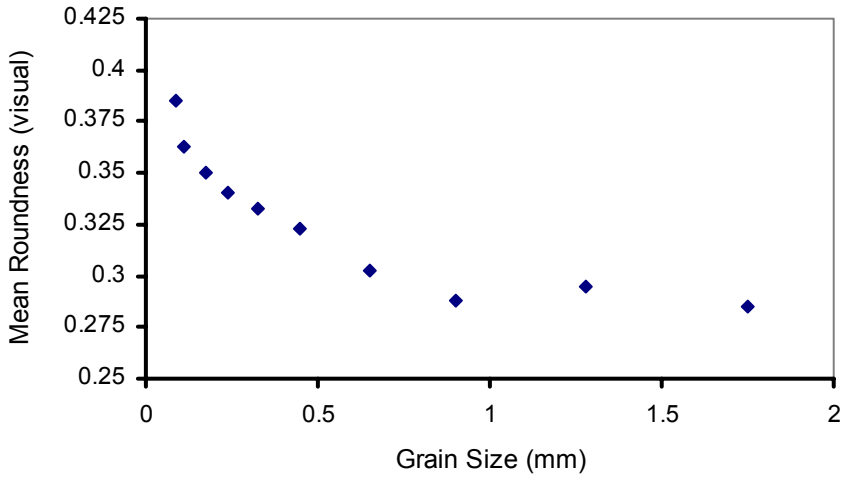

Figure 2.12 Mean Roundness Values of Eight Samples Plotted Against Mid-Points of Size Grades
[Source: Banerjee, 1964]

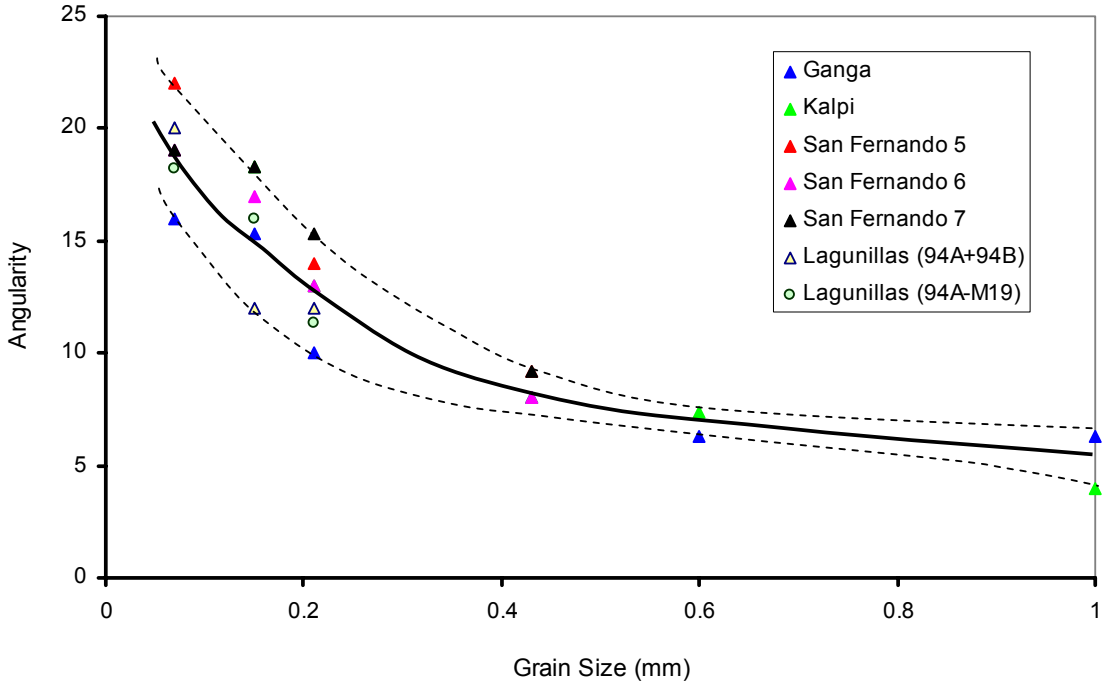

Figure 2.13 Relationship Between Particle Angularity and Particle Size
[Source: Yudhbir and Abedinzadeh (1991)]

Another study was conducted by Goudie and Watson (1981) to investigate the roundness of quartz grains from different dune areas around the world and the study revealed that the majority of the samples were sub-rounded and more angularity was observed in smaller grains compared to larger ones and the grain roundness varied from one dune location to the next. In addition, it is suggested that the shape of dune sand particles depends on the transport and sedimentation conditions, as well as the nature and origin of the material (Thomas, 1987). In a study conducted by Mazzullo et al. (1992) grains were divided into three bins based on the grain size distribution and for each bins higher order harmonics were used to study the effect of grain size on grain roundness for increasing distance of transport. In that study, no major variation in grain roundness was observed among the three bins.

The available literature exploring the relationship between grain size and grain shape sometimes fails to demonstrate consistent results. In various research studies it has been observed that roundness of sand grains is extremely susceptible to abrasion and wear to which particles are subjected during transportation by wind or water (Krumbein, 1941). An increase in roundness of very coarse sand (Plumley, 1948) and a slight decrease in roundness of fine sand (Russell and Taylor, 1937) with distance of transport by fluvial action were documented in the literature, whereas Pollack (1961) reported negligible changes in roundness in the direction of transport in the South Canadian River (Balazs, 1972). The shapes of individual particle in a composite soil sample also depend on the extent of gradation. Likewise, an increase in roundness was observed when sand particles are separated from gravel during segregation by tidal currents since the presence of gravel results in decrease in roundness of sand (Balazs, 1972; Anderson, 1926; Russell, 1939; Twenhofel, 1946).

Abrasion of sand grains also depends on the environment in which they are being transported. It has been observed in literature (Kuenen, 1960) that abrasion (in terms of weight loss) of quartz grains in aeolian environment is 100 to 1000 times more than that in fluvial environment over the same distance of transport because sand grains have to resist more friction in air than in water (Sorby, 1877). Another factor controlling grain shape is the mineralogical composition of the individual grain. Hunt (1887) indicated that

quartz and feldspar are highly resistant to abrasion. Moreover, prolonged transport results in abrasion in feldspar and hence feldspar is expected to be less rounded than quartz (Balazs, 1972).

Mazzullo et al. (1986) suggested that the shapes of quartz grains can be influenced by different mechanical (abrasion, fracturing, grinding and sorting) and chemical (silica dissolution and precipitation) processes and the variability in resulting grain shapes is likely to be dependent on the variation in mechanical and chemical processes to which the grains are subjected. In this research, Fourier descriptors are used to verify any existing relationship between grain size and shape.

2.3 Modeling Particle Shape in Two Dimensions

Discrete element method (DEM) is being considered as a significant achievement in the area of micromechanical modeling. The recent development of DEM has made it possible to model particle morphology in two and three dimensions and examine soil behavior from micromechanical standpoint. The Discrete Element Method was first developed to model rock slopes (Cundall, 1971) and the mechanical behavior of 2-D assemblies of circular discs (Strack and Cundall, 1978). Later, the method was extended to three dimensions to model 3-D assemblies of spheres (Cundall & Strack, 1979) by the program TRUBAL. Extensive research has been conducted to study the constitutive behavior of coarse grain soil using the modified versions of TRUBAL. In DEM, material is modeled as a random assembly of discrete elements interacting with each other through contact forces.

2.3.1 Existing Methods of Modeling Irregular Particle Shape

The DEM tool has been adopted by numerous researchers to study the mechanical response of granular soil from macroscopic to microscopic level (Mustoe et al., 1989; Williams & Mustoe, 1993). Traditional approaches in DEM modeled soil mass as an assembly of discs or spheres (Cundall and Strack, 1979). The first DEM code, BALL was introduced by Strack and Cundall (1978), where a two-dimensional system was modeled as an assembly of discs. Following this procedure, various DEM formulations were

proposed during the last two decades using circular and spherical particles, such as TRUBAL (Cundall and Strack, 1979), CONBAL (Ng, 1989; Ng and Dobry, 1991), GLUE (Bathurst and Rothenburg, 1989), DISC (Ting et al., 1989), DMC (Taylor and Preece, 1989) and others. The circular or spherical particles have a higher tendency to rotate compared to the actual particle. Hence the angle of internal shearing resistance of the material comprising of circular or spherical particles will be much less than that of actual material and the use of spherical particles in discrete element modeling simulation would be too idealized to study the microscopic behavior of soil mass (Lin and Ng, 1997). To overcome these limitations and to better understand the soil behavior through numerical simulation, different modeling techniques were proposed in many research studies where the non-circular particle outlines were approximated by various mathematical functions, such as ellipses (Ting et al, 1993; Ng, 1994), super-quadratics (Williams and Pentland, 1992; Cleary, 2000), and continuous circular segments (Potapov and Campbell, 1998) to model highly irregular particle shape.

Barbosa and Ghaboussi (1992) and Matuttis et al (2000) suggested polygon-shaped particles which is a more realistic representation of modeling irregular particle shape. However, the contact detection algorithm was very time consuming for polygon-shaped particles (Jensen et al., 1999) and the method is computationally intensive as the particle outline becomes more complex and irregular, especially in three dimensions.

Ting et al. (1993) developed an algorithm for DEM simulation using two-dimensional ellipse-shaped particles to compute particle-to-particle and particle-to-wall contacts and good agreement was observed between the numerical simulation and the behavior of real soil. Though ellipse-shaped particles have fewer tendencies to rotate compared to circular particles, the shape of irregular particle could not be represented accurately by ellipse.

Potapov and Campbell (1998) used oval-shaped particles in order to generate representative assemblies in DEM environment where ellipse was approximated by oval shape whose boundary was determined by four circular arches of two different radii that are joined together in a continuous way. More complex shapes can be reproduced by

changing the radii of the arches. Though the procedure was computationally efficient, the application of the method in thee dimensions was not verified.

Favier et al (1999) modeled axisymmetrical particles as multi-sphere discrete elements by using overlapping spheres with fixed rigidity. The method was capable of modeling any axisymmetrical shape, however highly angular particles cannot be modeled properly using the procedure.

2.3.2 Modeling Angular Particles as Clusters

Jensen et al. (1999) proposed a new clustering technique where a number of circular discrete elements were clumped together in a semi-rigid configuration to capture the shape of irregular particle (Figure 2.14). The main concept behind this clustering technique is that each cluster rotates and translates as a rigid body. The relative translation and rotation among the discs within a cluster can also be prevented by enforcing kinematics restrictions on discs forming the cluster (Thomas and Bray, 1999). In both methods, only non-overlapping elements were used within each cluster and the number of discs within a cluster was limited to three or four to decrease computation time. Therefore, the simulated particle outlines did not resemble that of actual particles.

2.3.3 Overlapping Discrete Element Clusters

Ashmawy et al (2003) proposed the Overlapping Discrete Element Cluster (ODEC) technique to model angular particle shapes accurately in two dimensions by using discrete element modeling code PFC^{2D} and Itasca's software-specific programming language, *Fish*. In the ODEC method, two-dimensional particle shape was modeled by clumping a number of overlapping discs within the particle boundary so that the resulting outline resembles the outline of the actual particle (Figure 2.15). The ODEC method is computationally efficient, because the built-in clump logic cannot detect contacts between disc elements belonging to the same clump. The number of overlapping discs needed to accurately model the irregular particle shape depends on the degree of non-uniformity in the original particle shape and angularity, the desired level of geometric accuracy and the required computation time limit (Ashmawy et al., 2003). It was

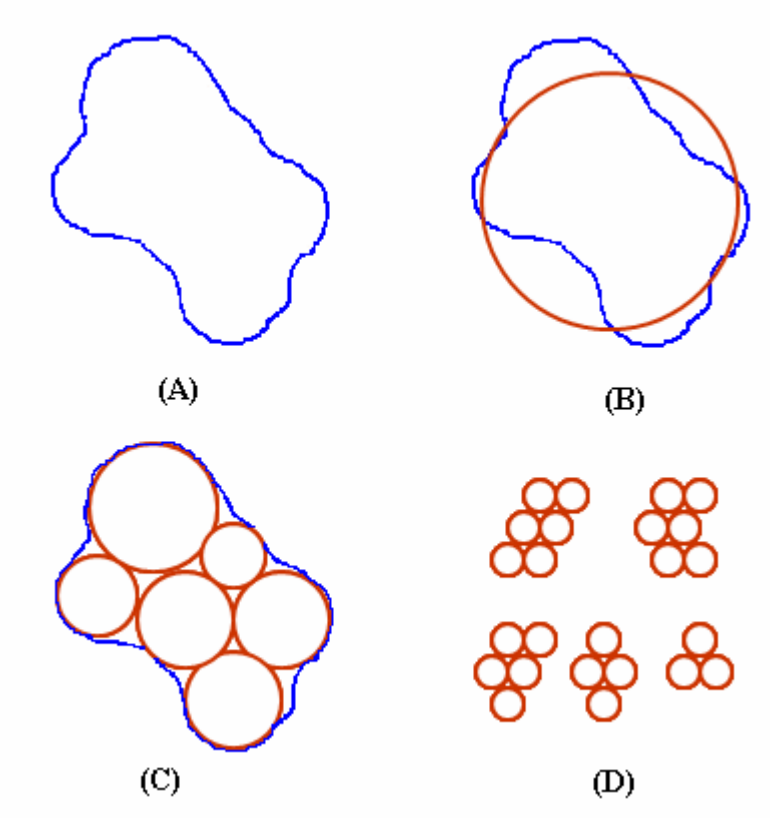

Figure 2.14 (A) Outline of Sand Particle, (B) DEM Disc Element Superimposed Over Sand Particle, (C) DEM Disc Particles are Joined Together in a Rigid Configuration (Cluster), (D) Several Possible Combination of Discs to Form Clusters [Source: Jensen et al. (1999)]

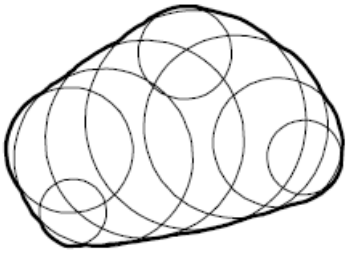

Figure 2.15 Disc Elements Inscribed within a Particle Outline to Capture the Shape
[Source: Ashmawy et al. (2003)]

observed that ten to fifteen discs are sufficient to capture the shape of a particle accurately.

Due to overlapping, the density scaling should be necessary for each disc belonging to a particular clump so that the mass of the particle remains proportional to the area. An approximate method was proposed by Ashmawy et al. (2003) to scale the density of overlapping discrete elements as follows:

$$\rho_d = \frac{A_p}{\sum A_d} \times \rho_p \tag{2.17}$$

where ρ_d is the density of the discs, A_p is the area of the particle, A_d is the sum of the areas of the disc elements and ρ_p is the density of the particle. Equation (2.11) does not guarantee the moment of inertia and the center of mass of the model particle to be identical to those of the actual particle. Sallam (2004) introduced a modification to the ODEC method where the compatibility of the particle centroid and inertia was satisfied after generating all the discs inside the particle.

The ODEC method was implemented within PFC^{2D} by means of a series of *Fish* functions that convert a particle assembly of discs into their corresponding angular particle as follows:

- Particles were first generated as circular discrete elements within the desired range of grain sizes using the built-in particle generation techniques.
- Each circular particle was then transformed into its angular equivalent by using the shape conversion algorithm that replaced each circular outline with a corresponding set of circular discrete element cluster, selected randomly from the particle shape library.
- A random rotation between 0 and 360º was applied to each transformed particle to ensure uniform particle orientations within the assembly. (Ashmawy et al., 2003). Figure 2.16 shows a random assembly of circular particles generated in PFC^{2D} and transformed to their equivalent angular shapes using the ODEC technique.

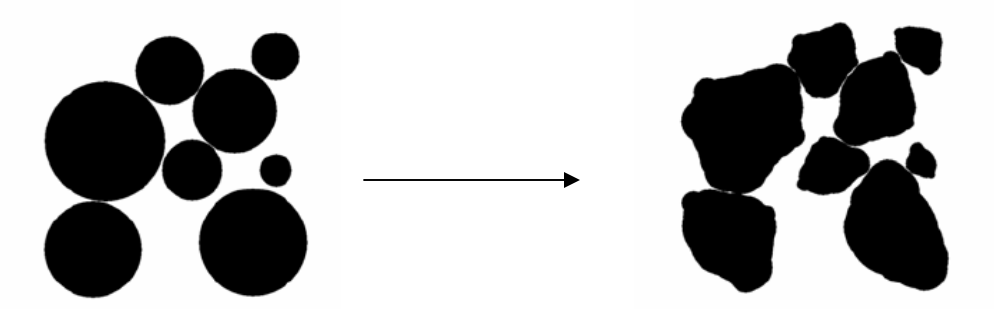

Figure 2.16 Random Assemblies of Eight Circular Particles (Left) and the Transformed Equivalent Angular Particles (Right)
[Source: Ashmawy et al. (2003)]

Sallam (2004) experimentally verified the ability of DEM using the ODEC technique developed by Ashmawy et al. (2003) to model the behavior of irregular particle shapes. An experimental set-up was built to study the translations and rotations of particles and inter-particle contact resulting from external disturbance. Good agreement was observed between experimental results and numerical simulations. In the current research the two-dimensional particle shapes are modeled using the ODEC technique. An algorithm is developed to automate the ODEC technique.

2.4 Modeling Particle Shape in Three Dimensions

Most of the available literature on modeling irregular particle shape is limited to two dimensions with minimal progress in the three-dimensional domain. Lin and Ng (1997) developed a three-dimensional DEM code, ELLIPSE3D where the three-dimensional irregular particle shape was approximated by ellipsoid. Numerical simulations were performed to study the mechanical behavior of mono-sized particle arrays using the ELLIPSE3D program. The use of non-spherical particles in discrete element modeling showed an improvement in the results of numerical simulations. However, the highly irregular three-dimensional particle shape cannot be modeled accurately using ellipsoid. Another DEM formulation was proposed by Ghaboussi and Barbosa (1990) where three-dimensional granular particles were modeled as polyhedron. None of the methods used the shape of real sand particles for DEM simulation.

Matsushima (2004) first suggested a 3-D image-based method to model irregular particle shapes in three dimensions. 3-D images of Toyoura sand were obtained with a micro X-ray CT and they were directly converted into Discrete Element models (Figure 2.17). A number of primitive elements of different sizes were placed within the particle surface and a virtual attraction was assumed between each point on the grain surface and the element closest to the point. Due to this attraction, elements moved from their initial position and increased or decreased in size to reduce the distance from the surface point and the procedure was continued until an optimized converged solution was obtained (Matsushima, 2004). The accuracy of the model was estimated and an average error of 5.8% was found in terms of grain radius and the volumes of most of the modeled grains were 10 to 15% less than that of actual grains. The volumes of some grains were even bigger than the original volumes of the corresponding grains and these errors were considered as an inaccuracy of the modeling technique.

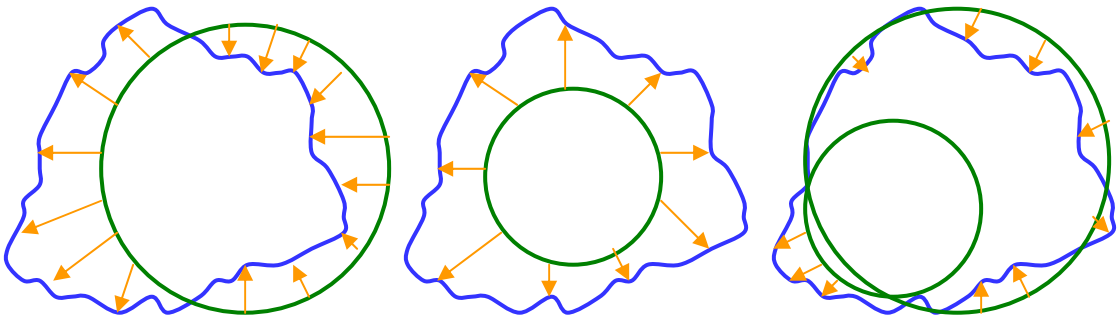

Figure 2.17 Virtual Force Acting on the Elements
[Source: Matsushima, 2004]

In this research, the ODEC method (developed by Ashmawy et al., 2003) is extended to three dimensions. A number of overlapping spherical discrete elements is clumped together within the particle volume. The number of spheres necessary to cover the particle volume depends on the overall shape and angularity of the particle. Three-dimensional shapes are implemented within 3-D DEM code, PFC^{3D} by using Itasca's software-specific programming language, *Fish* that converts a particle assembly of spheres into their equivalent angular particles.

2.5 Effect of Particle Shape on Shear Strength Behavior of Cohesionless Soil

Shear force in cohesionless soil is derived from the frictional resistance of soil which depends on the inter-particle friction, particle interlocking, packing density, grain crushing, rearrangement and dilation during shearing. These factors can also be influenced by inherent soil properties, such as particle size, shape and surface roughness. Grain shape is one of the major contributing factors that affect the mechanical behavior of granular assembly. Shear strength and liquefaction characteristics of granular soil depend on particle size, grain size distributions, shape and surface texture of the individual grains. Granular packing which is governed by the void ratio of the assembly is another important factor influencing the shear strength behavior of soil (Holtz and Kovacs, 1981). The maximum (loosest state) and minimum (densest state) void ratio of a soil mass depend on the grain shape and grain size distribution of the assembly of grains. Early research found an increase of maximum (e_{max}) and minimum (e_{min}) void ratio and void ratio difference ($e_{max} - e_{min}$) with increasing particle angularity or decreasing roundness and sphericity (Youd, 1973; Cho et al., 2006; Fraser, 1935; Shimobe and Moroto, 1995; Miura et al., 1998; Cubrinovski and Ishihara, 2002; Dyskin et al. 2001; Jia and Williams, 2001; and Nakata et al., 2001). Based on several experiments published in the literature, the angle of internal friction (ϕ) decreases with an increase in void ratio (Zelasko et al., 1975; Shinohara et al., 2000). Therefore, the shear strength of soil also decreases since ϕ is a measure of shear strength of cohesionless soil. The angle of shearing resistance of soil can also be influenced by the angularity (or roundness) and the surface texture of the individual grains. The increase in angularity and surface roughness of the soil particles results in an increase of ϕ (Zelasko et al., 1975; Alshibi et al., 2004). A reverse relationship was documented in literature where the void ratio was increased with increasing particle angularity (Jensen et al, 2001). Angular particles cannot produce dense packing since the grains are separated by sharp corners (Dodds, J., 2003).

Conflicting knowledge is available in the literature describing the relationship between particle size and the angle of internal friction. Koerner (1970) observed a decrease in ϕ with increasing mean grain size. In another study, the authors demonstrated a decrease in void ratio with increasing grain size whereas the friction angle reduces or

remains almost constant for each sand sample. Though the larger grains show greater initial interlocking, it is compensated by the greater degree of grain crushing and fracturing due to the greater force per contact of larger grains (Lambe & Whitman, 1969). Norris (1976) and Zelasko et al. (1975) also suggested that the angle of internal friction of soil is not influenced by particle size considering the void ratio, angularity and roughness remaining constant (Jensen et al., 2001), rather the shear strength of soil is greatly influenced by gradation or particle size distribution (Zelasko et al. 1975). The relationship between grain size and angle of internal friction can be explained by the phenomenon of interlocking. For example, the angle of internal friction of well graded soil is higher than that of poorly graded sand, because the smaller size particles fill the void spaces between larger size particles; hence the void ratio is reduced resulting in an increase in the strength of soil mass. The effect of particle shape on void ratio was investigated by Zelasko et al. (1975) and the study demonstrated an increase in shear strength and ϕ value with a decrease in particle roundness. More interlocking is observed between angular grains and hence the angular particles are found to exhibit more shearing resistance than do rounded particles. Sukumaran and Ashmawy (2001) conducted a study to evaluate the relationship between shear strength and shape and angularity factor and found that the large-strain drained friction angle increases with an increase in shape and angularity factor. An increase in large-strain angle of shearing resistance with increasing surface roughness was also observed by Santamarina and Cascante (1998). In general, dense specimen with angular particles will provide more resistance to shearing than rounded particles (Shinohara et al., 2000) due to increase in interlocking effect. The shearing resistance of soil is developed due to particle rotation and translation (rolling and sliding). Frictional resistance will increase if the particles are 'frustrated from rotating' (Santamarina and Cascante, 1998). If the density of soil is low, particles are free to rotate which results in lower frictional resistance to shearing. In densely packed soil (low void ratio), higher density and higher coordination number (number of contacts per particle) hinder rotation, causing slippage at particle contacts and this will results in dilation and thus an increase in the shearing resistance of soil (Santamarina and Cascante, 1998). The two major components influencing the shearing resistance of granular soil are

dilatancy (developed from particle rearrangement and interlocking) and interparticle sliding resistance (Taylor, 1948; Santamarina and Cascante, 1998; Alshibi et al., 2004). Dilatancy of granular soils is defined as the change in soil volume during shear and dilatancy of granular soil is greatly influenced by the angularity of the grains, void ratio and confining pressure (Chen et al., 2003). Dilation is usually represented by the angle of dilation (ψ) which is defined as the ratio of volumetric strain rate to shear strain rate. Dense sand under undrained condition exhibits strain hardening behavior. After an initial tendency to contract, dilation starts and causes the pore pressure to decrease and effective stress to increase.

Liquefaction susceptibility of granular soil also depends on particle size, shape and size distribution. Poorly-graded sands with rounded particles are more susceptible to liquefaction than well-graded sands with angular particles since the shearing resistance of angular particles is higher due to high coordination number and thus the particle interlocking is stronger compared to rounded particles.

Liquefaction is a phenomenon that may take place during earthquake shaking and is one of the major causes of ground failure in earthquakes. Loose, saturated, uniformly-graded, fine grain sands are very susceptible to liquefaction. Liquefaction takes place when seismic shear waves pass through a saturated granular soil layer, distorting its particle arrangements and breaking the inter-particle contacts. During earthquake loading, the shearing stage is so rapid that the pore water pressure cannot get enough time to dissipate, resulting in rapid increases of pore water pressure and accompanying very low effective stress such that the shear strength of the soil can no longer sustain the weight of the overlying structures and the soil flows like a viscous fluid. To mitigate the post earthquake hazards, areas susceptible to liquefaction should be identified.

The effect of particle shape and angularity on shear strength, dilation and liquefaction characteristics of granular media in two dimensions has already been investigated by several researchers and the findings are documented in literature (Sallam, 2004, Ashmawy et al., 2003). Not much progress has been made in evaluating the dilation angle of granular soils in three dimensions and influence of three-dimensional particle shape on liquefaction behavior of cohesionless soil. To simulate the real

micromechanical behavior of granular media, accurate characterization and modeling of particle shape in three dimensions are necessary. The current study presents a detailed description of particle shape modeling technique both in two and three dimensions using Discrete Element Method to evaluate the influence of particle shape on the shear strength behavior of granular assembly.

CHAPTER 3
MATERIALS

The previous chapter has offered a review of the conceptual developments in particle shape quantification and modeling techniques. The current chapter presents the properties of various granular materials collected from different geographical locations and those obtained from various sources in the literature.

3.1 Sand Samples Collected for the Present Study

A wide variety of natural and processed sand samples having different roundness and angularity are collected from various locations around the world in conjunction with the current study. The intent was to obtain materials from as wide a geographical coverage as possible so that they would be more likely to be different in mean grain size, size distribution, and morphology due to differences in the deposition process. The sand samples collected for the current study encompass natural sands from beaches, rivers, dunes and manufactured crushed sands. The two-dimensional projection images of the sand samples collected for the study are documented in Appendix A.

3.1.1 Sample Selection Procedure

A detailed description of different sand samples obtained from various sources in the literature and their engineering properties such as gradation (mean grain size, uniformity coefficient, coefficient of curvature), packing (minimum and maximum void ratio and dry density) are documented in the form of a spreadsheet. These parameters can be a useful source for selecting materials for the present study. Figure 3.1 through Figure 3.8 present the variation of minimum and maximum void ratio for different types of sand samples.

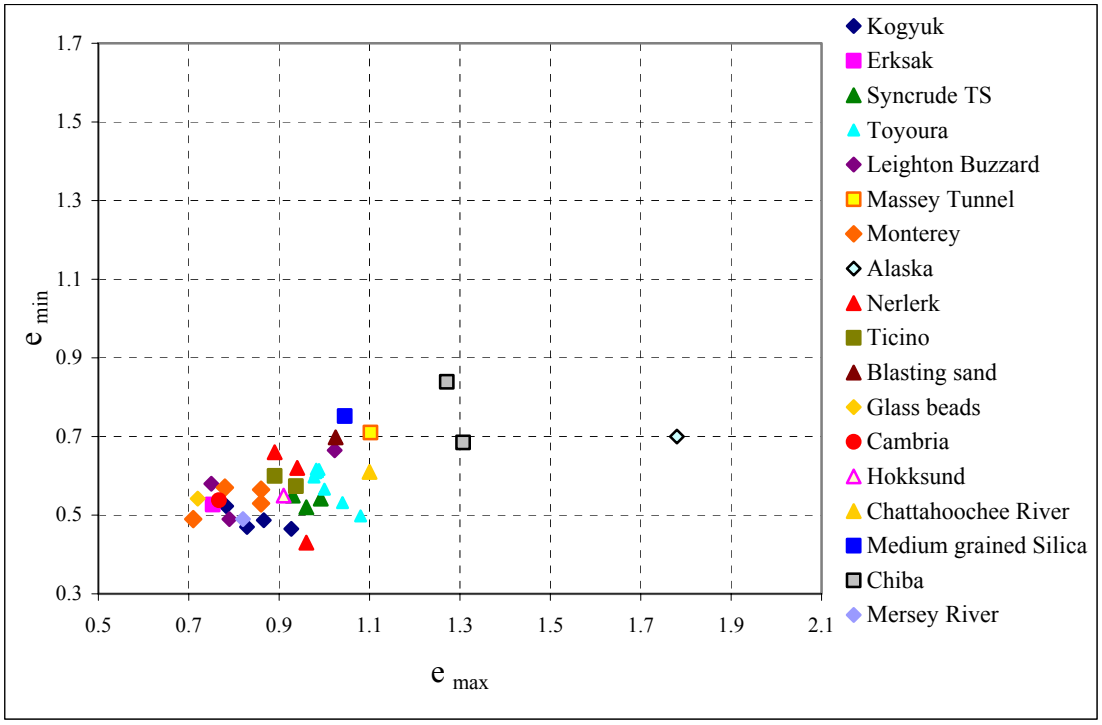

Figure 3.1 Variation of Minimum and Maximum Void Ratio (Group # 1)

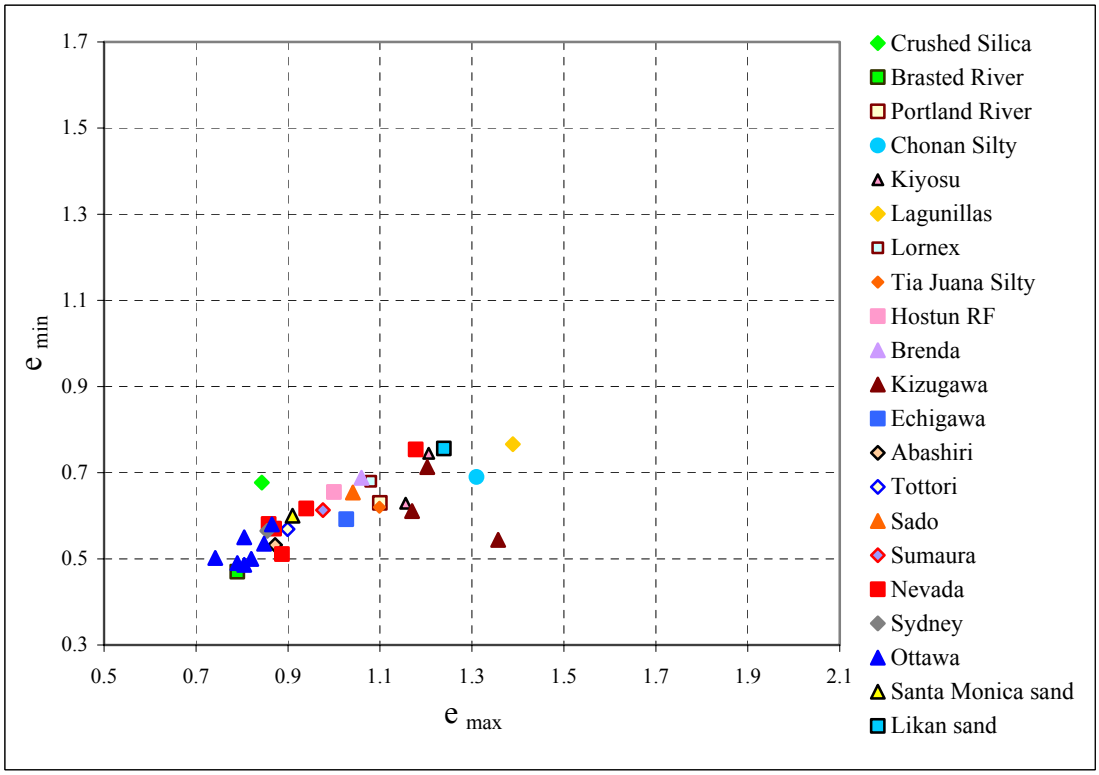

Figure 3.2 Variation of Minimum and Maximum Void Ratio (Group # 2)

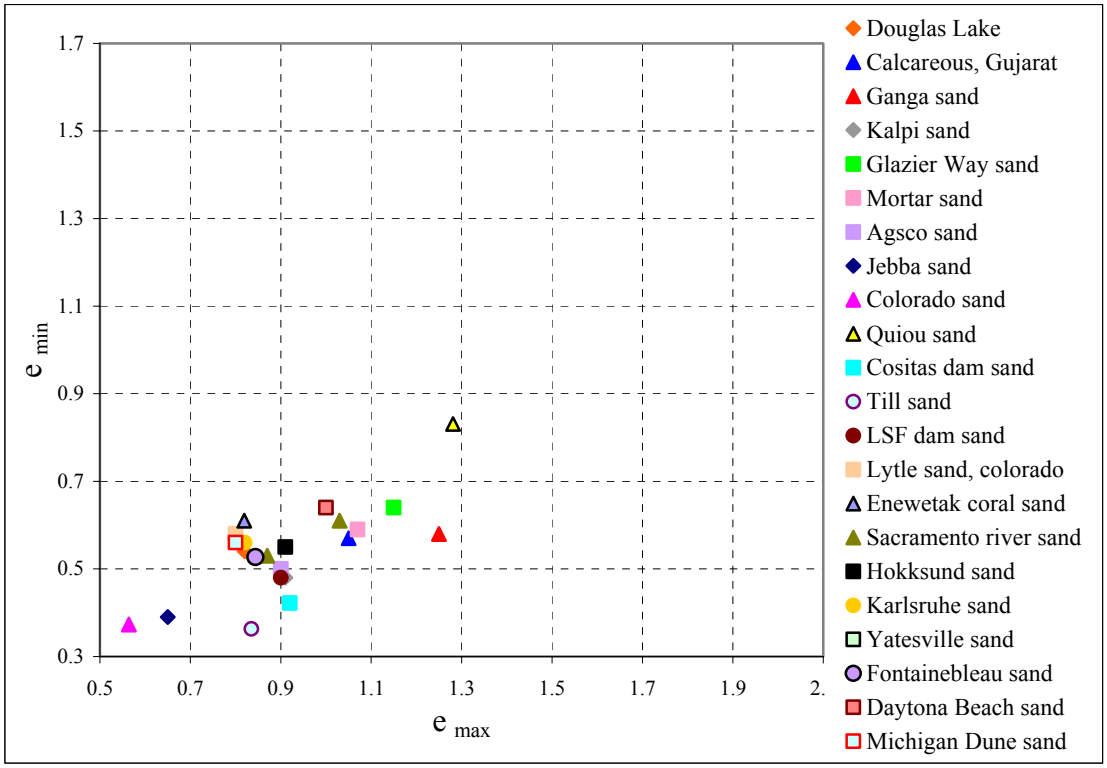

Figure 3.3 Variation of Minimum and Maximum Void Ratio (Group # 3)

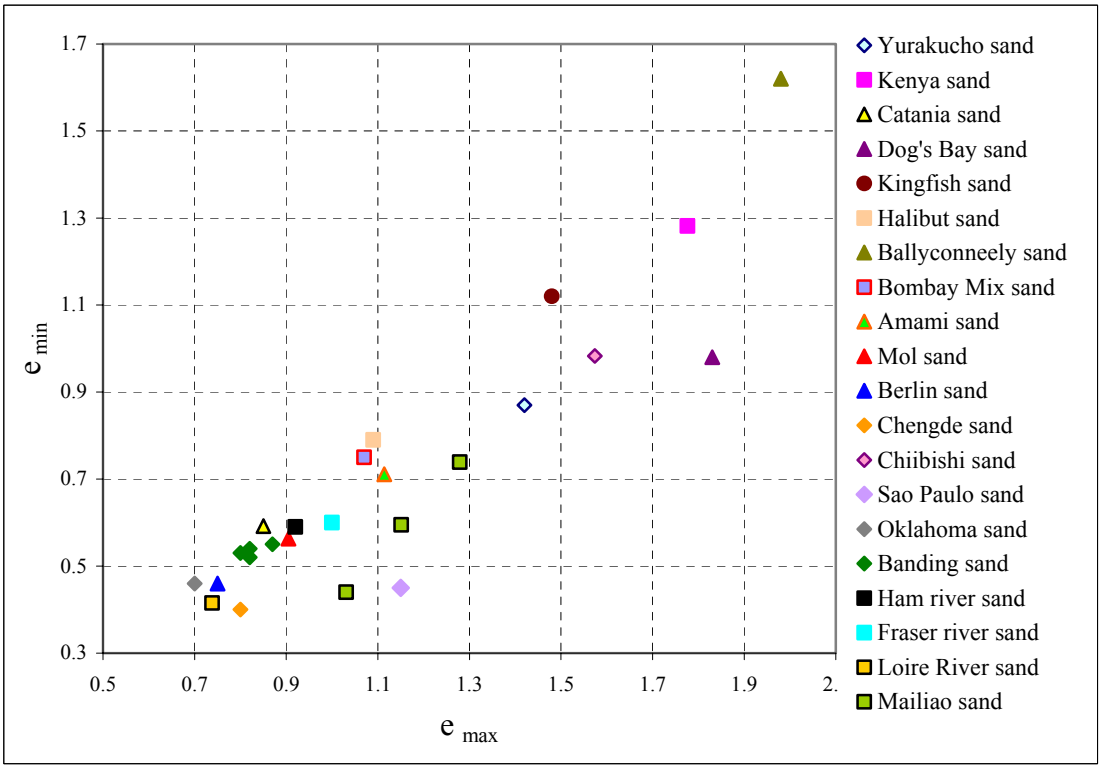

Figure 3.4 Variation of Minimum and Maximum Void Ratio (Group # 4)

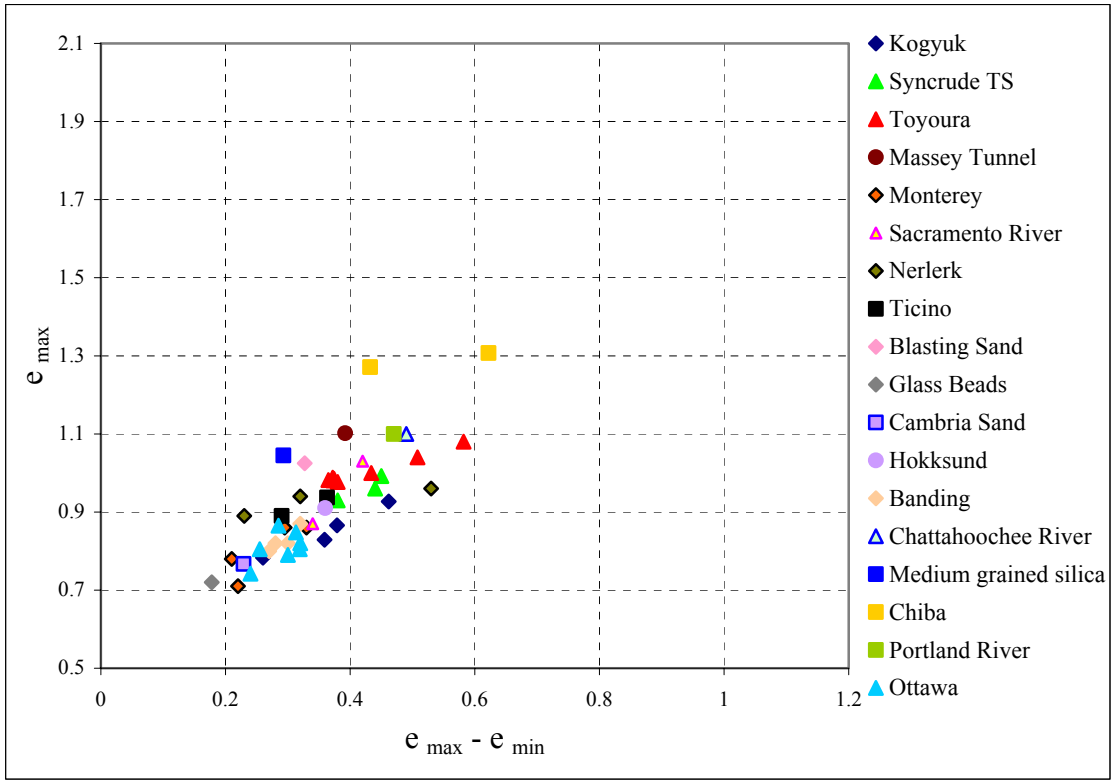

Figure 3.5 Variation of Maximum Void Ratio with e_{max} - e_{min} (Group # 1)

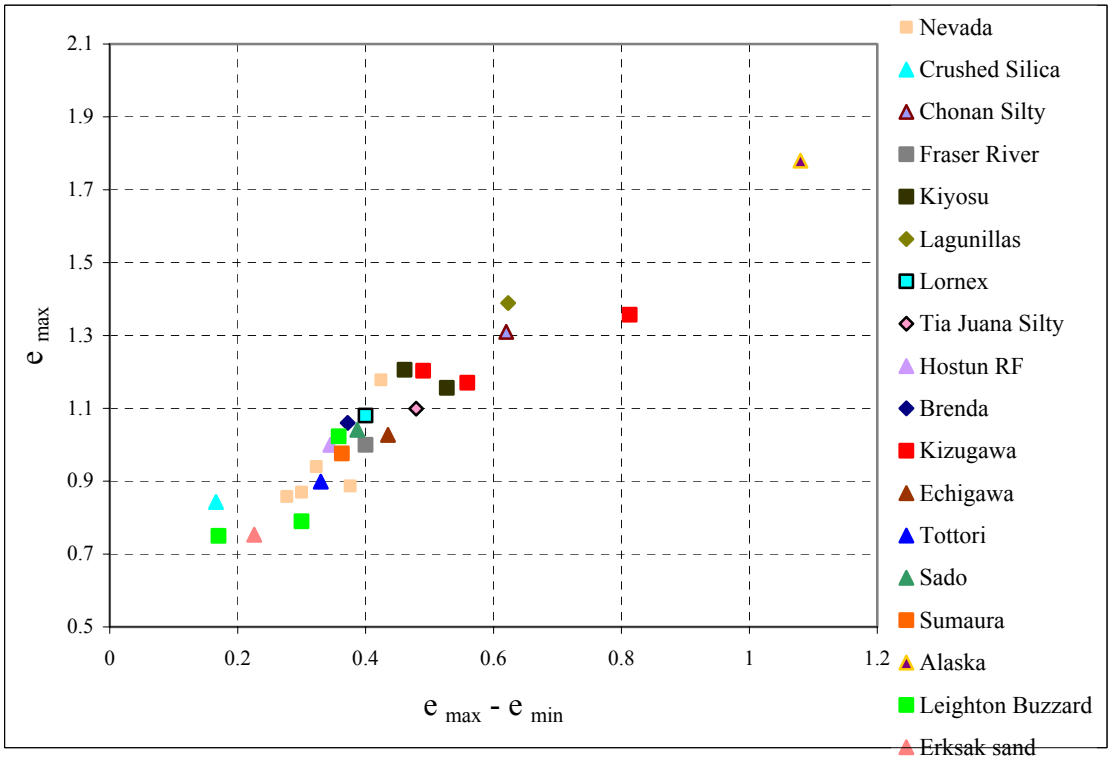

Figure 3.6 Variation of Maximum Void Ratio with e_{max} - e_{min} (Group # 2)

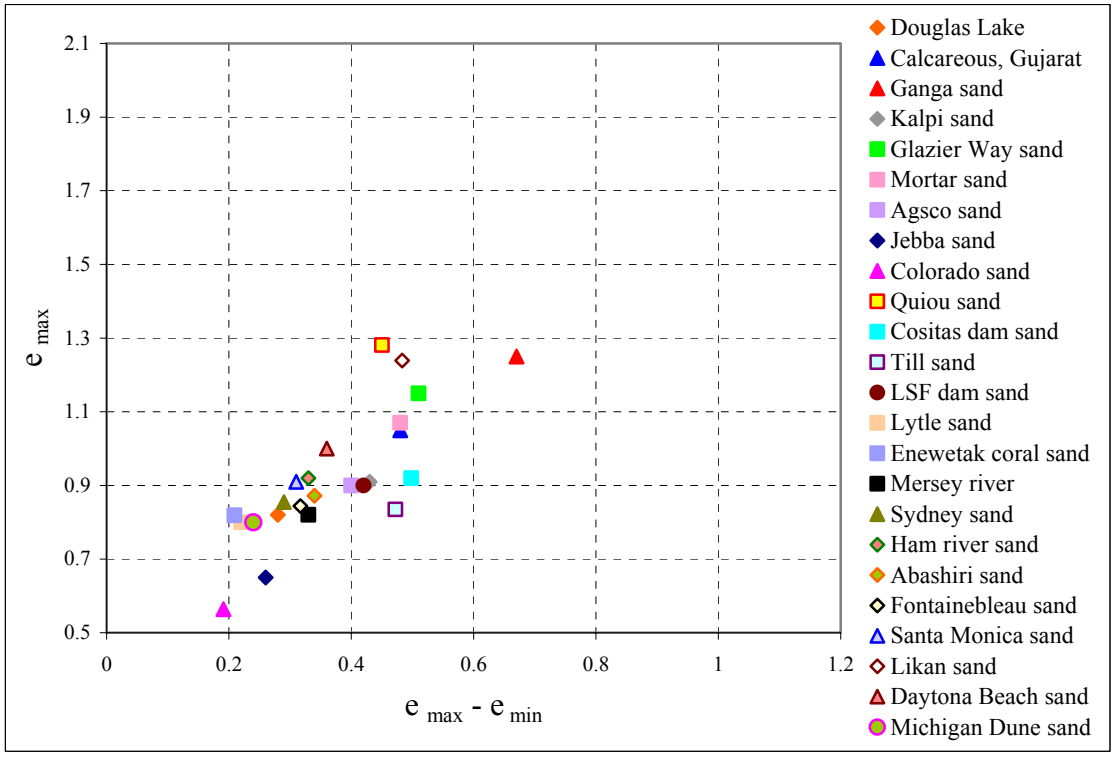

Figure 3.7 Variation of Maximum Void Ratio with e_{max} - e_{min} (Group # 3)

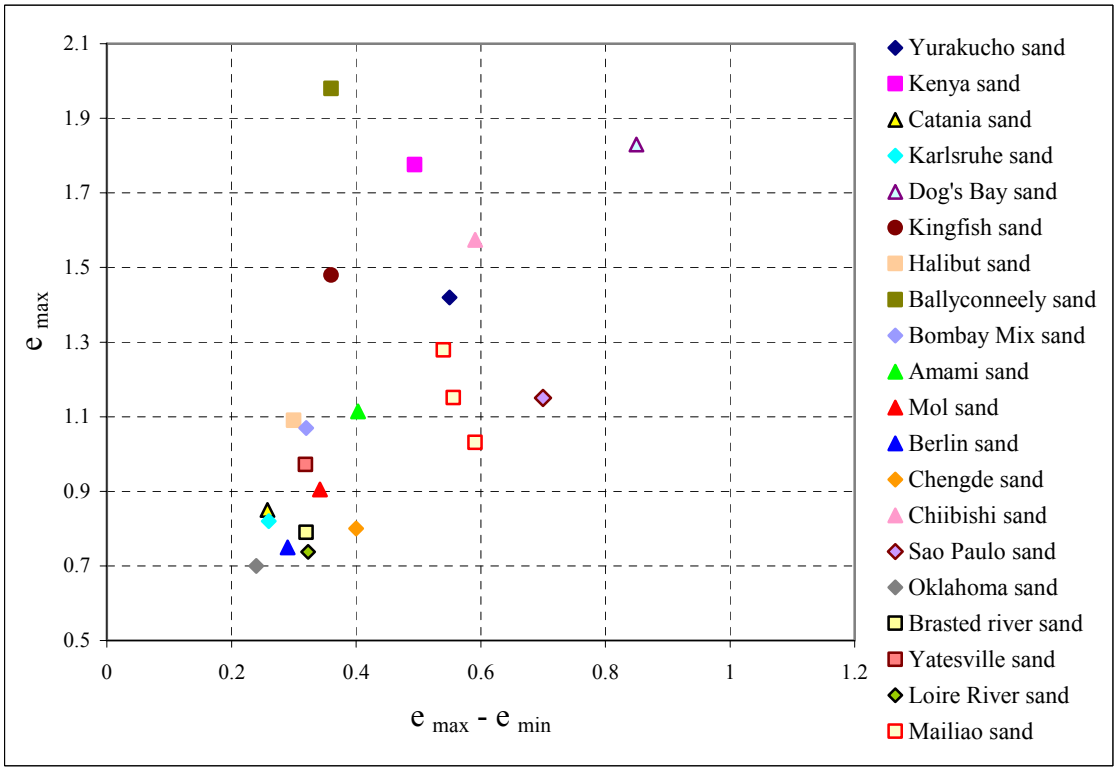

Figure 3.8 Variation of Maximum Void Ratio with e_{max} - e_{min} (Group # 4)

Granular packing is represented by the void ratio of the assembly and the shear strength behavior of soil is influenced by the packing density of the granular mass (Holtz and Kovacs, 1981). The maximum and minimum void ratios of a soil mass depend on the shape of the individual grain and grain size distribution. Research had been documented in the literature describing the relationship between void ratio and angle of internal friction of cohesionless soil and the studies suggested an increase of maximum (e_{max}) and minimum (e_{min}) void ratio and void ratio difference ($e_{max} - e_{min}$) with increasing particle angularity or decreasing roundness and sphericity (Youd, 1973; Cho et al., 2006; Fraser, 1935). Based on several experiments published in the literature, a decrease in void ratio results in an increase in angle of shearing resistance (ϕ) and therefore an increase in shear strength of granular soil mass (Zelasko et al., 1975; Shinohara et al., 2000). Materials can be selected based on the above figures. For example, Chiba, Alaska, medium grained Silica, Lagunillas, Kizugawa, crushed Silica, Quiou, Jebba, Colorado, Till, Ganga, Glazier Way, Dog's Bay, Kenya, Ballyconneely, Kingfish, Sao Paulo, Oklahoma, Erksak, Leighton Buzzard sands can be some of the interesting materials to study since their void ratios fall a way above or a way below on the plot. Though it was intended to acquire these materials for the purpose of the present study, it was difficult to obtain all these materials from different parts of the world. Instead, the materials collected for the current study are easily available, but still cover a wide range of geographic locations and have various degrees of angularity and roundness. Therefore, it is expected that they are likely to be different in grain size, shape, mineralogical composition and other engineering properties. The properties of sand samples collected for this study are presented next.

3.2 Data Sets and Sample Characteristics

Total 26 types of different sand samples are collected for the present study. Their locations and engineering properties are presented in table 3.1. Figure 3.9 through Figure 3.11 presents the particle size distribution for some of the materials collected. For some samples, sieve analysis is not performed because of insufficient amount of sample.

Instead, the particle size distributions for those materials are obtained through image analysis.

Table 3.1 Sand Samples Collected for the Study

Type of Sand	Gradation			Location
	D_{50}	D_{10}	C_u	
US-Silica, #1 Dry	0.270	0.130	2.462	Newport, NJ
US-Silica, Std. Melt	0.280	0.140	2.286	Newport, NJ
Daytona Beach	0.130	0.080	1.875	Daytona Beach, FL
Rhode Island	0.250	0.190	1.421	Rhode Island
Nice	0.200	0.073	3.014	Var River bed, Nice, France
Fontainebleau	0.200	0.110	1.909	Fontainebleau, France
Loire River	0.730	0.520	1.500	Loire River bed, Orléans, France
Hostun	0.580	0.410	1.659	Hostun, France
Toyoura Beach	0.200	0.170	1.235	Toyoura Town, Japan
Indian Rocks Beach	0.220	0.160	1.500	Clearwater, FL
Belle Air Beach	0.420	0.182	2.802	Clearwater, FL
Clearwater Beach	0.180	0.095	1.947	Clearwater, FL
Gulf Beach	0.220	0.170	1.353	Clearwater, FL

Table 3.1 (Continued)

Type of Sand	Gradation			Location
	D_{50}	D_{10}	C_u	
Madeira Beach	0.200	0.105	1.952	Clearwater, FL
Redington Shores	0.215	0.140	1.643	Clearwater, FL
Belmont Pier	0.245	0.170	1.559	Long Beach, CA
Boca Grande Beach	0.200	0.160	1.313	Cartagena, Columbia
Tecate River	0.950	0.760	1.316	Tecate, Mexico
Oxnard	0.800	0.525	1.600	Oxnard, CA
Arroyo Alamar	0.900	0.600	1.550	Alamar River, a tributary of Tijuana River in Tijuana
Rincon Beach	0.680	0.460	1.609	Beaches of Rincon, Puerto Rico
Panama Malibu Beach	0.250	0.180	1.472	Malibu Beach, Gorgona, Panama
Michigan Dune	0.345	0.260	1.385	Michigan
Ala Wai Surfers Beach	1.050	1.010	1.054	Ala Wai Surfers Beach, Oahu, Hawaii
Kahala Beach	0.700	0.500	1.520	Kahala Beach, Oahu, Hawaii
Red Sea Dune	0.900	0.600	1.550	Suez, Egypt

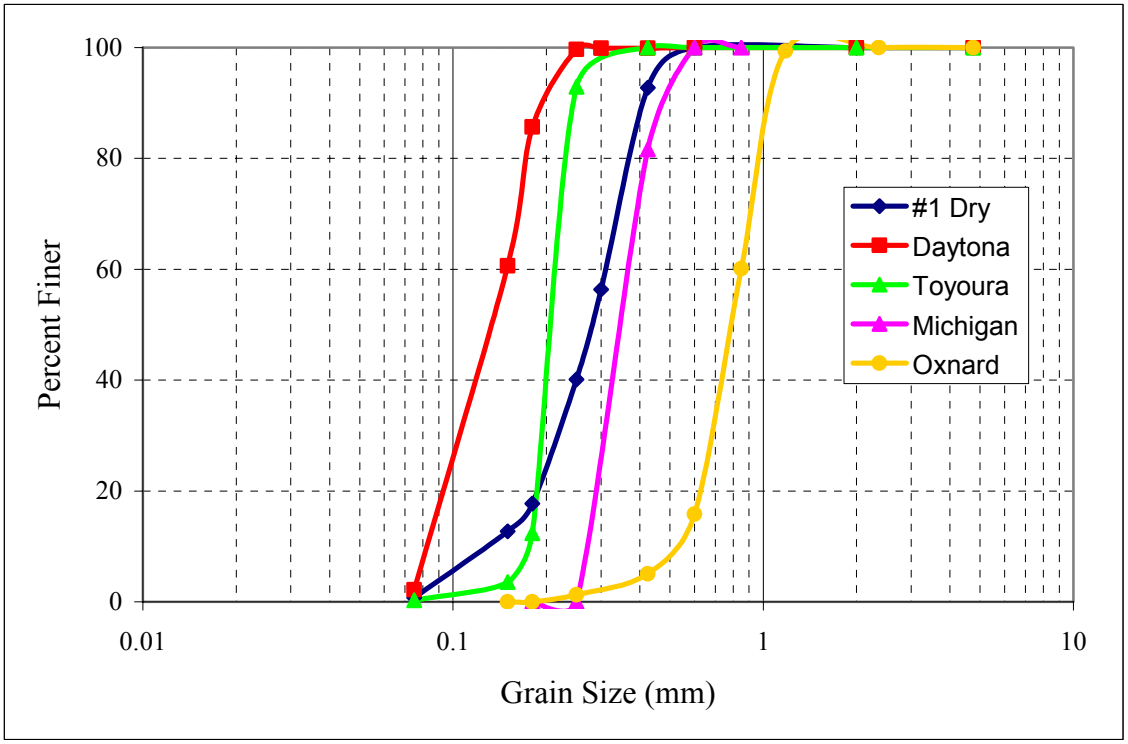

Figure 3.9 Particle Size Distributions (Sand Samples, Group # 1)

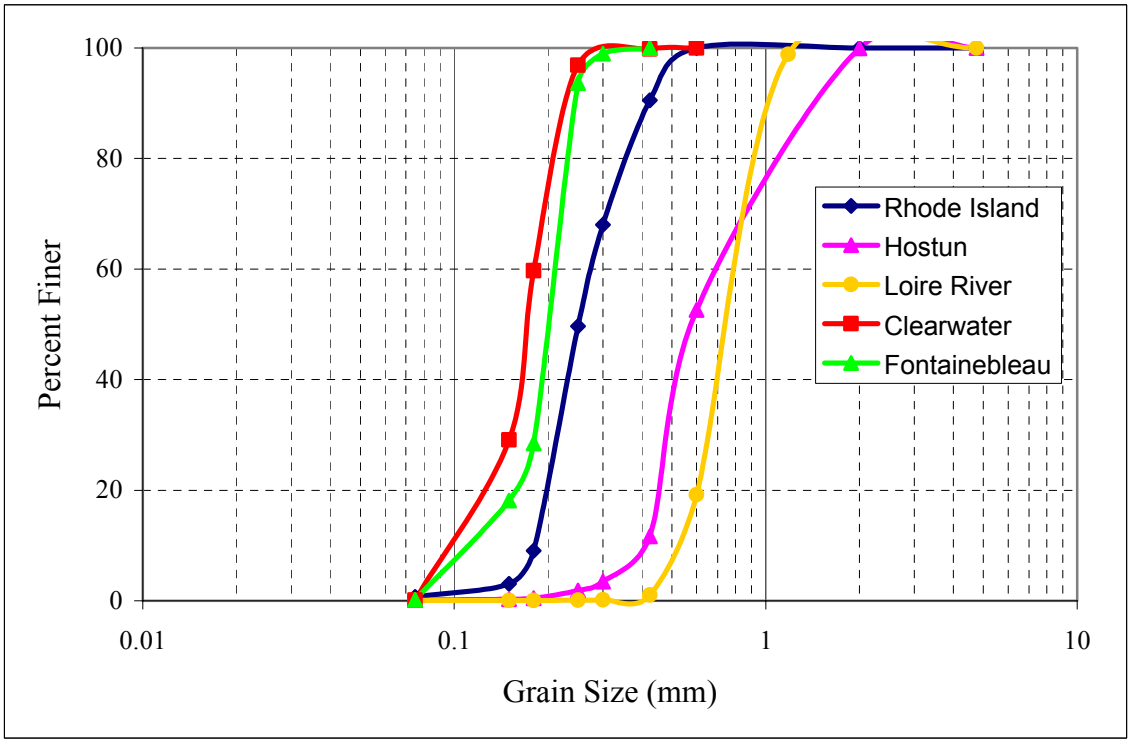

Figure 3.10 Particle Size Distributions (Sand Samples, Group # 2)

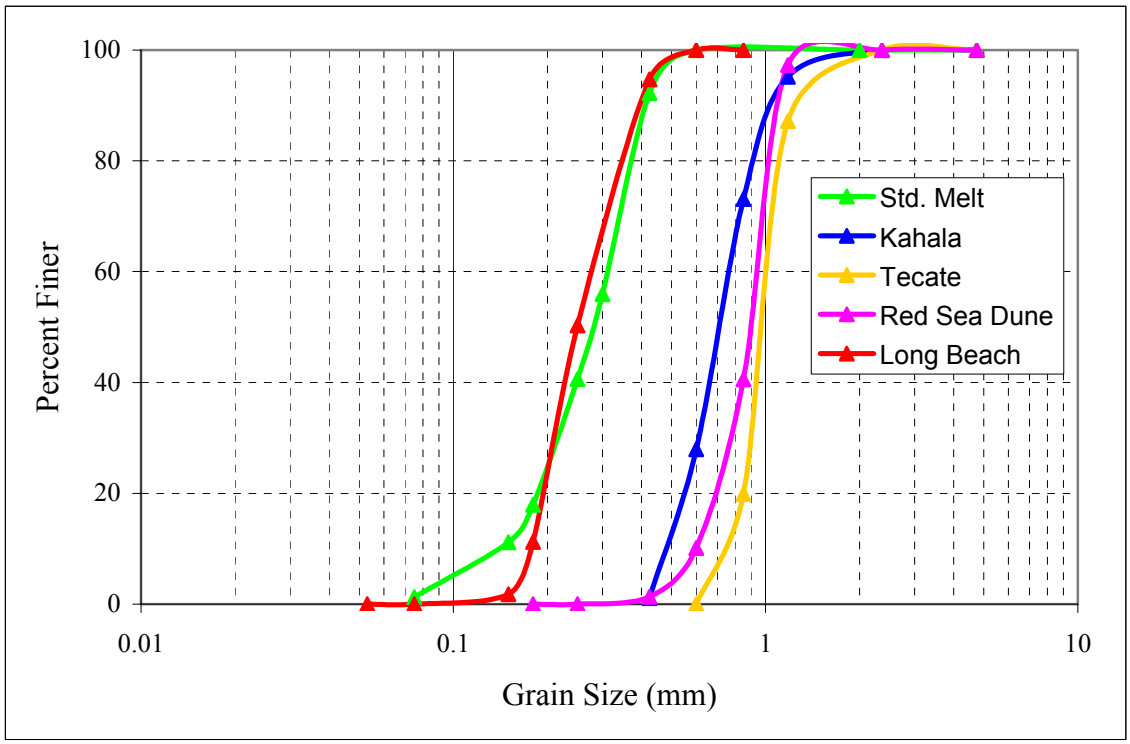

Figure 3.11 Particle Size Distributions (Sand Samples, Group # 3)

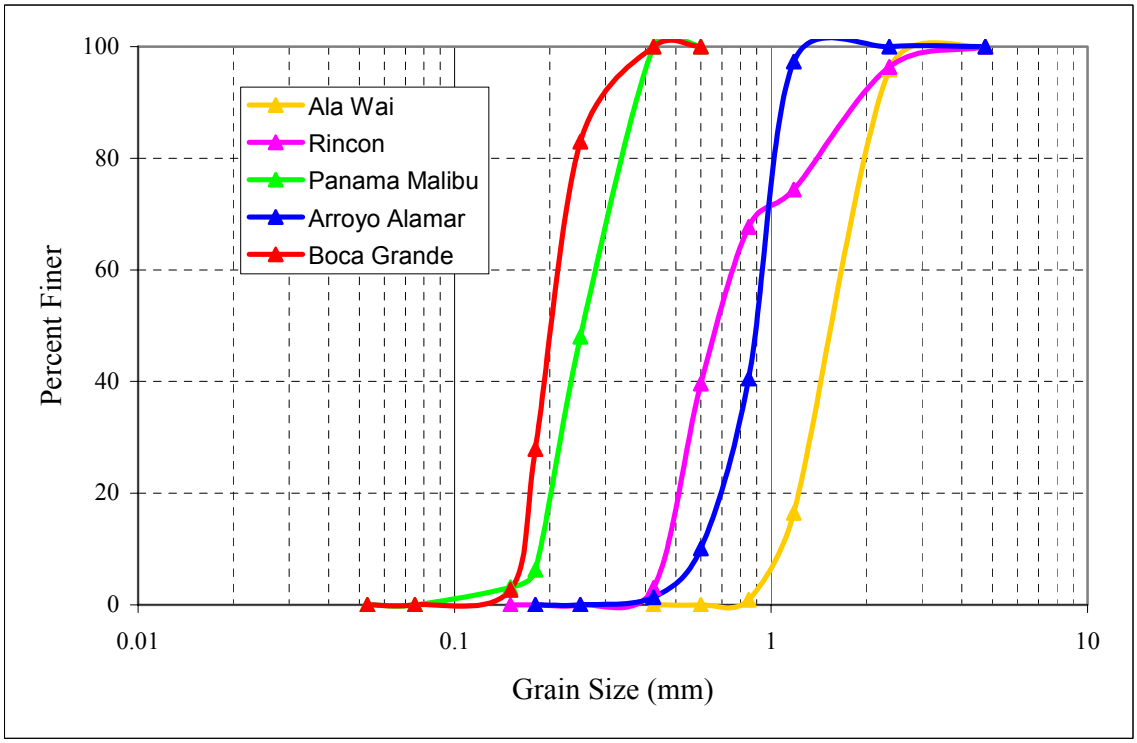

Figure 3.12 Particle Size Distributions (Sand Samples, Group # 4)

CHAPTER 4
PARTICLE SHAPE CHARACTERIZATION AND QUANTIFICATION

The previous chapter has discussed about the material selection procedure and engineering properties and locations of sand samples collected for the present study. The current chapter includes a detailed description of microscope system, image analysis software and X-ray CT as well as the particle shape characterization and quantification techniques in two and three dimensions.

4.1 Characterizing Particle Shape in Two Dimensions

An automated procedure is established to characterize particle shape in two dimensions using photo microscopy and an image processing software package from Media Cybernetics, Inc: Image-Pro Plus 5.1 and the add-ins Scope-Pro 5.0, Sharp Stack 5.0 and 3D Constructor 5.0. Different illumination systems and filtering techniques is also suggested (Rivas, 2005). A semi-automated routine is implemented within the software to capture a large number of images of sand particles at a time. The microscopes used in this study are Motic SMZ-168 Stereo Microscope with Magnification of 0.75X to 5X (Figure 4.1) and Motic AE31 Inverted Microscope with Magnification of 4X to 40X (Figure 4.2) manufactured by Motic Instruments, Inc. Various sand samples collected for the present study are analyzed using the optical microscopes and digital camera system. Two-dimensional images of particle outline are obtained by orthogonal projection. The captured images of the sand particles are processed through successive steps of erosion, dilation and contrast enhancement technique using the image-processing software and different shape parameters in terms of aspect ratio, roundness, diameter, perimeter etc. are obtained.

Figure 4.1 Motic SMZ-168 Stereo Zoom Microscope

Figure 4.2 Motic AE-31 Inverted Microscope

4.2 Characterizing Particle Shape in Three Dimensions

Characterizing the particle surface accurately in three dimensions is a challenging task. Serial Sectioning has been found to be a very accurate method for three-dimensional reconstruction of particle surface. In this destructive technique, the grains are embedded in epoxy-resin matrix and successive thin layers are removed using a polishing machine. The first slice of a particular thickness is removed and the remaining portion is observed in a microscope to acquire the image. The same process can be repeated to remove successive layers of same thickness and each time the images of the remaining portion of the grains are captured. Then all the stacks of images are combined to reconstruct three-dimensional shapes of the sand grains. Though reliable, the experimental procedure, especially the sample preparation is very time consuming and laborious. X-ray Computed Tomography is an alternative technique for three-dimensional reconstruction of particle shape where no prior sample preparation is necessary. X-ray CT is a completely nondestructive technique for visualizing internal structure of solid objects and obtaining digital information about their three-dimensional geometries and properties. The fundamental principle behind computed tomography is to acquire multiple views of an

object over a range of angular orientations. Computed Tomography is based on the x-ray principle: as x-rays pass through the object, they are absorbed or attenuated, creating a profile of x-ray beams of different strength. This x-ray profile is captured by a detector within the CT to generate an image.

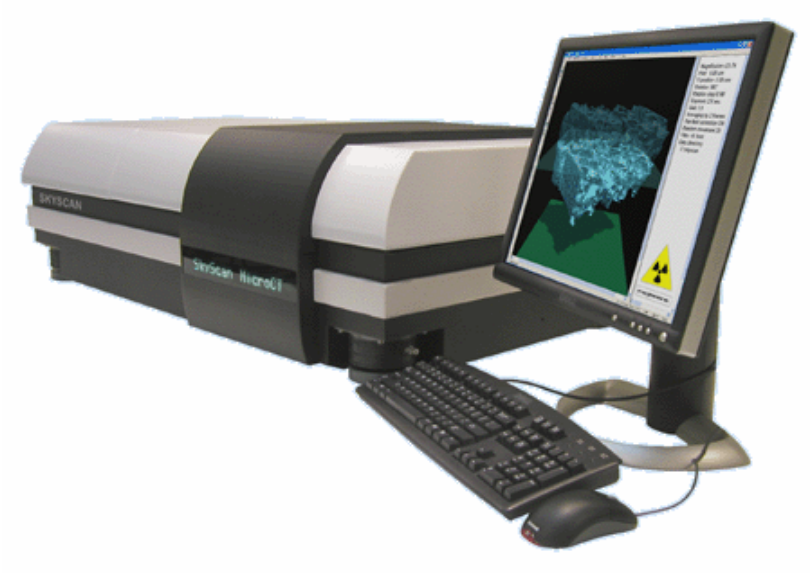

Figure 4.3 SkyScan 1072 X-Ray CT System
[www.rowan.edu/colleges/engineering/clinics/shreek/database.html]

In the present study the three-dimensional particle shape is characterized using X-ray CT since it allows visualizing and measuring a complete 3D object without any special sample preparation. The machine is located at the Rowan University, NJ (Figure 4.3). Two-dimensional grayscale image stacks are obtained from the online geomaterial database developed at the Rowan University. The grayscale image stacks are then processed through successive steps of erosion and dilation to obtain binary image stacks. Three-dimensional coordinates (x, y, z) of boundary and internal voxels are extracted from the two-dimensional image stacks using Matlab 7.2.

4.3 Quantification of Particle Shape

In various research studies the particle shapes are quantified using different shape descriptors. A detailed description of shape descriptors can be found in Chapter 2. In the current study, particle shape is quantified using Fourier shape descriptors in two dimensions.

4.3.1 Particle Shape Quantification in Two Dimensions

Fourier analysis is a mathematical approach to quantify grain shape in two-dimensions. In this research, two-dimensional signature descriptors of each shape are obtained by measuring the radial distance between the centroid and particle boundary at constant sampling interval, and Fourier transforms are used to obtain the spectral information of each shape. A starting point on the boundary is selected and periphery radii (R) are measured from the centroid to the boundary of the particle at a uniform sampling interval θ (Figure 4.4). This periodic function is then expanded in a Fourier series to obtain a set of harmonic amplitudes, each at a different frequency. The first harmonic indicates the deviation from the center of gravity. It can be represented as circularity. The second, third and fourth and fifth harmonics add a component of elongation, triangularity, sqaureness and pentagonality respectively. The *n*th harmonic contributes a sinusoidal wave of frequency *n* to the R_0 (Diepenbroek, et al., 1992). These shape descriptors can be a measure of angularity or roundness of grains.

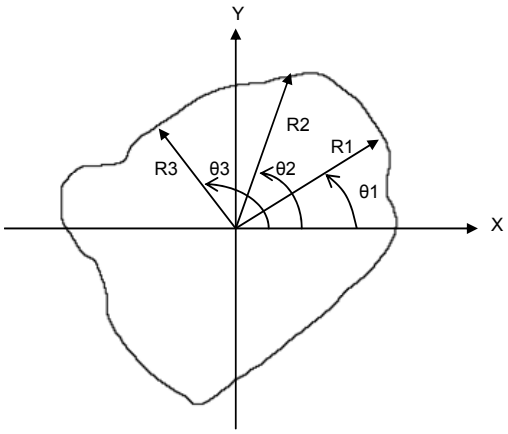

Figure 4.4 Fourier Transform on Particle Boundary

The equation of the profile is:

$$R(\theta) = R_0 + \sum_{n=1}^{N} [A_n \cos(n\theta) + B_n \sin(n\theta)] \tag{4.1}$$

Where, $R_0 = \frac{1}{2\pi} \int_0^{2\pi} R(\theta) d\theta$ (4.2-a)

$$A_n = \frac{1}{\pi} \int_0^{2\pi} R(\theta) \cos(n\theta) d\theta \tag{4.2-b}$$

$$B_n = \frac{1}{\pi} \int_0^{2\pi} R(\theta) \sin(n\theta) d\theta \tag{4.2-c}$$

$N =$ total number of discrete samples taken = 256; $\theta =$ total sampling angle = 2π ;

$\Delta\theta =$ sampling interval = $\frac{\theta}{N} = \frac{2\pi}{256} = 0.02454$ radian = 1.40625 degree;

$f_s =$ sampling frequency = $\frac{1}{\Delta\theta} = \frac{N}{\theta} = 40.74367$ cycles/radian;

$\Delta f =$ frequency increment = $\frac{1}{\theta} = \frac{1}{2\pi} = 0.15916$ cycles/radian = fundamental frequency of the Fourier series.

In this study, total 256 data points are taken along the periphery of the grain at a sampling interval of 1.40625 degree and the first 128 shape descriptors (in terms of amplitude) are used to quantify the shape. Figure 4.5 and Figure 4.6 show the mean amplitude spectra for Tecate River sand and Daytona Beach sand respectively for the first 24 harmonics. FFT is performed on each grain of six different sand samples to quantify the grain shapes in terms of Fourier shape descriptors. These shape descriptors are used as parameters to determine the sample size of different sand samples and to explore the relationship between grain size and grain shape.

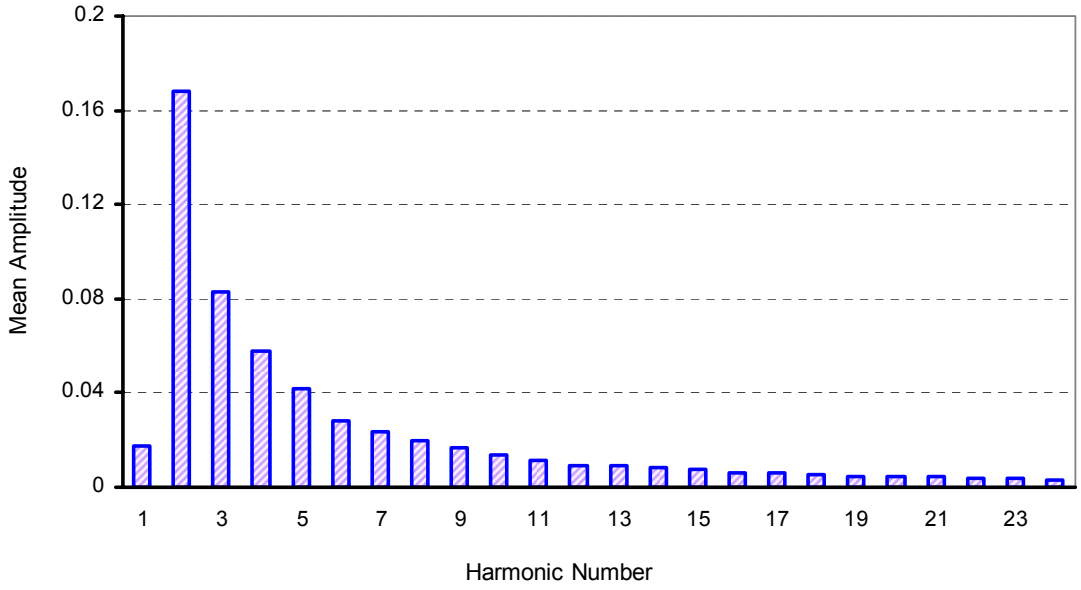

Figure 4.5 Mean Amplitude Spectra for Tecate River Sand

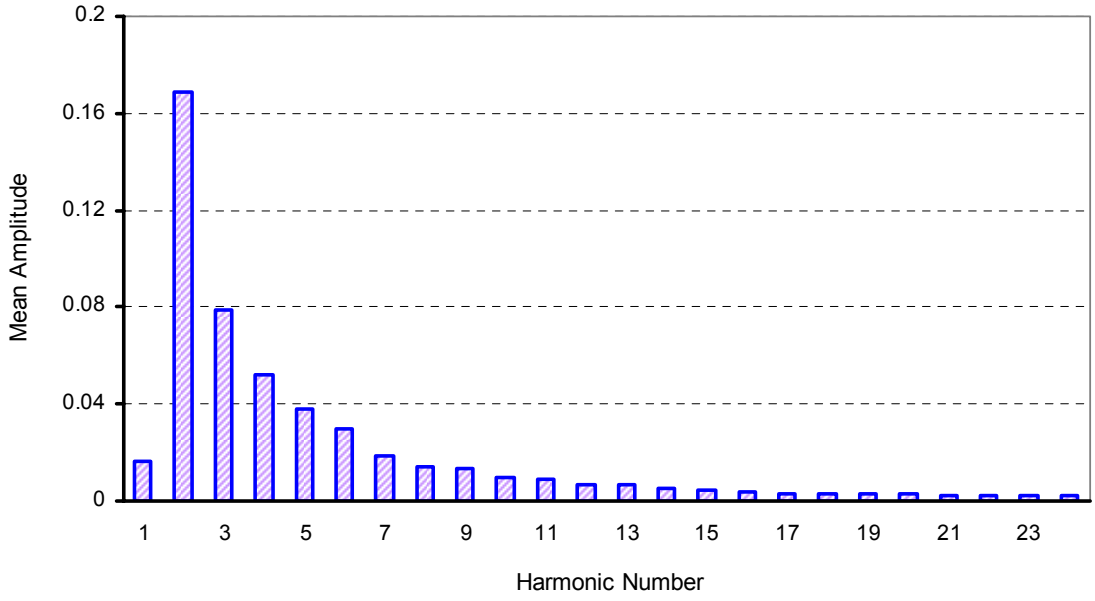

Figure 4.6 Mean Amplitude Spectra for Daytona Beach Sand

Meloy (1977) found a straight line relationship between log (descriptor number) and log (amplitude) above order 8. These higher order descriptors give an idea about the surface texture along the periphery of the grain. Surface texture is a measure of roughness of the particle. Figure 4.7 follows the same pattern as obtained by Bowman et al. (2001) where the surface roughness was quantified by slope and intercept. As explained by the authors, a higher intercept indicates a greater degree of roughness and a steeper gradient suggests a greater decay of roughness toward the finer scale. Therefore, this plot can be used to measure the surface roughness of sands. In Figure 4.7, the gradients are almost identical for all the sands but the Tecate River sand shows the highest intercept and Michigan Dune sand shows the lowest intercept. Therefore, Tecate River sand should possess highest surface roughness and Michigan Dune sand should have lowest surface roughness.

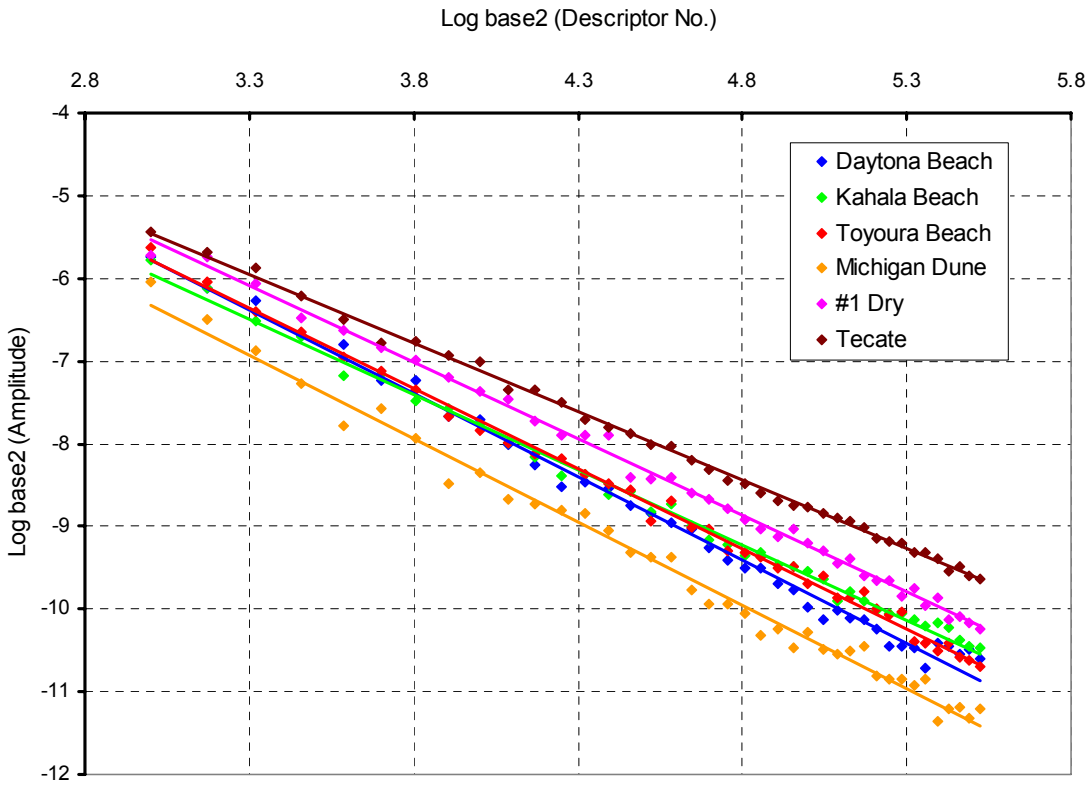

Figure 4.7 Variation of Harmonic Amplitude with Descriptor Number for Different Sand Samples

CHAPTER 5
RELATIONSHIP BETWEEN GRAIN SIZE AND SHAPE

The previous chapter has described particle shape characterization and quantification techniques in two and three-dimensions. The current chapter explores the relationship between grain size and shape of different natural and processed sand samples. It also offers a methodology to determine the sample size that will be the representative of the population for each type of sand sample collected for the study.

5.1 Introduction

In order to generate and reconstruct particle assemblies of highly irregular geometric shapes of a particular sand sample, the relationship between grain size and shape needs to be evaluated. For example, size-shape relationships are necessary to generate representative assemblies of angular particles for discrete element modeling simulations. The present study develops a methodology to determine an optimum sample size for a given sand sample. Determination of sample size is important to verify any existing relationship between grain size and shape since size-shape relationship depends on the number of particles used in the analysis. Moreover, design of an optimum sample size can save significant amount of resources.

5.2 Methodology to Determine Sample Size

The present study focuses on determining sample size (optimum number of particles within a particular sand sample) for different natural and processed sand samples using different shape descriptors such aspect ratio, elongation, triangularity and squareness. Aspect ratio is found to have greater influence on sample size determination than Fourier

shape descriptors. The minimum number of particles needed to be to be analyzed for a particular sand sample depends on the variability of particle size and shape within that sand sample. Statistical analysis is performed to find out the sample size for sand samples from different locations based on relevant shape parameters like aspect ratio, roundness, elongation, triangularity and squareness. Sample size depends on the following factors:

Confidence Level is the estimated probability that a population estimate lies within a given margin of error.

Margin of error (E) measures the precision with which an estimate from a single sample approximates the population value. The margin of error is same as the *confidence interval* which is a range of values. For example, if $\bar{x}$ is the sample mean, $\bar{x} \pm$ confidence will be the range of population mean. The margin of error is the maximum difference between the sample mean $\bar{x}$ and the population mean μ.

$$\bar{x} - E \le \mu \le \bar{x} + E$$

The value of *population standard deviation*.

The formula for calculating the sample size for a simple random sample is:

$$n = \left[\frac{z_{\alpha/2}\sigma}{E} \right]^2 \tag{5.1}$$

Where, $z_{\alpha/2}$ is the standard normal variate; α is the risk of rejecting a true hypothesis and it is called the significance level. For α=0.05, confidence level is 95%. ($z_{\alpha/2}$ = 1.645 for 90% confidence level, 1.96 for 95% confidence level, and 2.575 for 99% confidence level). σ is the population standard deviation; n is the sample size. The sample standard deviation, $s = \frac{\sum (x_i - \bar{x})^2}{n-1}$. s is the consistent estimator of the population standard deviation, so σ can be replaced by s in equation (5.1).

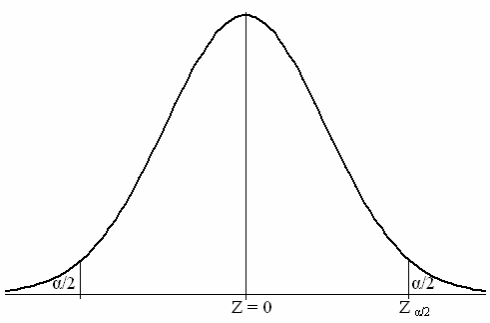

Figure 5.1 Standard Normal Distribution

Table 5.1 presents the values of the variances of different shape descriptors for the sand samples. In the present study, sample size is calculated based on aspect ratio of the particle shape, because (1) more variation is observed in aspect ratio compared to other shape parameters for each sand sample; (2) the gross shape of the particles can be defined by elongation and in various research studies, the two-dimensional particle shapes were approximated by ellipse. Elongation is closely related to aspect ratio of a given shape. The higher the aspect ratio, the more elongated is the shape of the particle; (3) the magnitude of error in terms of aspect ratio is stabilized at a magnitude of 0.04 or below for all the sand samples tested whereas no specific error threshold can be established for elongation, triangularity and squareness since the magnitude of error for each of these parameters varies from one sand sample to the next.

The magnitude of error is plotted against sample size for Toyoura sand in Figure 5.2 and Figure 5.3 presents the variation in change of error per unit sample with sample sizes for the same sand. It can be found from Figure 5.2, that the variation in errors is marginal at a magnitude of 0.04 and beyond and the same trend was observed for all other sand samples. Corresponding to the error magnitude of 0.04, the sample size is 90.

The threshold for change of error per unit sample is chosen as ±0.001or less (Figure 5.3) and the corresponding sample size is 70 and after that the change of error per unit sample is negligible and gradually approaching to zero.

Error as percent of mean (e_p) is also considered as a criterion for the determination of sample size (Figure 5.4) and a value of 5% is selected as a reasonable threshold for this experimental design and based on the value of e_p, a sample size of 50 is

obtained. The maximum of these three values is selected as the required sample size for the particular sand sample. Therefore, a sample size of 90 was chosen for Toyoura sand. Table 5.2 provides the sample sizes estimated for different sand samples used in the analysis.

Table 5.1 Values of Variances of Different Shape Parameters

Type of Sand	Aspect Ratio	Elongation	Triangularity	Squareness
Daytona Beach	0.077	0.006	0.002	0.0008
Toyoura Beach	0.045	0.006	0.003	0.0006
Tecate River	0.088	0.007	0.002	0.0009
Michigan Dune	0.054	0.006	0.001	0.0006
US-Silica #1 Dry	0.101	0.008	0.002	0.0008
Kahala Beach	0.112	0.010	0.001	0.001

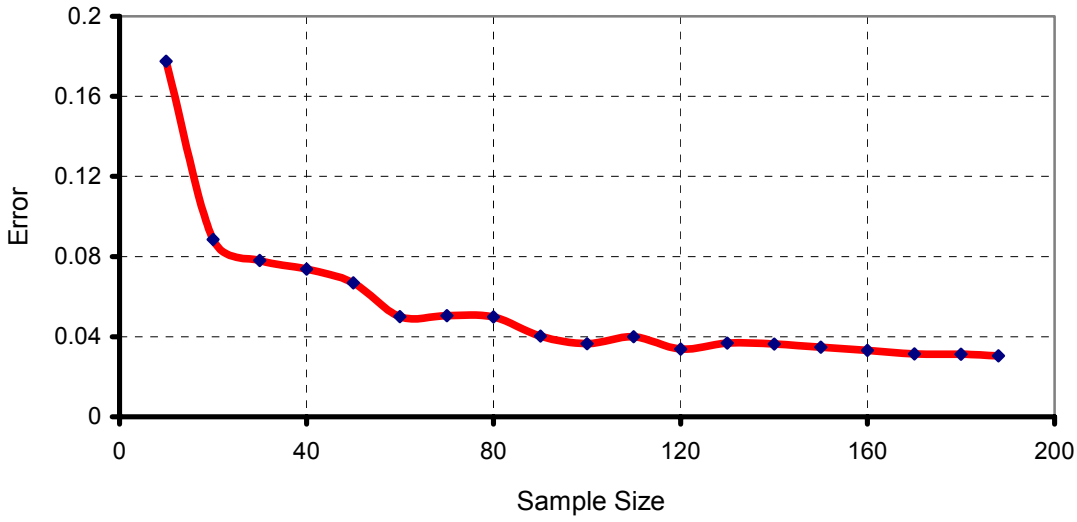

Figure 5.2 Variation of Error with Sample Size for Toyoura Sand

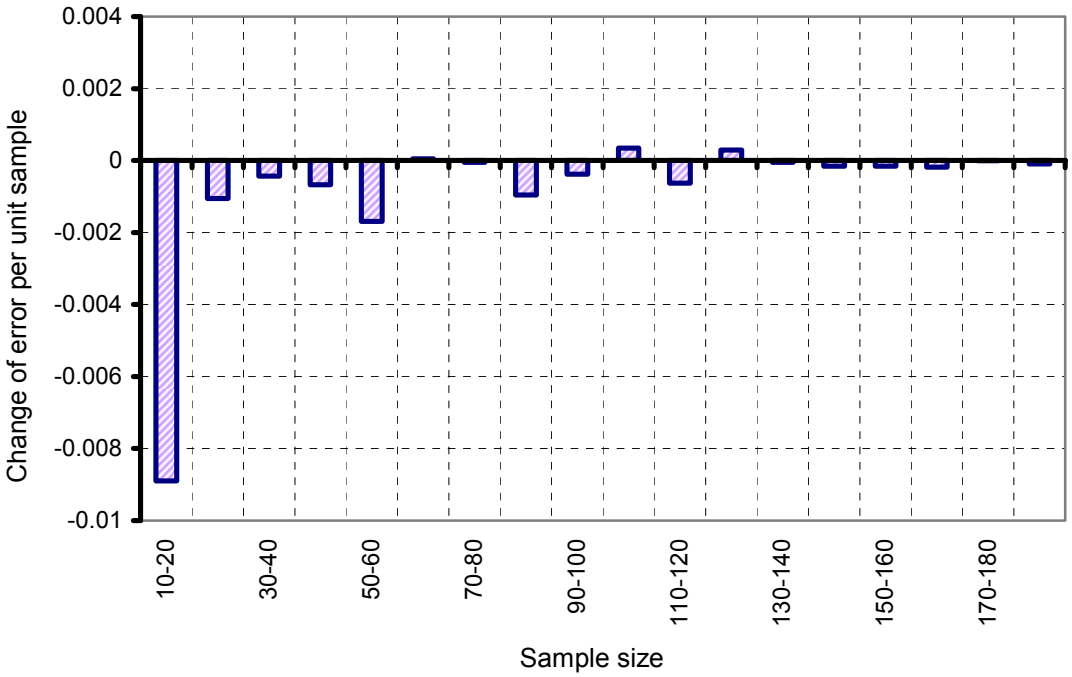

Figure 5.3 Variation of Change of Error Per Unit Sample with Sample Size

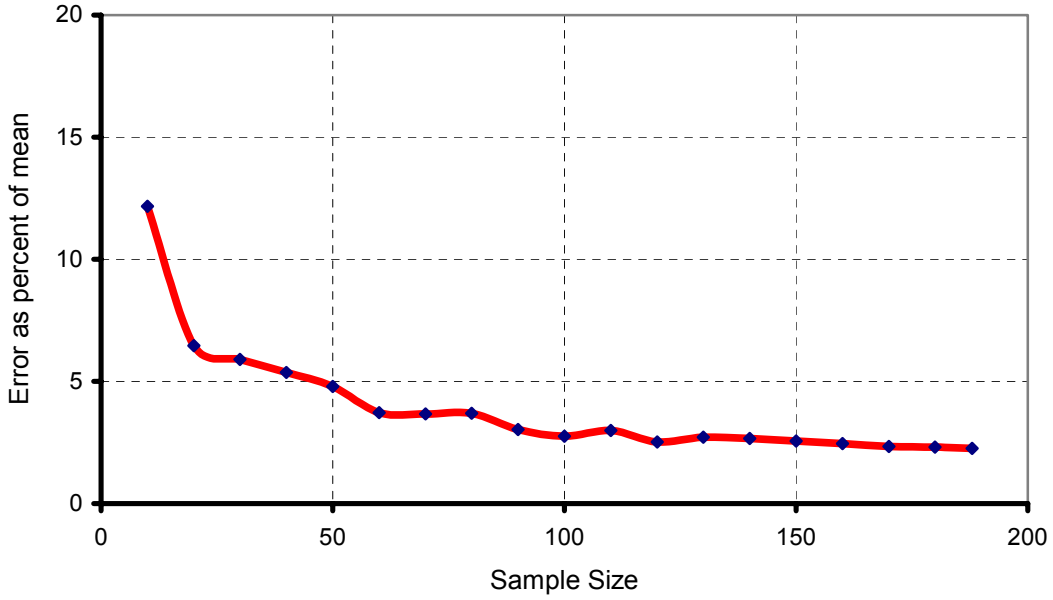

Figure 5.4 Variation of Error as Percent of Mean with Sample Size

Table 5.2 Estimated Sample Size for Sand Samples Used in the Study

Material	Sample Size
Hostun Sand	110
US-Silica Std. Melt	200
Boca Grande Beach Sand	230
US-Silica #1 Dry	150
Daytona Beach Sand	130
Loire River Sand	130
Toyoura Beach Sand	90
Oxnard Beach Sand	120
Kahala Beach Sand	170
Ala Wai Beach Sand	200
Michigan Dune Sand	100
Rincon Beach Sand	110
Arroyo Alamar River Sand	140
Rhode Island Sand	150
Tecate River Sand	150
Clearwater Beach Sand	150
Red Sea Dune Sand	90
Fontainebleau Sand	110
Long Beach Sand	130
Panama Malibu Beach Sand	70

5.3 Relationship Between Grain Size and Grain Shape

The relationship between particle size and shape for a given sand plays an important role in generating and reconstructing particle assemblies for micromechanical modeling. However, limited and conflicting knowledge is available in the literature describing the relationship between particle size and particle shape. The present study focuses on verifying any existing relationship between grain size and grain shape using different natural and processed sand samples. The findings can provide important information in understanding the nature of variation – or lack thereof – of shape parameters such as elongation, triangularity, squareness with grain size.

5.3.1 Data Sets

Total 6 sand samples are used to find out the size-shape relationship and they encompass natural sands from beaches (Daytona, Toyoura, Kahala), rivers (Tecate), dunes (Michigan) and a manufactured crushed sand (#1 Dry). Figure 5.5 shows the two-dimensional projection images of the sand samples and Table 5.3 summarizes the relevant engineering properties and locations of various materials.

Table 5.3 Relevant Properties of Granular Materials

Material	No. of particles	D_{50} (mm)	C_u	Location
Daytona Beach	100	0.13	1.87	Florida
Toyoura Beach	90	0.20	1.24	Japan
Tecate River	130	0.95	1.32	Mexico
Michigan Dune	100	0.33	1.5	Michigan
US Silica #1 Dry	150	0.27	2.46	New Jersey
Kahala Beach	170	0.70	1.52	Hawaii

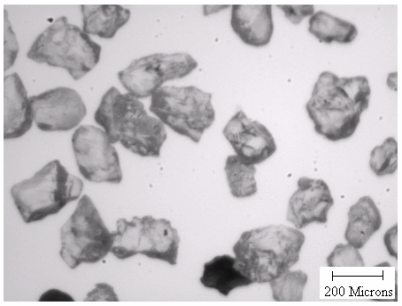

Daytona Beach Sand

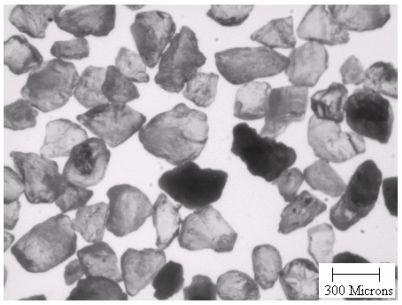

Toyoura Sand

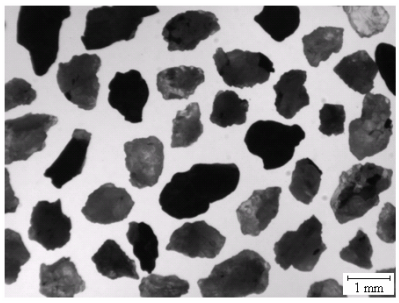

Tecate River Sand

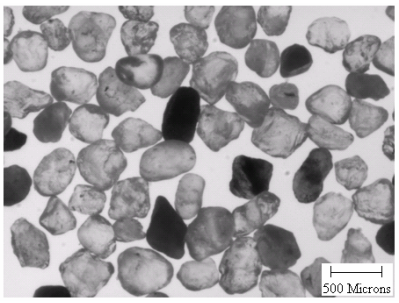

Michigan Dune Sand

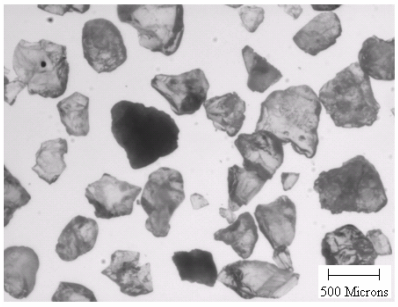

US-Silica #1 Dry

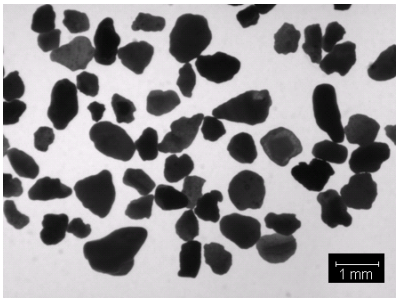

Kahala Beach

Figure 5.5 Two-Dimensional Images of Sand Samples

5.3.2 Fourier Shape Descriptors

Fourier transform is performed to characterize grain shape in two dimensions by fitting a *Fourier* series to the unrolled particle outline. In the present study, grain shapes are quantified by (R, θ) Fourier method in closed form (Ehrlich & Weinberg, 1970). Table 5.4 presents the average values of the first four shape descriptors for different sand samples and Figure 5.6 and Figure 5.7 show the mean amplitude spectra for Toyoura Beach sand and Michigan Dune sand respectively for the first 24 harmonics.

Table 5.4 Average Values of Fourier Descriptors for Different Sand Samples

Type of Sand	Harmonic1 (Circularity)	Harmonic2 (Elongation)	Harmonic3 (Triangularity)	Harmonic4 (Squareness)
Daytona Beach	0.016378	0.168487	0.078809	0.052109
Toyoura Beach	0.016165	0.139724	0.100307	0.0518
Tecate River	0.017707	0.168221	0.082782	0.057527
Michigan Dune	0.010951	0.140109	0.063223	0.04587
US-Silica #1 Dry	0.017826	0.167989	0.088005	0.054268
Kahala Beach	0.015493	0.167344	0.080716	0.048941

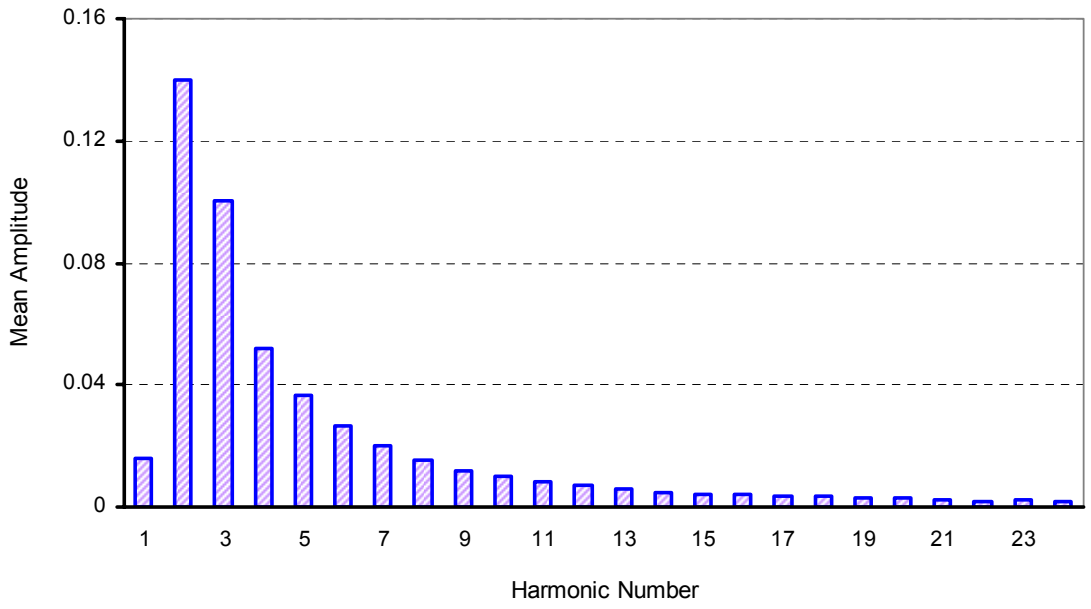

Figure 5.6 Fourier Amplitude Spectra for Toyoura Sand

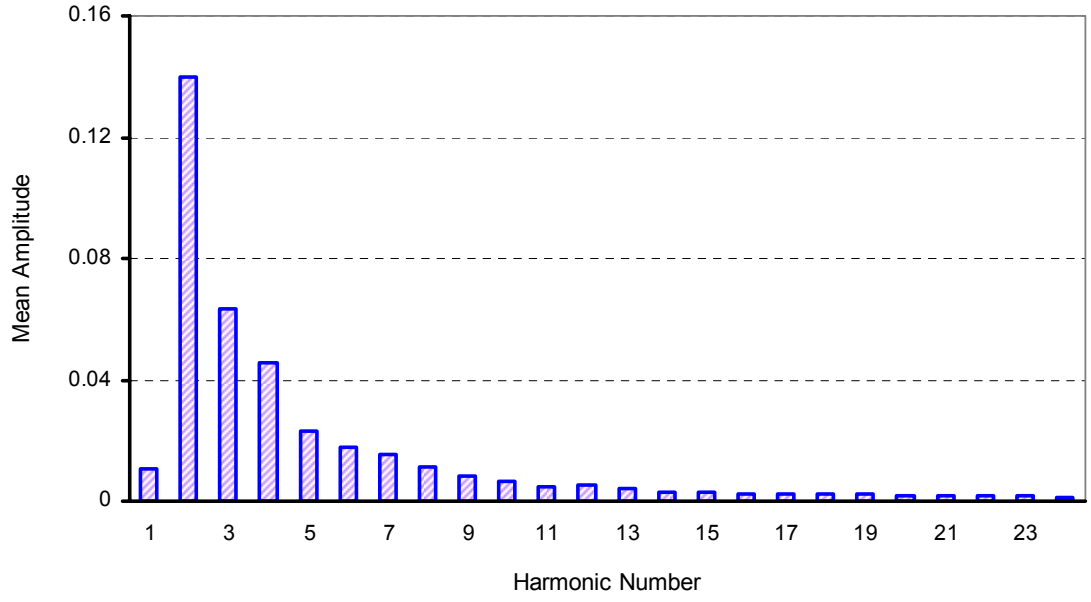

Figure 5.7 Fourier Amplitude Spectra for Michigan Dune Sand

5.3.3 Grain Size – Grain Shape Relationship

The study aims to explore the relationship between grain size (mean diameter) and grain shape (shape descriptors) for a given sand sample. Figure 5.8 presents the frequency distribution of the shape parameters such as diameter, elongation, triangularity and squareness respectively. The distributions are very close to standard normal distribution. Figure 5.9 through Figure 5.12 shows the variation of shape descriptors with grain size for Tecate River sand and Table 5.5 summarizes the R-square values obtained from regression analysis.

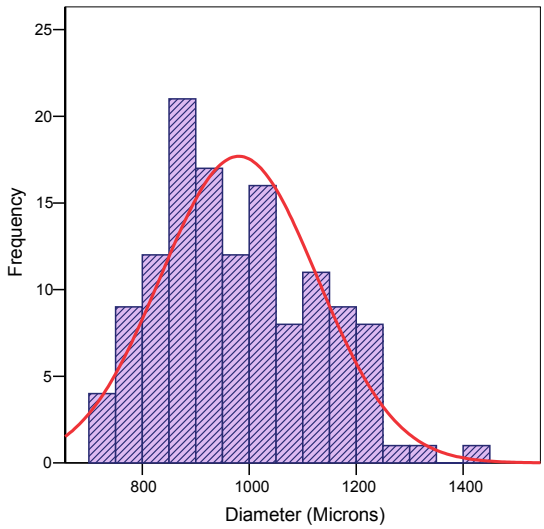

(A) Mean = 980.34, Std. Dev. = 146.57

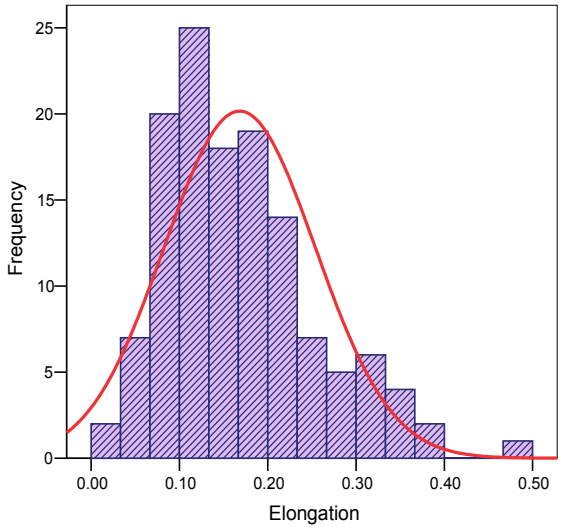

(B) Mean = 0.168, Std. Dev. = 0.086

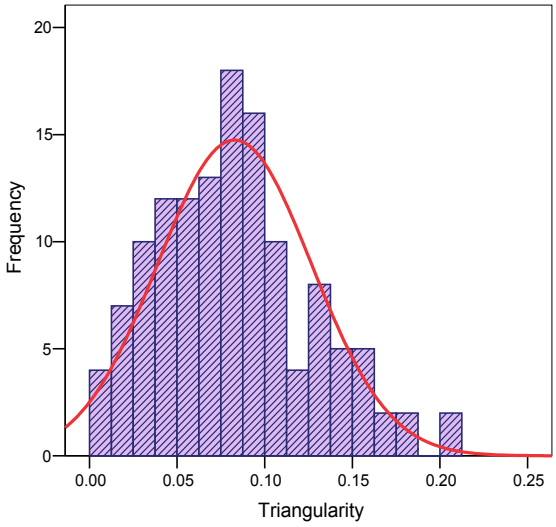

(C) Mean = 0.083, Std. Dev. = 0.044

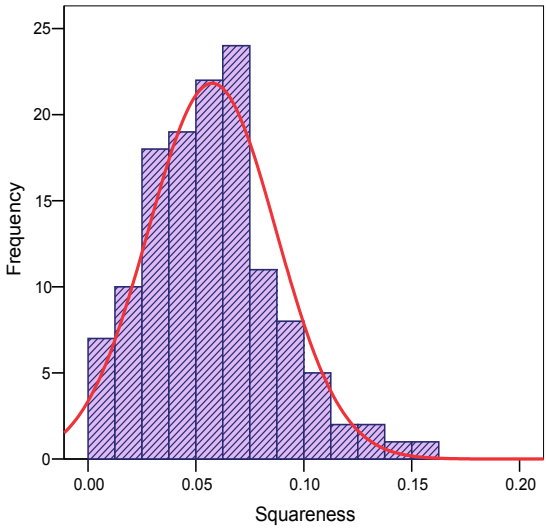

(D) Mean = 0.058, Std. Dev. = 0.03

Figure 5.8 Frequency Distributions of Shape Parameters: (A) Diameter, (B) Elongation, (C) Triangularity and (D) Squareness

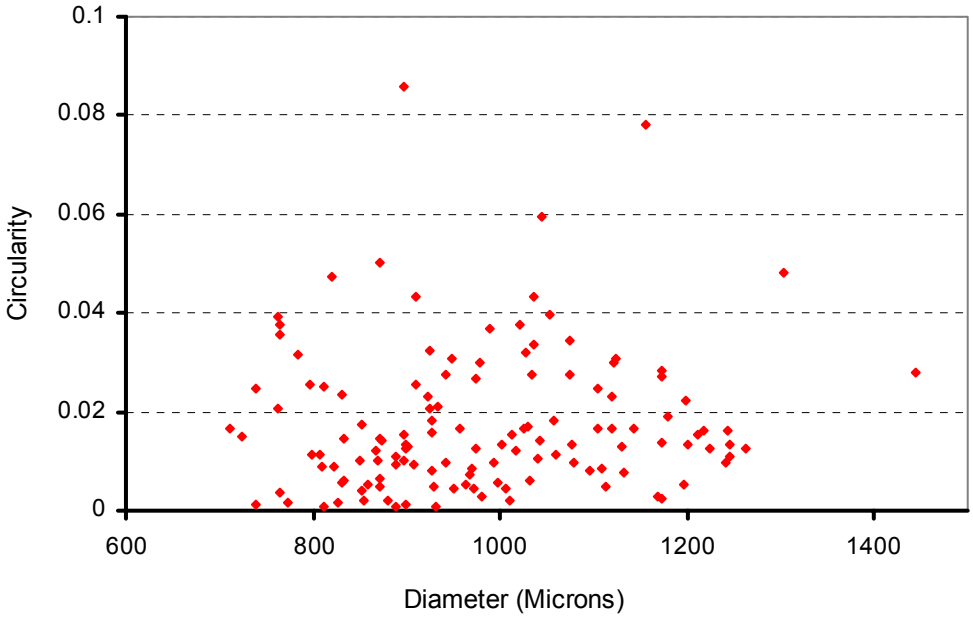

Figure 5.9 Variation of Circularity with Diameter

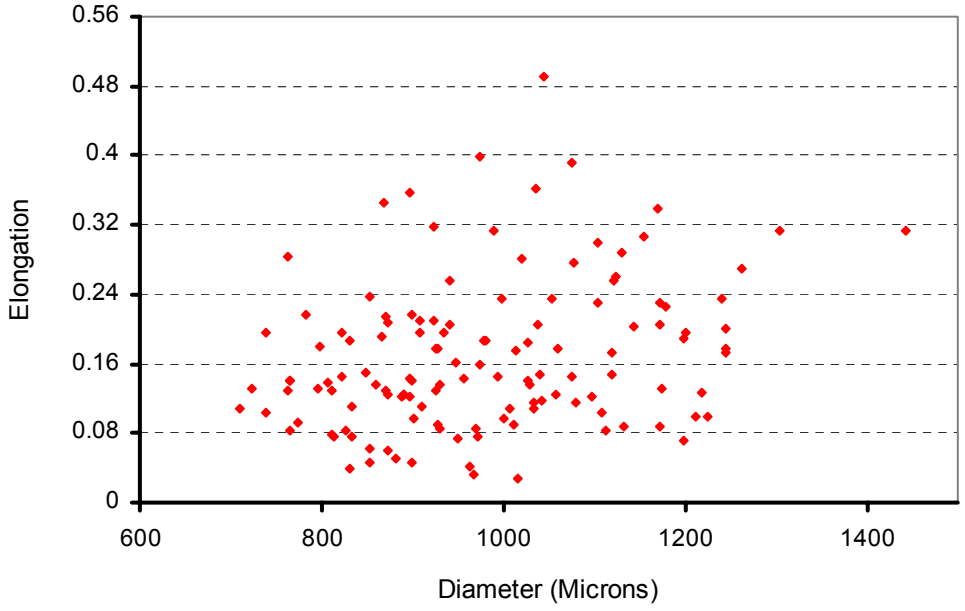

Figure 5.10 Variation of Elongation with Diameter

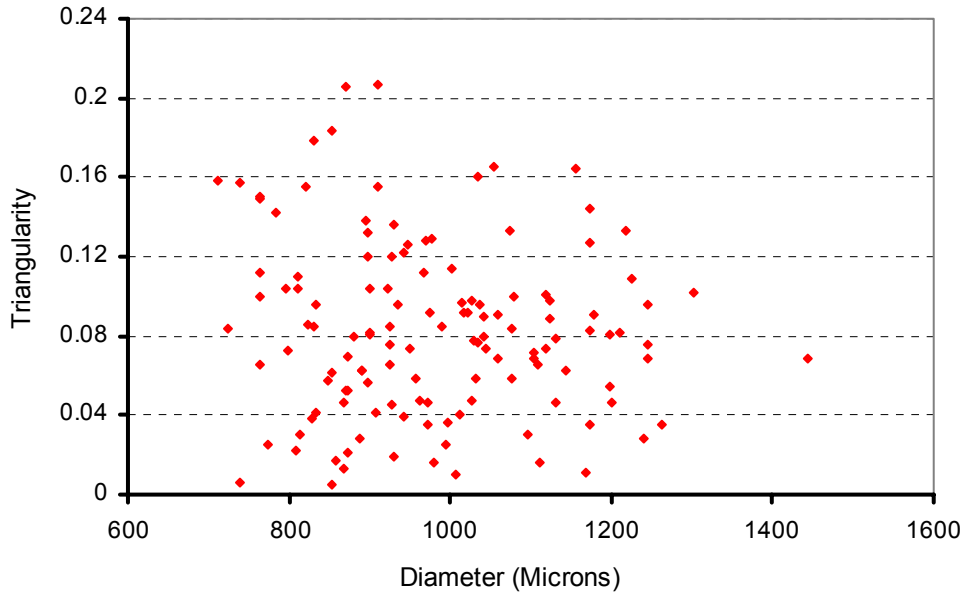

Figure 5.11 Variation of Triangularity with Diameter

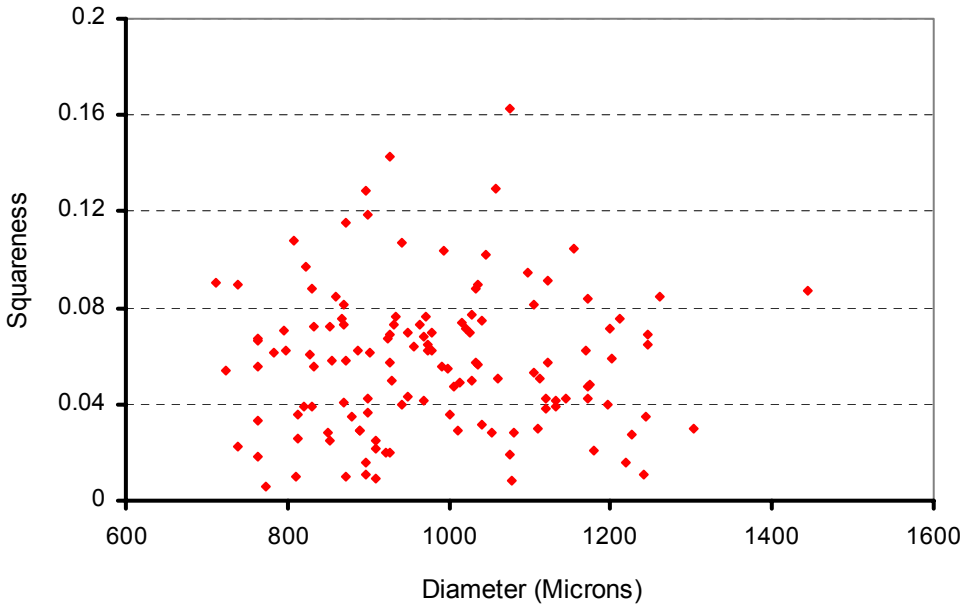

Figure 5.12 Variation of Squareness with Diameter

Table 5.5 Regression Analysis Results for Different Shape Descriptors

Circularity

Regression	R-square
Linear	0.0081
Logarithmic	0.0074
Polynomial (2^{nd} degree)	0.0097
Exponential	0.0301

Elongation

Regression	R-square
Linear	0.0804
Logarithmic	0.0786
Polynomial (2^{nd} degree)	0.0813
Exponential	0.0727

Triangularity

Regression	R-square
Linear	0.0093
Logarithmic	0.0104
Polynomial (2^{nd} degree)	0.0128
Exponential	0.00004

Squareness

Regression	R-square
Linear	0.0001
Logarithmic	0.0002
Polynomial (2^{nd} degree)	0.0024
Exponential	0.0016

5.3.4 Summary and Discussion

The current study focuses on the verification of any existing relationship between grain size and grain shape using six different natural and processed sand samples. To investigate the relationship, the first four Fourier descriptors are used to quantify the particle shapes. Though in previous literature a strong relationship has been documented between grain size and grain shape, it is evident from the current research that there is no relationship between grain size and grain shape in terms of circularity, elongation, triangularity or squareness for the sand samples analyzed. Considering the dependency of grain shape on various factors, such as origin and mineralogical compositions, distance of transport, mechanical and chemical processes, it is unlikely to obtain a universal relationship between grain size and grain shape for all sands. Even though the sands in the current study came from different sources and underwent considerably different depositional processes, no relationship was found between shape and size. The current findings have significant implications in terms of constructing discrete element model

assemblies of angular particles (e.g., Ashmawy et al., 2003). Because no relationship exists between particle size and shape, shapes belonging to a particular sand sample can be randomly selected from the particle shape library, and resized according to the desired grain size distribution, irrespective of size. However, if a particular sand is found to exhibit a correlation between shape and size, it would be necessary to separate the particles into different groups or bins based on their size in order to generate a representative assemblies of angular particles for discrete element simulation.

CHAPTER 6

SKELETONIZATION AND OVERLAPPING DISCRETE ELEMENT CLUSTER ALGORITHM

The previous chapter has presented a methodology to determine the sample size of various natural and processed sand samples. The analysis suggested that aspect ratio has greater influence on sample size determination compared to other shape descriptors. The relationship between grain size and shape has also been explored and no relationship was found for the sand samples analyzed. The current chapter explains the skeletonization and Overlapping Discrete Element Cluster (ODEC) algorithms to model irregular particle shape.

6.1 Skeletonization of Grain Shape

In the present study particle shape is modeled using the ODEC technique proposed by Ashmawy et al. (2003) where the irregular particle shape is covered by inscribing a number of overlapping circular or spherical discrete elements to generate representative assemblies of angular particles for discrete element modeling simulations.

To make the ODEC technique computationally efficient, skeletonization of the shape is necessary. Skeletonization is often called Medial Axis Transformation which is defined as the locus of centers of maximally inscribed discs. In 3-D, the medial surface is the locus of centers of all maximally inscribed spheres. One of the methods to generate skeleton is by thinning the object with a set of structuring elements. Figure 6.1 shows an example of successive thinning of a set A by structuring element B. The thinning procedure is performed on A by one pass with B^1. Then the thinning is continued on the resulting image by one pass of B^2, and so on, until A is thinned with one pass of B^n. The process is then repeated until A can not be thinned further. Figure 6.1 (A) shows a set of structuring elements commonly used for thinning and Figure 6.1(B) shows the successive

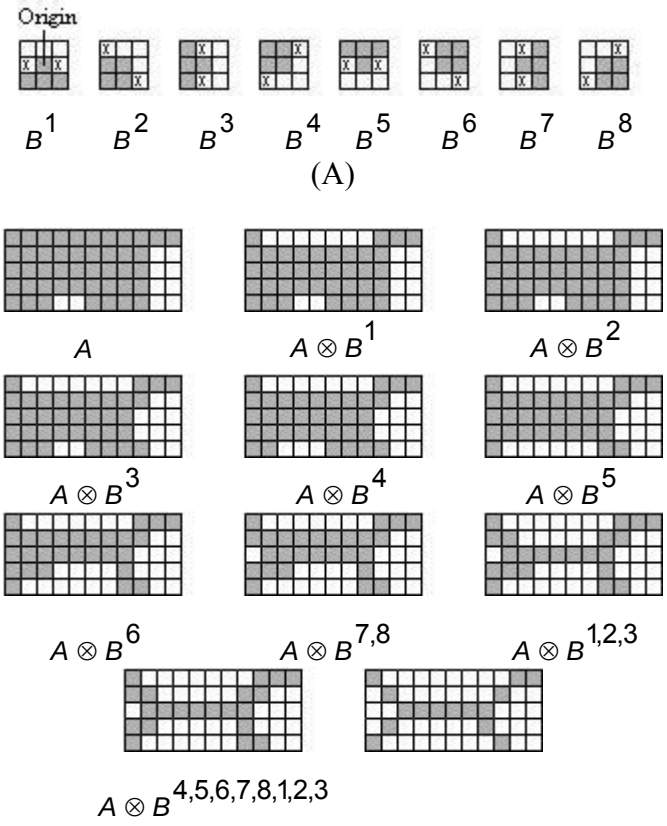

Figure 6.1 Thinning Algorithm: (A) A Set of Structuring Elements, (B) Successive Steps of Thinning
[Source: Gonzalez & Woods, 2003]

steps of thinning with passes of different structuring element. Finally the thinned set is converted to m-connectivity to eliminate multiple paths. Figure 6.2 presents the skeleton obtained using this method. Although the method is accurate for generating the skeleton of a regular "L" shaped object, it can not generate accurate skeleton for irregular object, such as Fraser River sand grain. It can be seen from Figure 6.2(B) that part of the medial axis (marked in red) is not equidistant from at least two non-consecutive points on the outline.

(A) (B)

Figure 6.2 Skeleton in Two Dimensions: (A) L-Shaped Object, (B) Fraser River Sand Grain

Contour thinning is another method to make skeleton of a binary region. In this method, the region points are assumed to have a value of 1 and the background points to have a value of 0. The procedure is based on two basic steps. The neighborhood arrangement is shown in Figure 6.3.

Step 1: Contour point P_1 is marked for deletion if the following conditions are satisfied:

(a) $2<=N(P_1)<=6$; (b) $T(P_1) = 1$; (c) $P_2 * P_4 * P_6 = 0$; (d) $P_4 * P_6 * P_8 = 0$

where, $N(P_1)$ is the number of non-zero neighbors of P_1, i.e.

$N(P_1) = P_2 + P_3 + \ldots\ldots\ldots\ldots + P_8 + P_9$

and $T(P_1)$ is the number of 0-1 transitions in the ordered sequence P_2, P_3, P_4, P_5, P_6, P_7, P_8, P_9, P_2.

Step 2: Conditions (a) and (b) remain the same, but condition (c) and (d) are changed to

(c) $P_2 * P_4 * P_8 = 0$; and (d) $P_2 * P_6 * P_8 = 0$

Step 1 is first applied to each border pixel and if all conditions are satisfied, the point is marked for deletion. After processing all border points, the marked points are deleted (changed to zero). Step 2 is then applied to the resulting image in the same manner as step 1. The entire process is repeated until no further points are deleted. The resulting image will be the skeleton of the region. Figure 6.4 (A) and Figure 6.4 (B) show the skeletons obtained by using this method. Though the skeleton was accurate for regular "T" shaped object, the method could not generate accurate skeleton for irregular shape, for example Michigan Dune sand grain because the red portion in the skeleton is not equidistant from at least two non-contiguous points on the outline. The skeleton obtained

through thinning algorithm may not be accurate since it is obtained by erosion of pixels, not by measuring the Cartesian distances from any internal point to the boundary.

P_9	P_2	P_3
P_8	P_1	P_4
P_7	P_6	P_5

Figure 6.3 Neighborhood Arrangement Used by the Thinning Algorithm

(A) (B)

Figure 6.4 Skeleton in Two Dimensions: (A) T-Shaped Object, (B) Michigan Dune Sand Grain

6.1.1 Skeletonization Algorithm in Two Dimensions

In the present study an algorithm is developed in Matlab to extract the skeleton of 2-D particle outline and it is capable of generating skeleton of any irregular shape. First the two-dimensional silhouette of the particle is obtained using edge detection algorithm. The edge pixel is a pixel for which one or more of the four neighbors is on the background. The edge of the particle is marked in red in Figure 6.5. The edge pixels are then numbered consecutively, starting from a particular point and then traversing either clockwise or anti-clockwise direction. The next step is to define any point on the skeleton. For this purpose, the centroid of the particle, which coincides with, say, the black pixel (Figure 6.6), is chosen as the first pixel to start the skeleton. The Cartesian distances (D) from the black pixel (centroid) to all the edge pixels are calculated and the minimum distance (D_{min}) from the centroid to the edge pixels is obtained. Now the edge pixels that are within a distance of D_{min} and D_{min} + 1 are marked in yellow/red dots. If all marked edge pixels are adjacent (i.e., their order is sequential, for example, 5, 6, 7 or

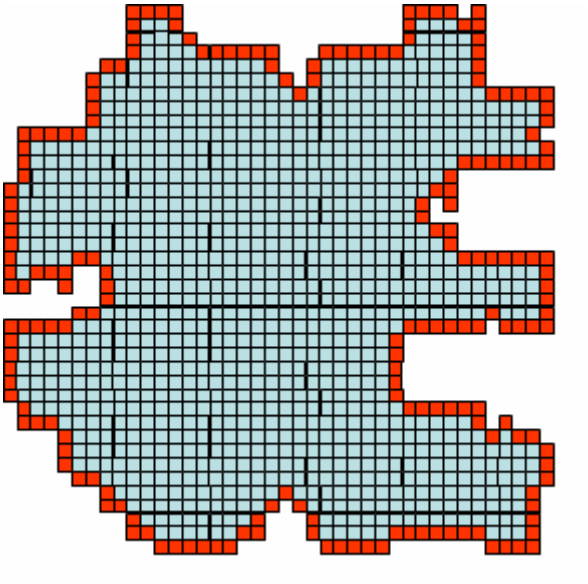

Figure 6.5 Edge Detection

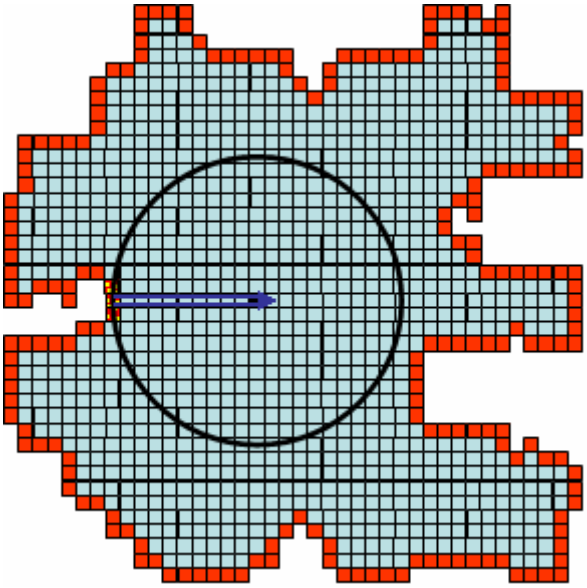

Figure 6.6 First Pixel to Start the Skeleton

separated by less than a previously defined threshold value, then the black pixel is not a skeleton point. In this study, a threshold of 10 pixels is considered. It should be noted that the first pixel and the last pixel on the boundary are adjacent. Since the black point is not a skeleton pixel based on the criteria, it is then marked in the same color as the internal pixels. The next pixel to be checked is the pixel that is one pixel along the D_{min} line away from the edge pixel as shown by blue arrow in Figure 6.6 and is marked in black (Figure 6.7).

At the new marked (black) point, the same process is repeated until the first skeleton point is obtained. First, the Cartesian distances (D) from the new black pixel to all the edge pixels are calculated. Now the edge pixels that are within a distance of D_{min} and $D_{min} + 1$ are marked in yellow/red dots. In this case, the marked edge pixels are not all adjacent (i.e., their order is not sequential). Therefore, the black point is a skeleton point (Figure 6.7).

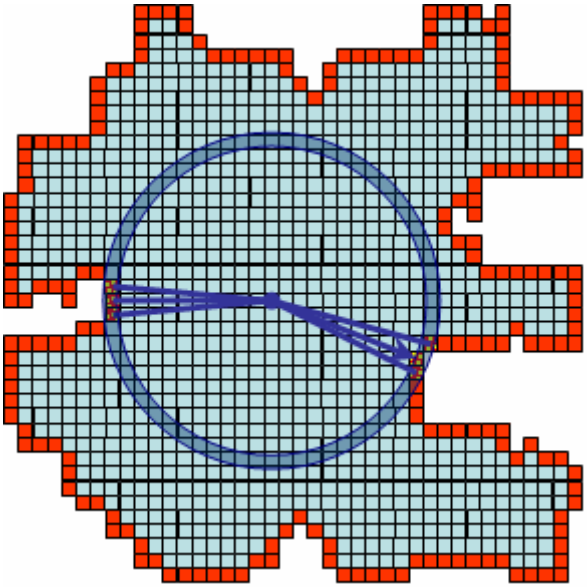

Figure 6.7 First Skeleton Point Obtained

The same process is then repeated on all 8 neighbors of the current skeleton point to check if they are the skeleton points or not. The distance between each of them and all the edge pixels are obtained. In this case, the yellow pixels satisfy the conditions required for a skeleton pixel (Figure 6.8) and the shaded yellow pixels do not. To move along the skeleton, anyone of those yellow pixels is chosen. This point is the next point on the skeleton and is then marked in black. It is noted that the yellow point at the bottom is also a skeleton point. This branch of the skeleton will be tracked later.

From the current point, the procedure is repeated, marking all 8-neighbors that satisfy the "skeleton pixel" condition (Figure 6.9) and any of the 8-neighbors that have been previously marked in black as a skeleton pixel and shaded yellow as a non-skeleton pixel are not considered.

When one branch of the skeleton reaches the edge pixel or being a certain threshold distance from the edge pixel, another branch is followed to continue the skeleton. The whole procedure is continued until the whole skeleton is defined (Figure 6.10). The output of the skeletonization algorithm is shown in Figure 6.11.

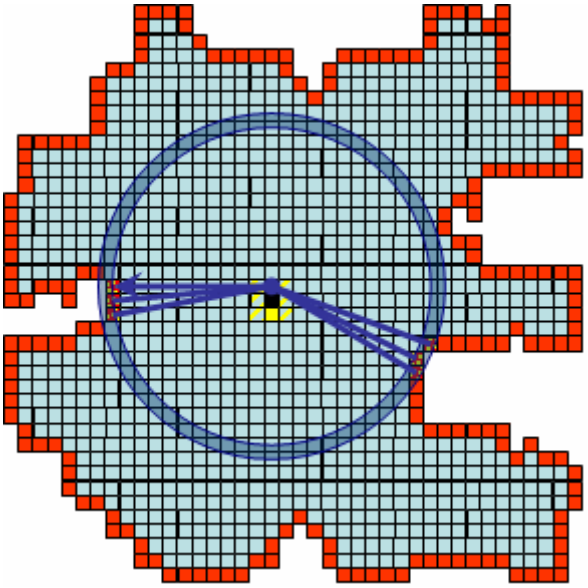

Figure 6.8 Next Skeleton Point

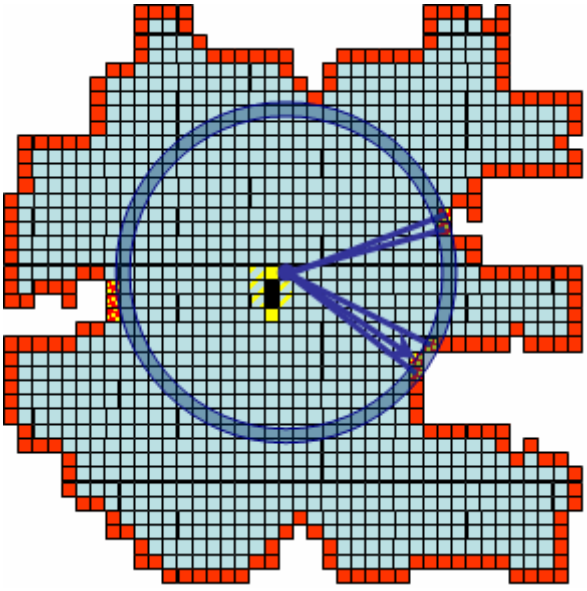

Figure 6.9 Skeleton Continued Following the First Branch

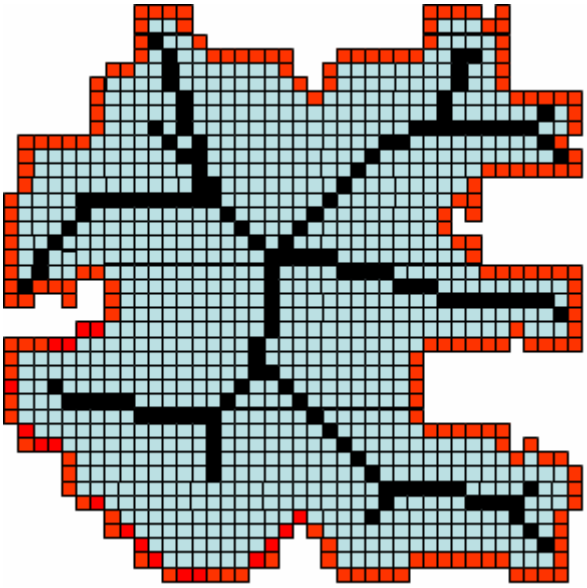

Figure 6.10 Final Skeleton Obtained Through the Algorithm

Figure 6.11 A Daytona Beach Sand Particle (Left) and the Skeleton (Right)

6.1.2 Skeletonization Algorithm in Three Dimensions

Different approaches have been suggested in early studies to extract skeleton of three-dimensional shape (Lien and Amato, 2005; Chuang et al., 2000; Wu et al., 2003). In the present study, three-dimensional skeleton of granular particles are extracted using the same method as developed in two-dimensions. After characterizing the grain shape, three-dimensional coordinates of each and every voxel of the particle are obtained. The centroid was chosen as the first voxel to start the skeleton. The distances from this voxel to all surface voxels are calculated and the minimum distance (D_{min}) from the centroid to the surface voxels is obtained. Now the surface voxels which are at a distance of D_{min} and

D_{min} + 1 are marked. If the marked voxels are non-adjacent (Figure 6.12), then the voxel at the centroid is a skeleton point. If not, this procedure should be continued on all of its 26 neighbors until the first skeleton point is obtained. The process is then repeated on all 26 neighbors of the current skeleton point to check if they are the skeleton points or not. When one branch of the skeleton reaches the boundary or being a certain threshold distance from the boundary, another branch is followed to continue the skeleton. The procedure is continued until the whole skeleton is defined. One problem that may arise during this skeleton generation procedure is explained below. Let's say the black voxels in Figure 6.13 are the marked surface voxels that are within a distance of D_{min} and D_{min} + 1 from a particular internal voxel. This kind of situation may occur if any particular region on the surface (as shown in red color) is protruded out of the neighboring region. Even though the marked black voxels are contiguous, the internal voxel should still be a skeleton point. The three-dimensional skeletons obtained by using the algorithm along with the original particles are shown in Figure 6.14 through Figure 6.21 for Daytona Beach sand grains (1 voxel = 0.003 mm) and Michigan Dune sand grains (1 voxel = 0.006 mm). The average computational time of this algorithm was 96 hours for Daytona Beach sand grains and 1 month for Michigan Dune sand grains.

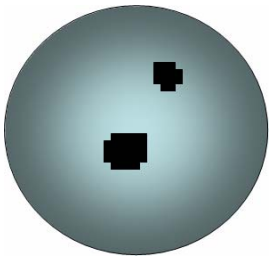

Figure 6.12 Non-Adjacent Boundary Voxels

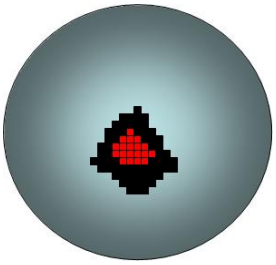

Figure 6.13 Surface Protrusion Marked as Red Voxels

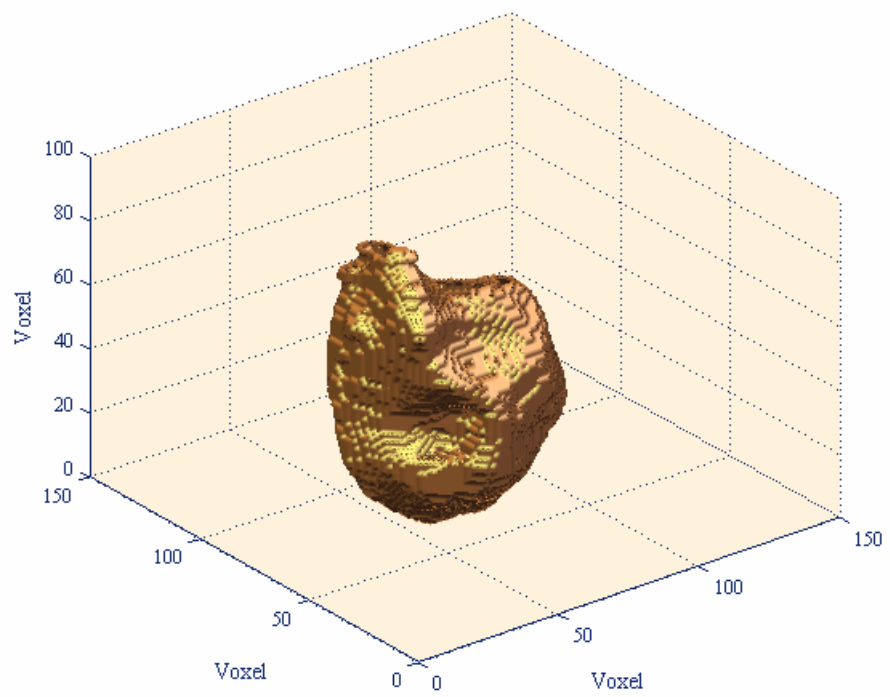

Figure 6.14 Original Particle of Daytona Beach Sand (DB #1)

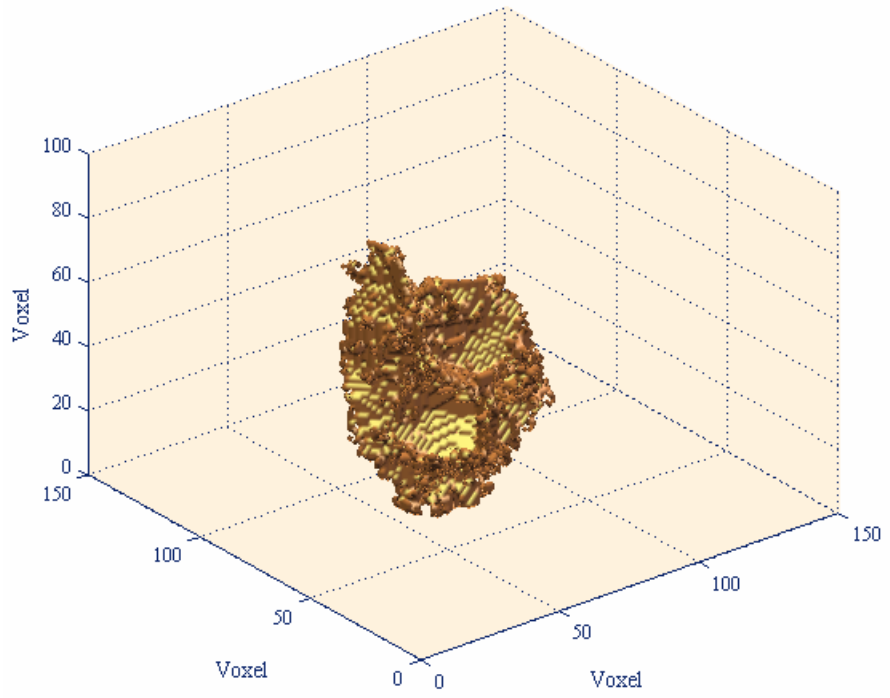

Figure 6.15 Three-Dimensional Skeleton of Daytona Beach Sand Grain (DB #1)

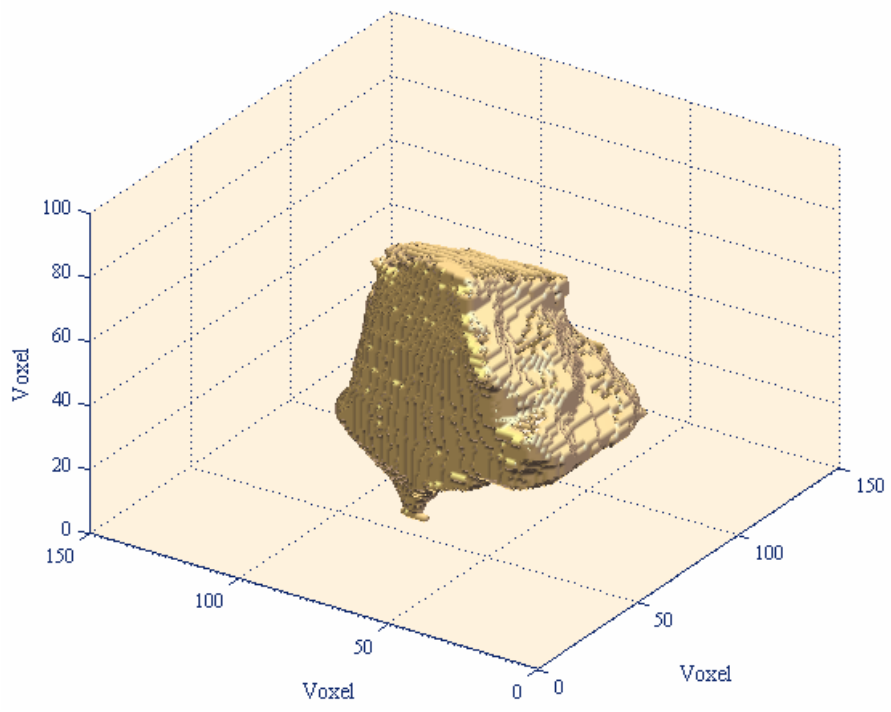

Figure 6.16 Original Particle of Daytona Beach Sand (DB #2)

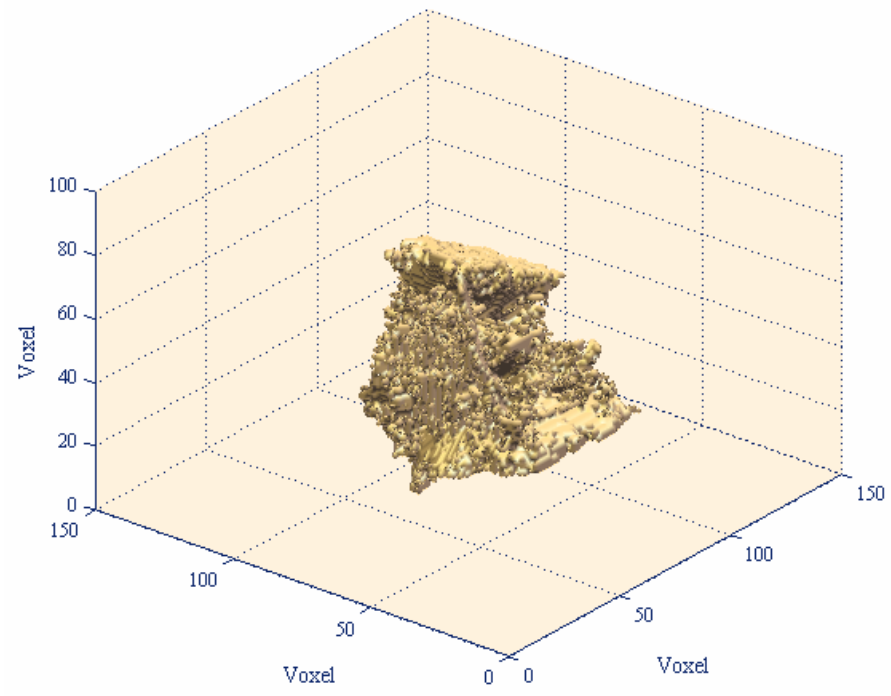

Figure 6.17 Three-Dimensional Skeleton of Daytona Beach Sand Grain (DB #2)

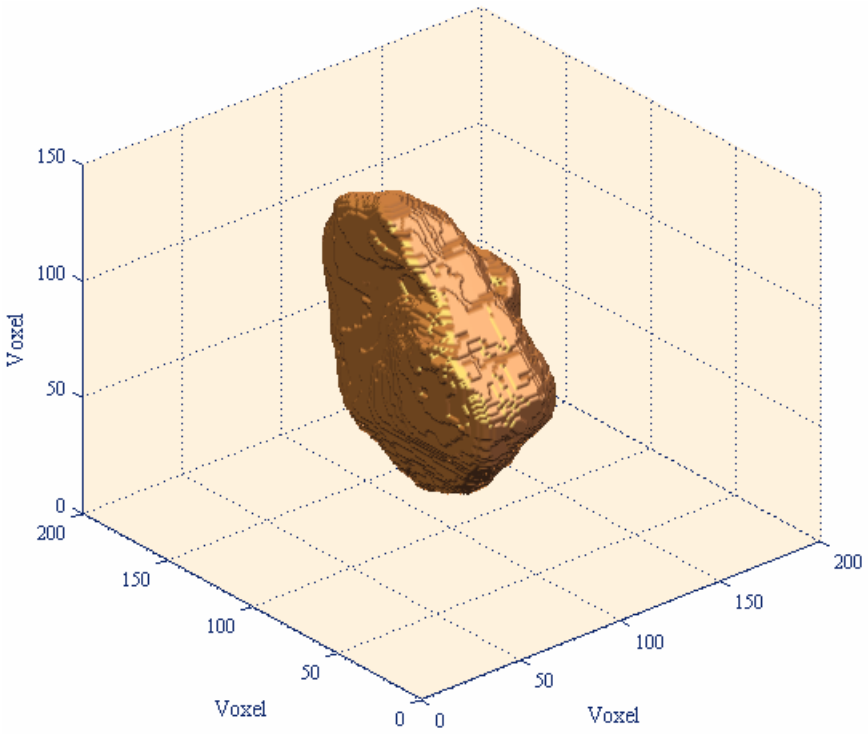

Figure 6.18 Original Particle of Michigan Dune Sand (MD #1)

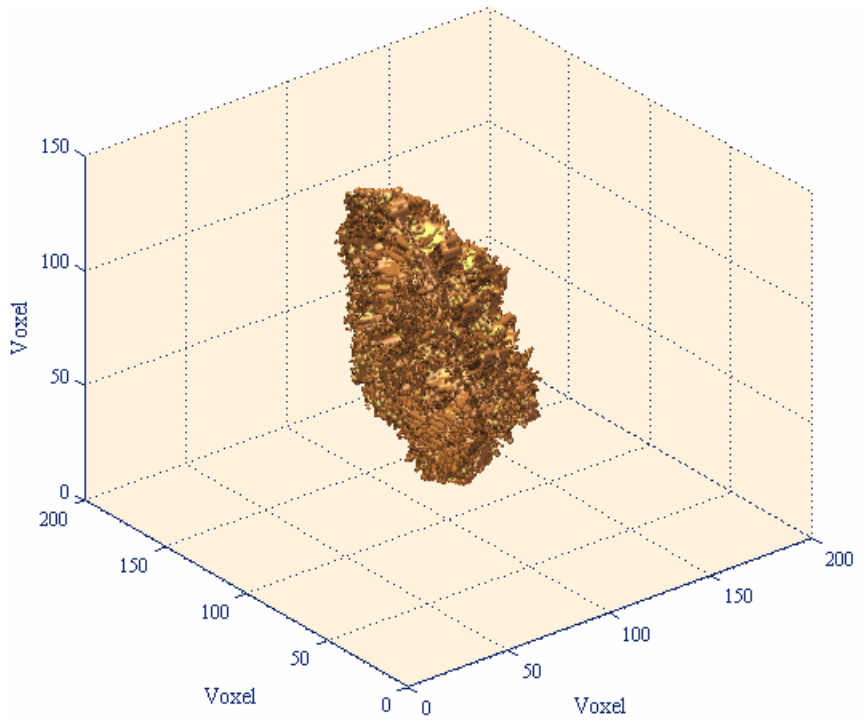

Figure 6.19 Three-Dimensional Skeleton of Michigan Dune Sand Grain (MD #1)

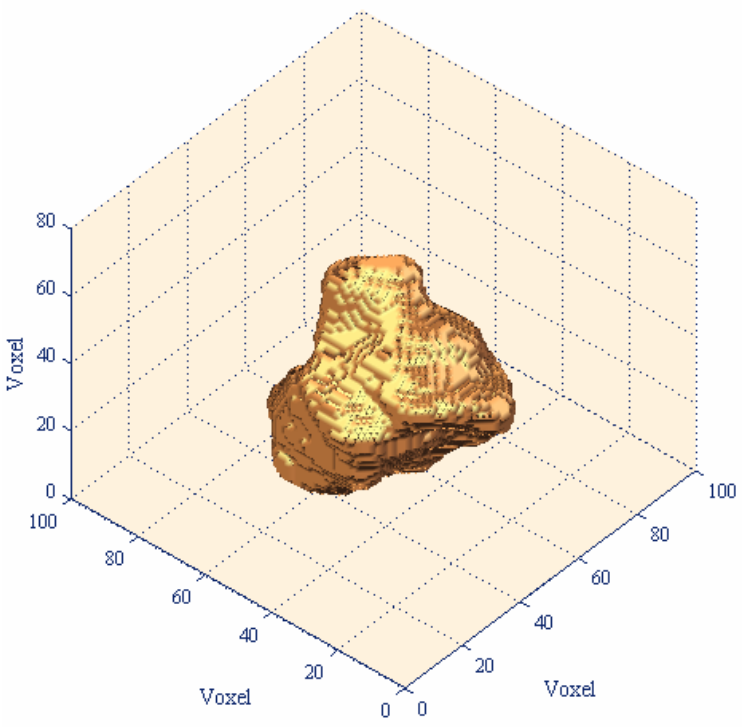

Figure 6.20 Original Particle of Michigan Dune Sand (MD #2)

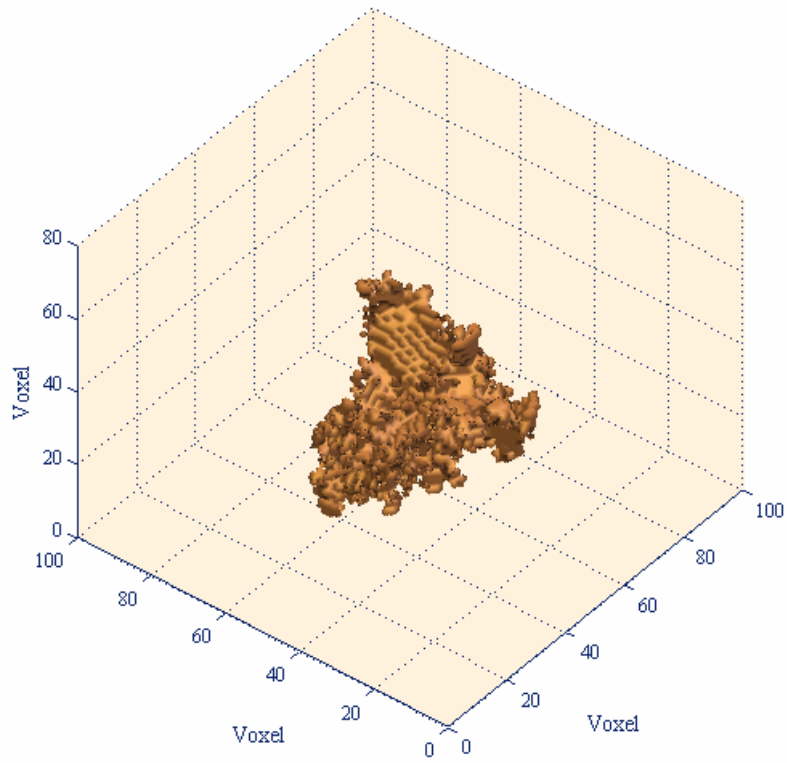

Figure 6.21 Three-Dimensional Skeleton of Michigan Dune Sand Grain (MD #2)

6.2 Overlapping Discrete Element Cluster

After extracting the skeleton of two-dimensional particle outline and three-dimensional particle surface, the irregular shapes of sand grains are modeled using the ODEC technique for implementation in discrete element modeling code PFC^{2D} and PFC^{3D}. In the current research, a fully automated procedure is developed to model two-dimensional particle shape using the ODEC technique proposed by Ashmawy et al. (2003). The procedure is also extended to three dimensions to model highly irregular particle surface for implementation in three-dimensional DEM simulation.

6.2.1 ODEC Algorithm in Two Dimensions

In the ODEC technique the two-dimensional particle outline is covered by inscribing a number of overlapping circular discrete elements so that the simulated particle outline resembles the outline of actual particle. To reduce the number of overlapping discs within the clump, the biggest disc covering maximum area is inscribed first. The next disc to be added is the disc that covers the maximum uncovered area and so on. The disc generation procedure is continued until at least a reasonable percentage of the grain area is covered. The output of the ODEC algorithm is shown in Figure 6.22 for Daytona Beach sand grain. Figure 6.23 and Figure 6.24 show the original particle of a Daytona Beach sand grain and the modeled particle obtained through the ODEC technique. Table 6.1 summarizes the number of discs required to capture the shapes of various grains of Daytona Beach sand sample.

Table 6.1 Number of Discs Required for Daytona Beach Sand Sample

Area Covered (in percent)	Number of Discs
98 %	9 – 14
95 %	4 – 8
90 %	3 – 6
85 %	2 - 4

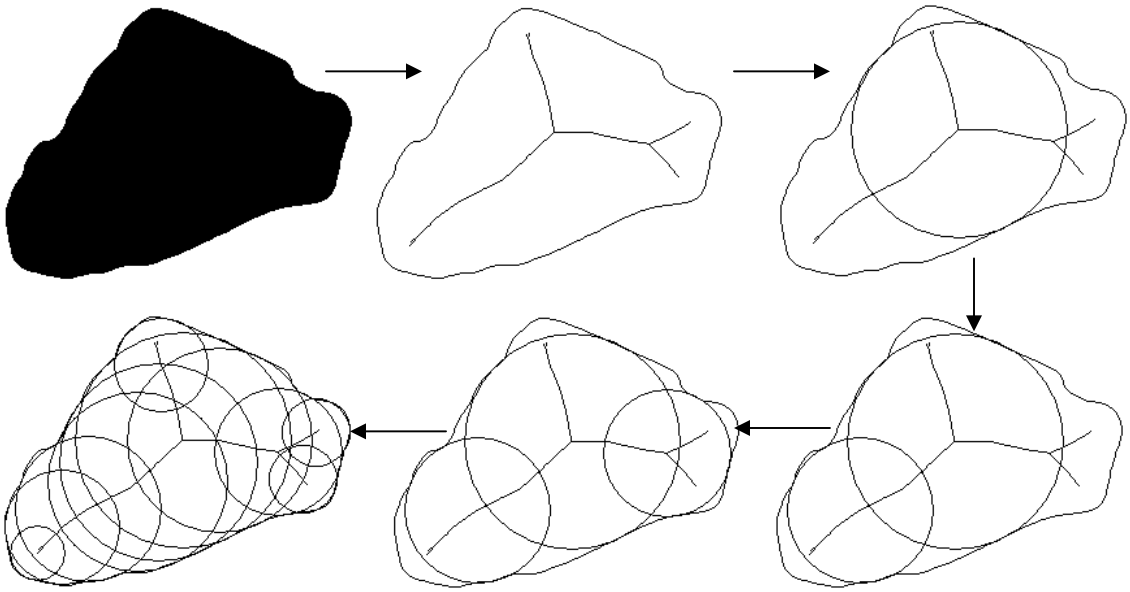

Figure 6.22 Overlapping Discrete Element Cluster for a Daytona Beach Sand Grain

Figure 6.23 Original Particle of Daytona Beach Sand in Two Dimensions

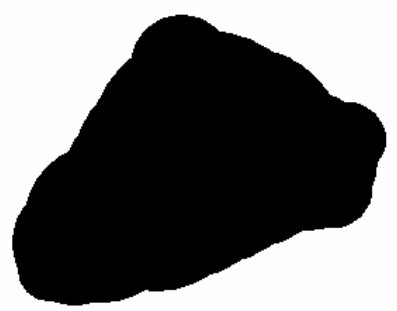

Figure 6.24 Particle Shape Obtained Through ODEC Technique

A significant difference between the number of discs is observed (Table 6.1) if the area coverage is increased from 95% to 98%, in comparison to the difference between the number of discs, when the area coverage is increased from 90% to 95%. Therefore, an area coverage of 95% was considered as a reasonable threshold for ODEC technique because a small increase in the number of discs can cover 5% more area if the threshold is increased from 90% to 95%.

6.2.2 ODEC Algorithm in Three Dimensions

In this case three-dimensional particle surface is covered by inscribing a number of overlapping spherical discrete elements so that the simulated particle surface resembles the surface of actual particle. To reduce the number of overlapping spheres within the clump, the biggest sphere covering maximum volume is inscribed first. The next sphere to be added is the sphere that covers the maximum uncovered volume and so on. The procedure is continued until at least a reasonable percent of the grain volume is covered. The output of the ODEC algorithm is shown in Figure 6.25 through Figure 6.36 for Michigan Dune sand (1 voxel = 0.006 mm) and Daytona Beach sand grains (1 voxel = 0.003 mm) respectively for different percentage of covered volume. The original particles for the corresponding Daytona Beach sand grains (DB #1 and DB #2) and Michigan Dune sand grains (MD #1 and MD#2) are presented in Figure 6.14, Figure 6.16, Figure 6.18 and Figure 6.20 respectively. Table 6.2 summarizes the number of spheres required to capture the shape of Michigan Dune sand and Daytona Beach sand grains. The average computational time of this algorithm was 96 hours for Daytona Beach sand grains and 56 hours for Michigan Dune sand grains with an error of 5% in grain volume.

Table 6.2 Number of Spheres Required for Michigan Dune and Daytona Beach Sand Grains

Volume Covered (in percent)	Number of Spheres	
	Michigan Dune	Daytona Beach
98 %	217 - 297	251 - 296
95 %	98 - 126	123 - 133
90 %	49 - 57	61 - 62
85 %	32	35 - 39

It is evident from the figures that that a threshold of 95% can model irregular particle shape accurately in three dimensions. However, a big difference between the number of spheres is observed if the volume coverage is increased from 90% to 95%, in comparison with the number of discs between 85% to 90% volume coverage. Due to large volume of data sets, only two particles are processed for Daytona Beach and Michigan Dune sand

samples, therefore it is not possible to set a threshold for percent volume covered. Sufficient number of grains needs to be analyzed to verify the threshold.

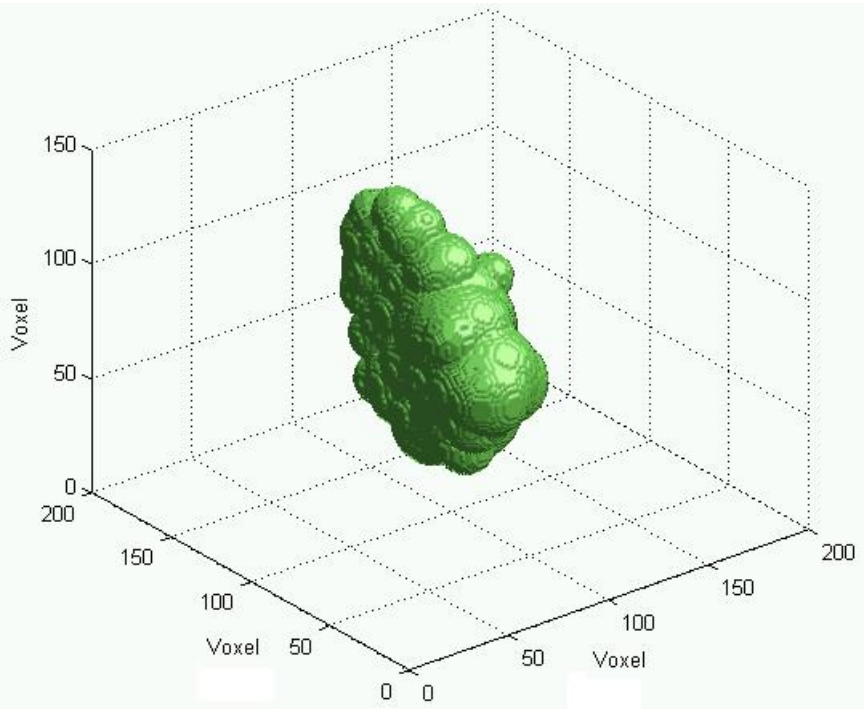

Figure 6.25 Overlapping Discrete Element Cluster (MD #1, Volume Covered =85%)

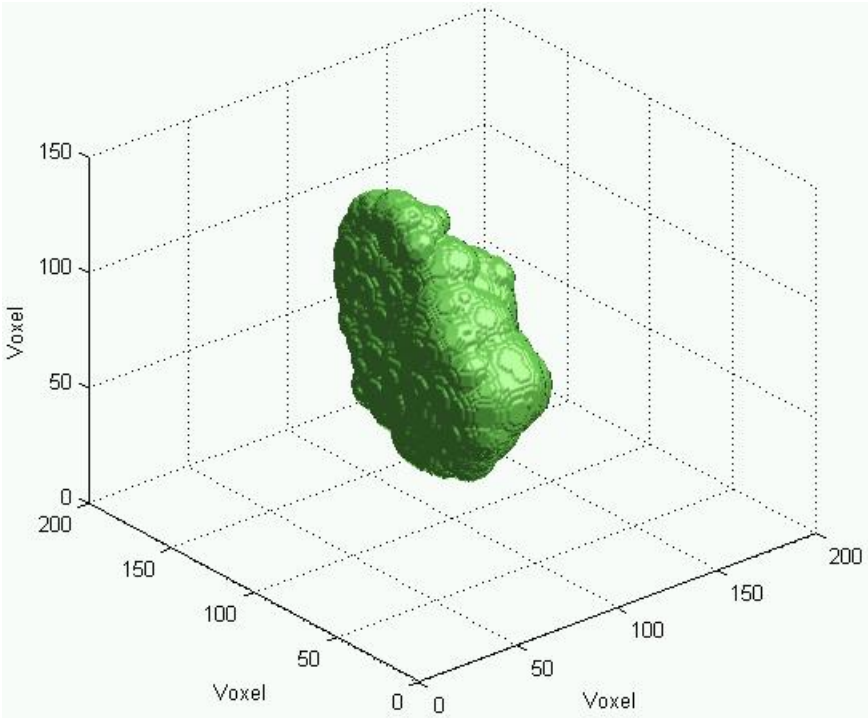

Figure 6.26 Overlapping Discrete Element Cluster (MD #1, Volume Covered =90%)

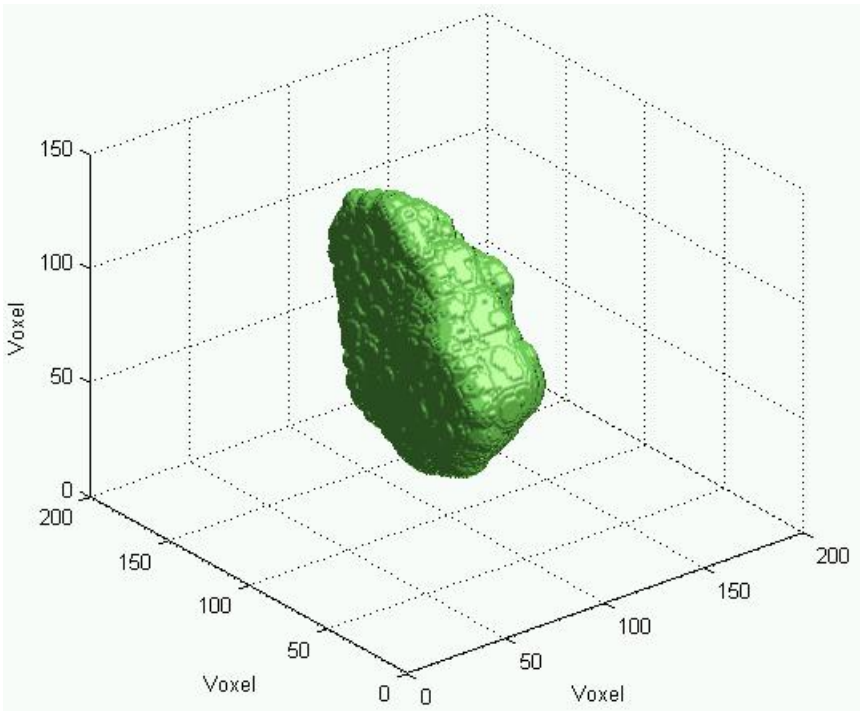

Figure 6.27 Overlapping Discrete Element Cluster (MD #1, Volume Covered =95%)

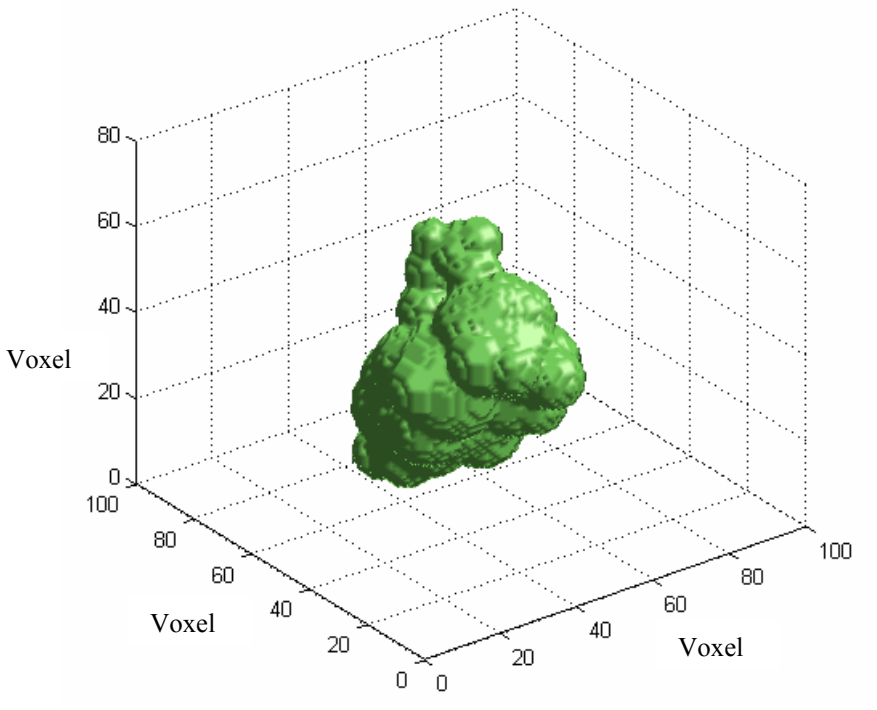

Figure 6.28 Overlapping Discrete Element Cluster (MD #2, Volume Covered =85%)

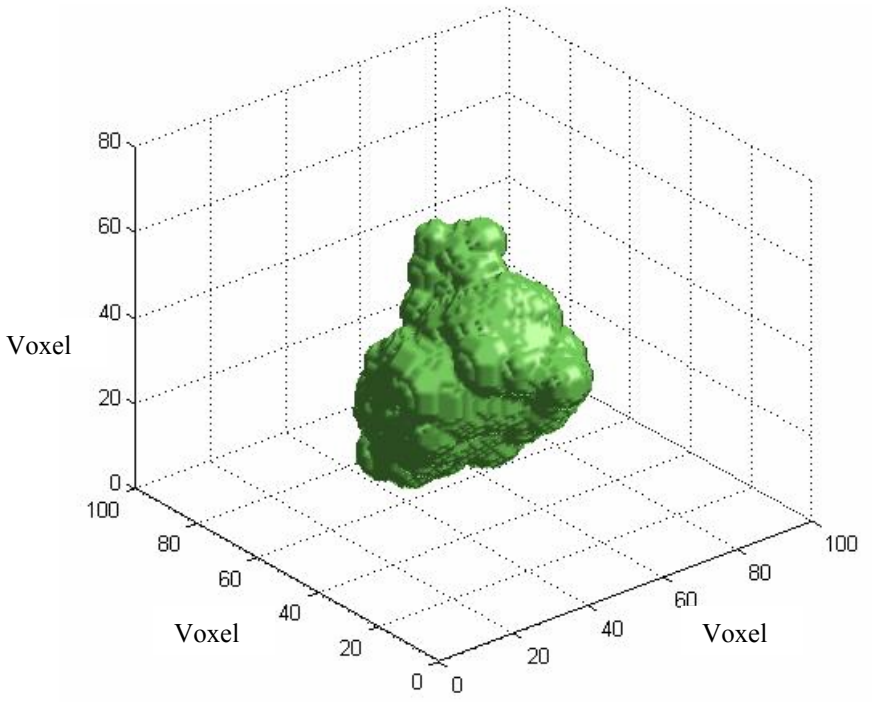

Figure 6.29 Overlapping Discrete Element Cluster (MD #2, Volume Covered =90%)

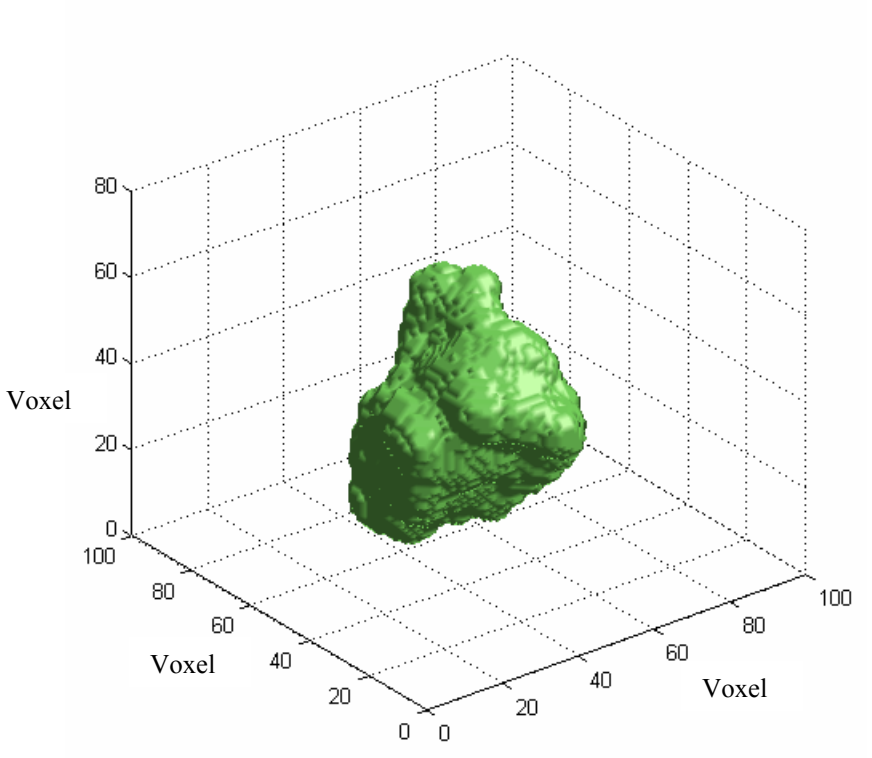

Figure 6.30 Overlapping Discrete Element Cluster (MD #2, Volume Covered =95%)

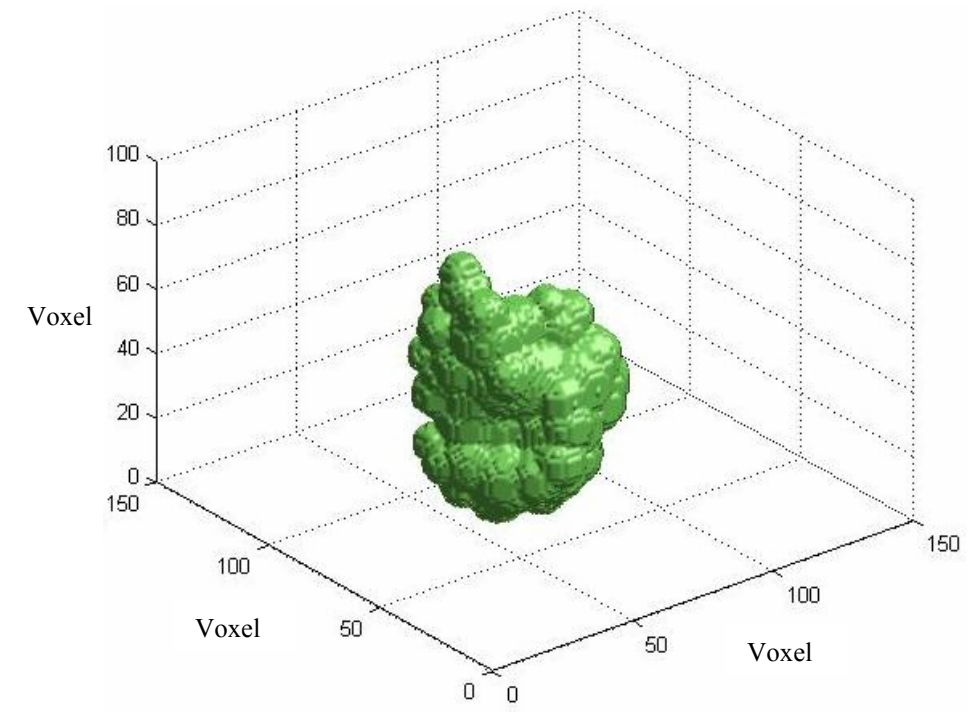

Figure 6.31 Overlapping Discrete Element Cluster (DB #1, Volume Covered =85%)

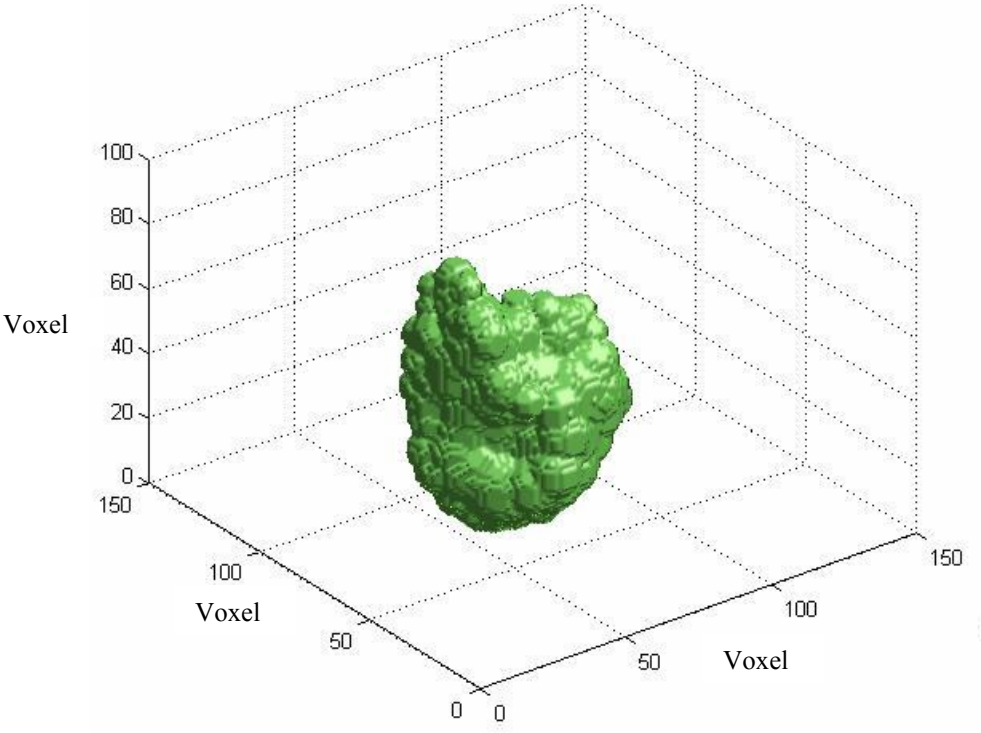

Figure 6.32 Overlapping Discrete Element Cluster (DB #1, Volume Covered =90%)

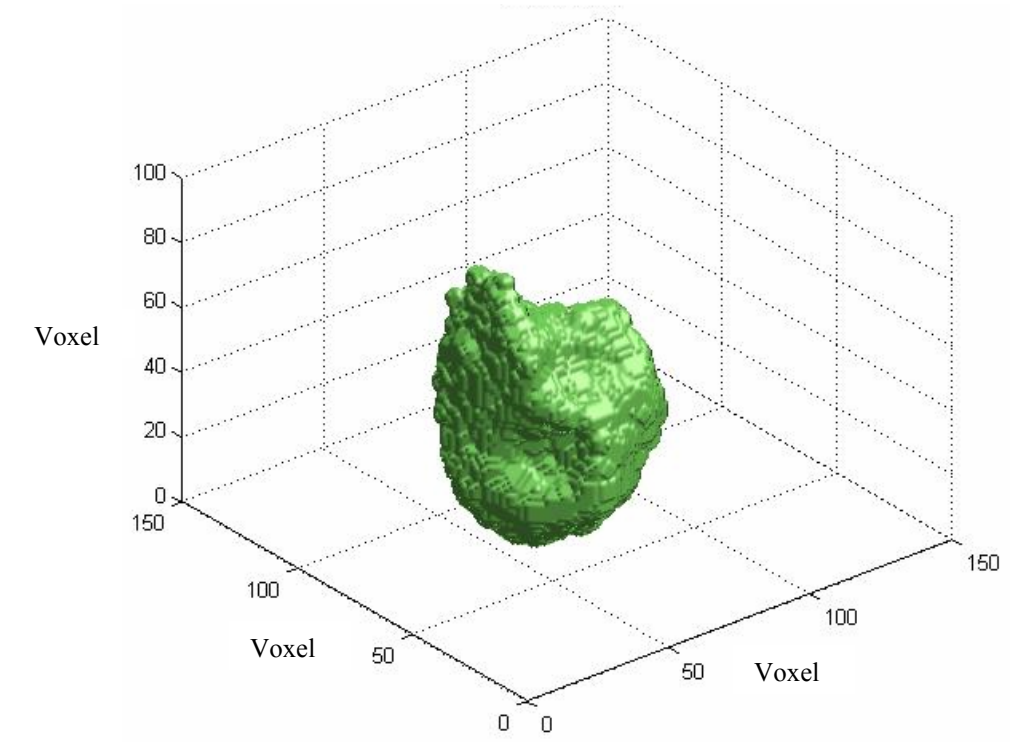

Figure 6.33 Overlapping Discrete Element Cluster (DB #1, Volume Covered =95%)

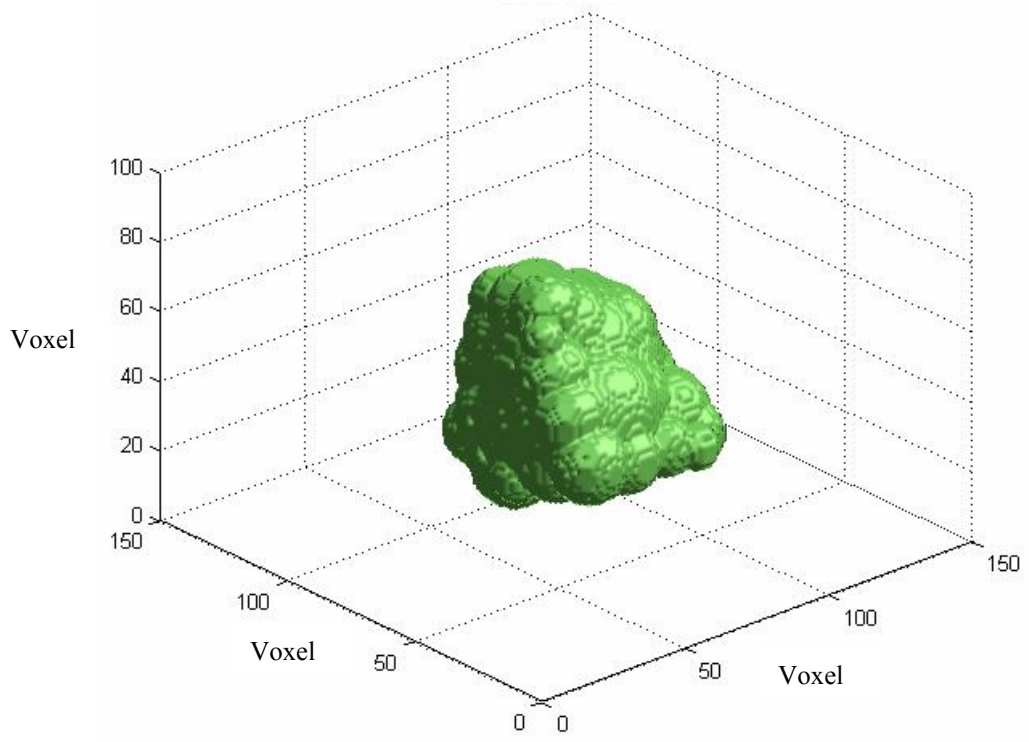

Figure 6.34 Overlapping Discrete Element Cluster (DB #2, Volume Covered =85%)

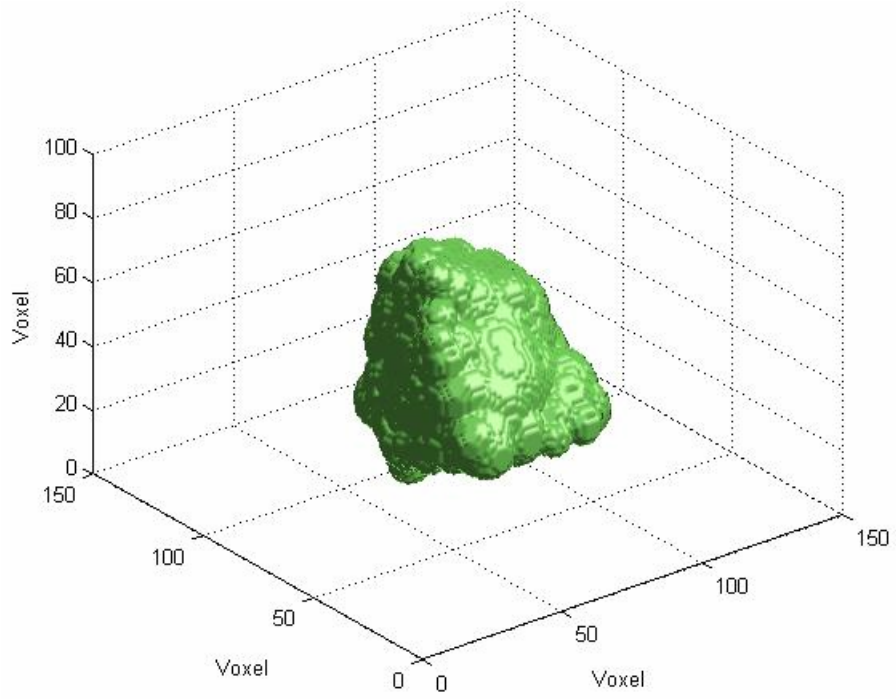

Figure 6.35 Overlapping Discrete Element Cluster (DB #2, Volume Covered =90%)

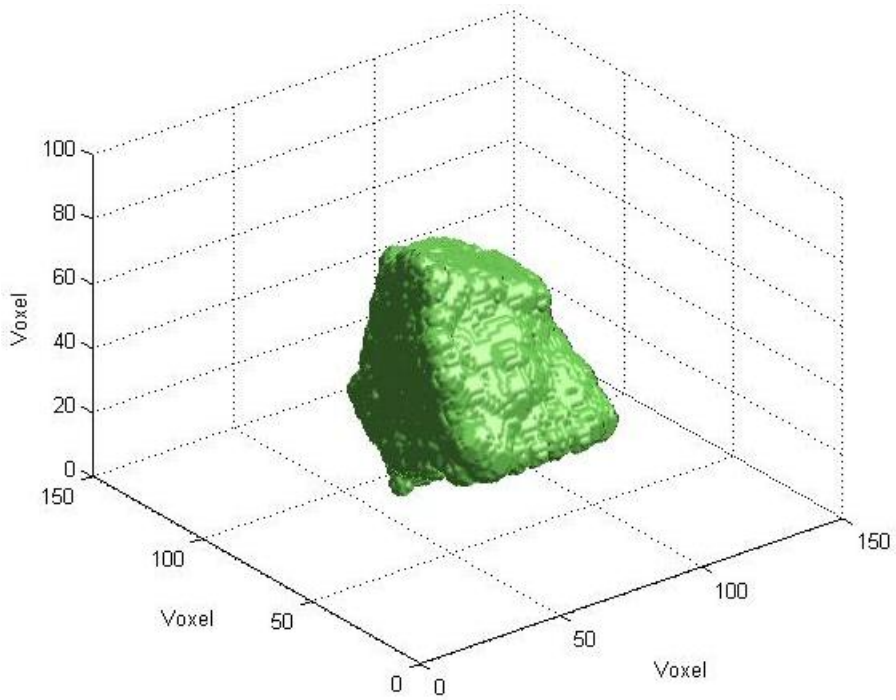

Figure 6.36 Overlapping Discrete Element Cluster (DB #2, Volume Covered = 95%)

CHAPTER 7

IMPLEMENTATION OF PARTICLE SHAPE WITHIN DISCRETE ELEMENT MODELING SIMULATION

The previous chapter presented the skeletonization and ODEC algorithms and it was observed that the algorithms are capable to modeling the irregular particle shape accurately. The current chapter describes the implementation of particle shape within DEM software and the effect of grain shape on the shear strength behavior of granular media.

7.1 Introduction

In recent years Discrete Element Method (DEM) has become an emerging technique to characterize irregular particle shapes in two and three dimensions. In the current research, the effect of particle shape on the micromechanical behavior of granular materials is studied using Discrete Element Method. The output of the ODEC algorithm is implemented within the DEM software, PFC^{2D} and PFC^{3D} (Itasca, 1999) to model angular particles by means of a series of *Fish* functions that will convert a particle assembly of discs and spheres into their corresponding angular particles using the technique described in chapter 2.

7.2 Two-Dimensional Discrete Element Simulation

Direct shear test is performed to evaluate the influence of grain shape on the shear strength response of cohesionless soil. Angular materials dilate and rounded materials contract when subjected to shear. In this study, Daytona Beach sand (angular materials) and circular particles (rounded materials) were selected to simulate the direct shear test numerically.

To implement particle shape within DEM simulation, the circular particles are first generated within the desired range of grain sizes using discrete element modeling code PFC^{2D}. The shape conversion algorithm (Ashmawy et al., 2003) is then invoked to transform each circular particle into its angular equivalent through replacement with a corresponding set of circular discrete element cluster, selected randomly from the particle shape library.

7.2.1 Model Set-Up

To simulate direct shear test numerically, the size of direct shear box is chosen as 5 mm in height and 12 mm in width, which can be split into two halves. Even though from practical standpoint, it is not possible to prepare such a small sample, numerical results can still be compared with the real-world experiments with respect to the nature of variation in stress-strain and volume change behavior between angular and rounded materials. Since the purpose of the current study is to compare the shear induced dilative or contractive response of otherwise similar materials of different particle shapes, the grain size distribution and particle density are kept constant in all simulations, with a mean grain size of 0.375 mm. The inter-particle friction coefficient is taken as 0.5. The shear and normal stiffness of the wall forming the box are set to 1×10^7 N/m. Total 416 circular particles are generated within the box with a void ratio of 0.3. The density, shear and normal stiffness of the particles are set to 2500 kg/m^3, 1×10^7 N/m respectively. The linear-stiffness contact model is used in the analysis. Figure 7.1 shows the simulated model for direct shear box with Daytona Beach sand grains that is generated in PFC^{2D}. The circular particles are considered in the analysis because of their perfectly round shape. The direct shear simulation of the sample with circular particles also started with the same setup including the same properties as the Daytona Beach sand sample.

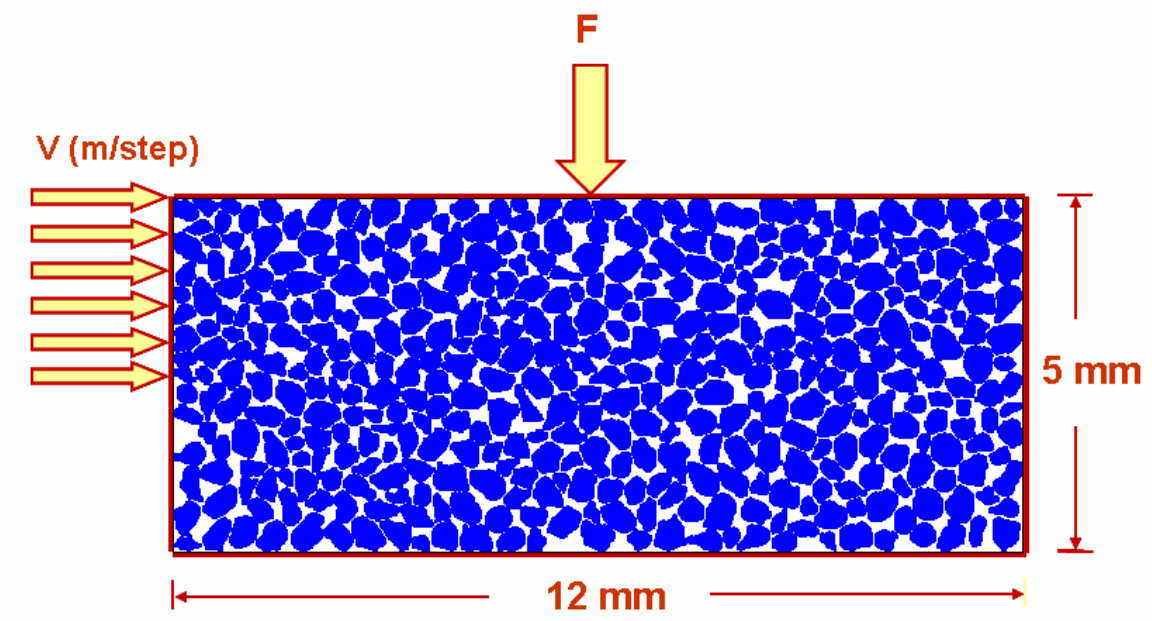

Figure 7.1 Two-Dimensional Direct Shear Test Simulation with Daytona Beach Sand Sample

7.2.2 Numerical Simulation

Soil specimen within the box is subjected to a vertical compressive load (F) and simultaneously sheared by applying a gradually increasing lateral load until the sample fails or the shear displacement reaches a certain value. The test is started by vertically moving the top wall of the box until a specific vertical stress (σ) is reached. The vertical force (F) is kept constant throughout the simulation by using Itasca's built-in servo-controlled *fish* functions that controls the movement of the top wall of the shear box. Figure 7.2 presents the history of servo-wall stress with time after application of normal load for Daytona Beach sand. After the vertical stress reaches a constant value, shearing stage is started by moving the upper half of the shear box laterally with a constant velocity of 5×10^{-3} m/step (V). The test is continued until the horizontal displacements are equal to 3.0 mm for Daytona Beach sand, and 2.8 mm for circular particles. Figure 7.3 shows the movement of the shear box after application of normal load and horizontal velocity after a certain time interval for Daytona Beach sand.

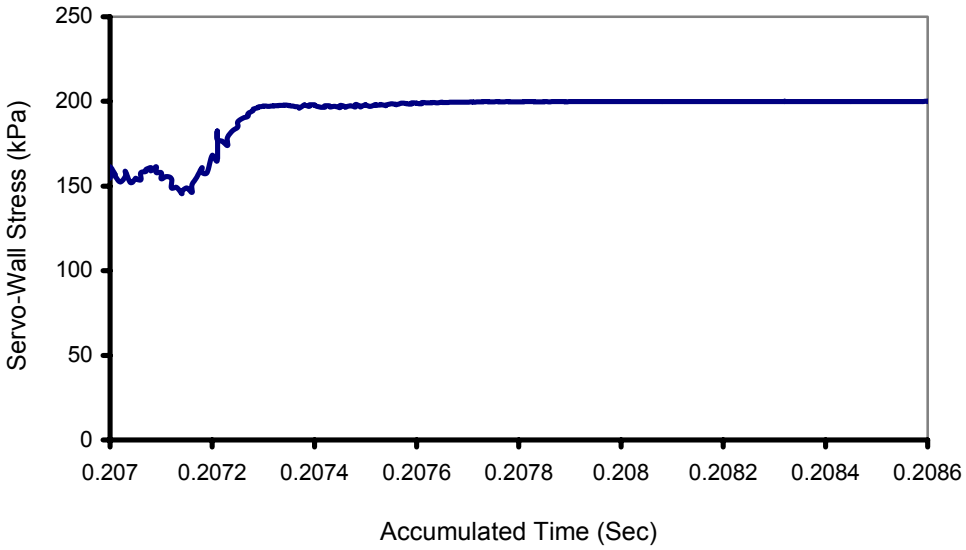

Figure 7.2 History of Servo-Wall Stress with Time

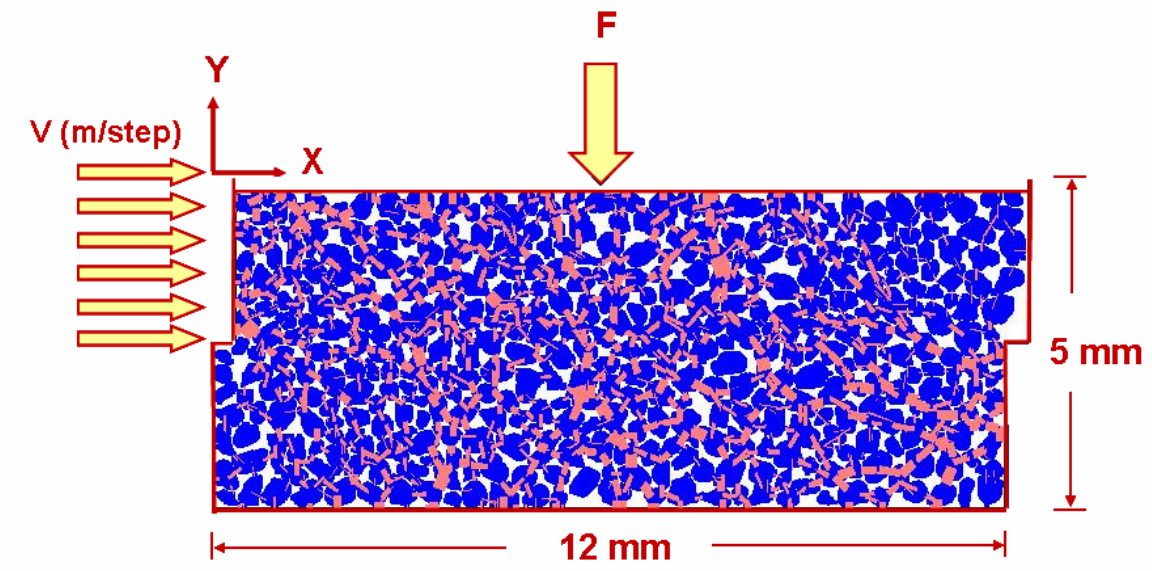

Figure 7.3 Movement of Shear Box with Daytona Beach Sand (2-D Simulation)

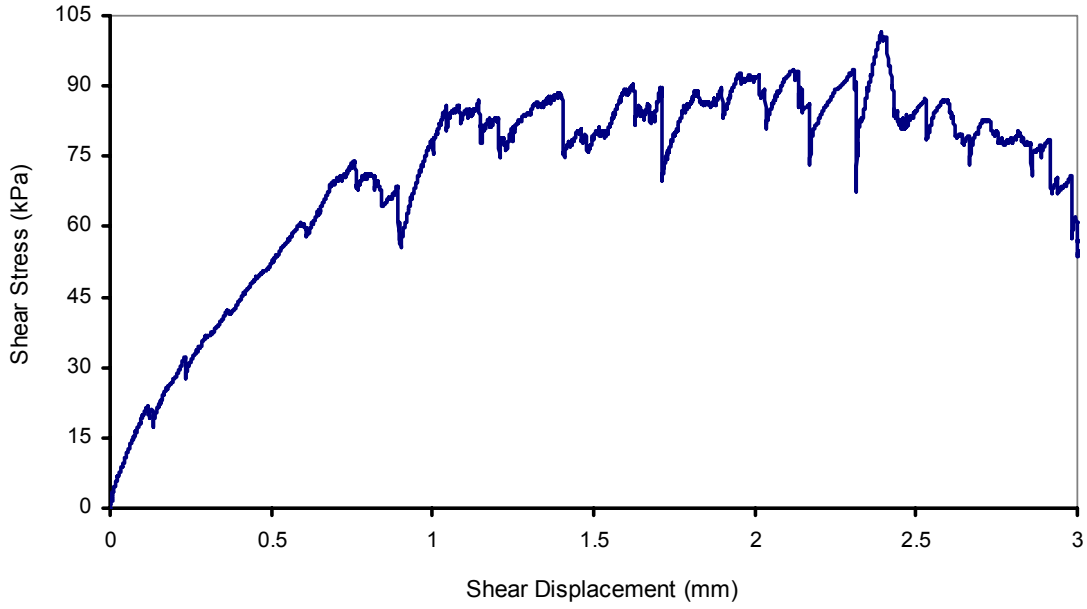

Figure 7.4 Variation of Shear Stress with Shear Displacement for Daytona Beach Sand Sample (Two-Dimensional Simulation)

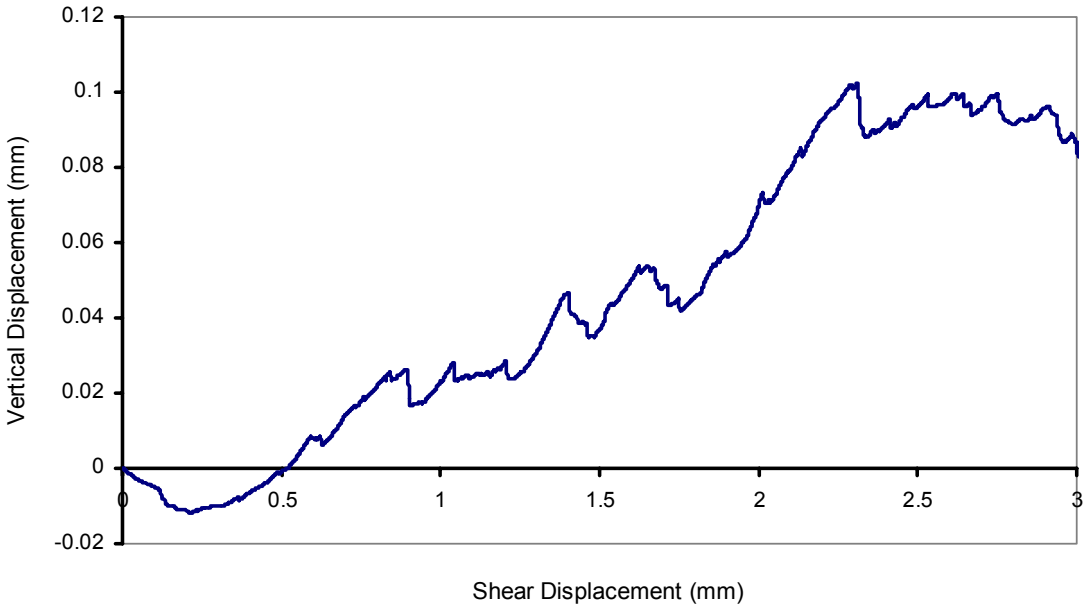

Figure 7.5 Variation of Vertical Displacement with Shear Displacement for Daytona Beach Sand Sample (Two-Dimensional Simulation)

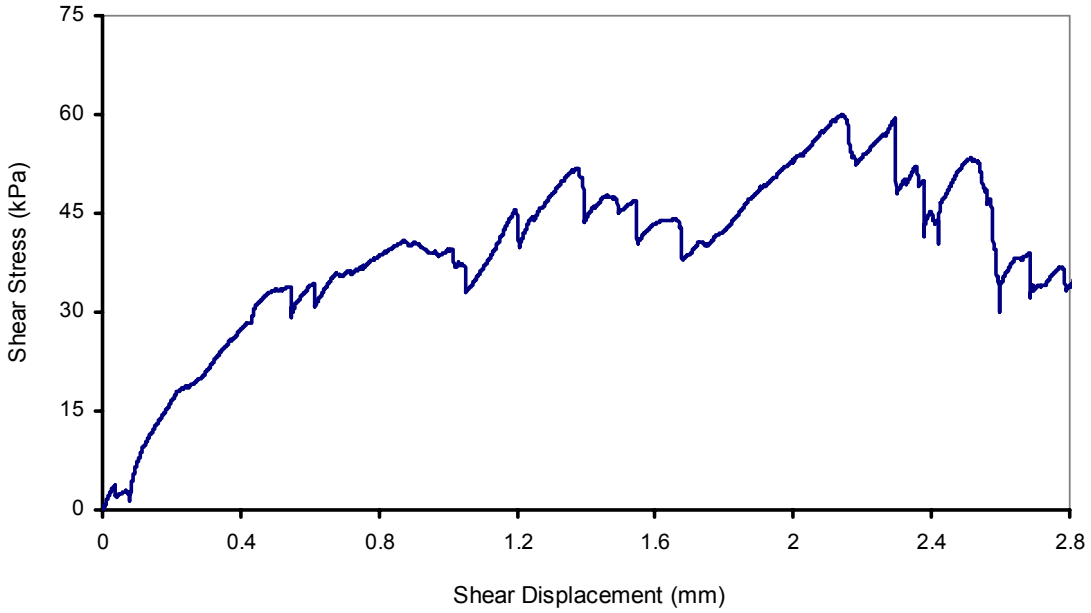

Figure 7.6 Variation of Shear Stress with Shear Displacement for Circular Particles (Two-Dimensional Simulation)

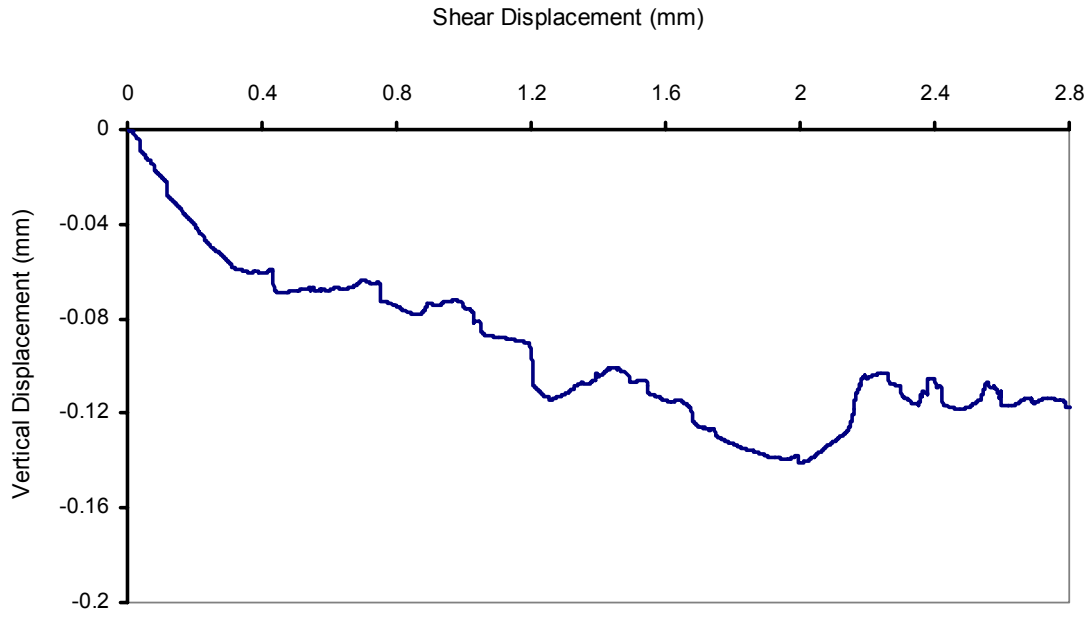

Figure 7.7 Variation of Vertical Displacement with Shear Displacement for Circular Particles (Two-Dimensional Simulation)

The variation of shear stress and vertical displacement with shear displacement are shown in Figure 7.4 through Figure 7.7 for Daytona Beach sand, and circular particles (σ = 200 kPa). From the stress-displacement plots, it is observed that the Daytona Beach sand sample possesses highest shear strength compared to the other material. Due to particle breakage and rearrangement, there are some spike drops in the stress-strain plot. From the displacements plots, it can be seen that, after initial contraction, the Daytona Beach sand exhibits dilation throughout the simulation due to the angularity of grains. On the other hand, the circular particles are predominantly contractive in nature which results from roundness of grains. The test is performed for four different normal stresses and the corresponding peak shear stresses are obtained. Table 7.1 presents the value of peak shear stresses for different applied normal stresses.

Table 7.1 Values of Maximum Shear Stresses for Different Vertical Stresses (Two-Dimensional Simulation)

Materials	Maximum Shear Stress (kPa)				$\tan\phi$	ϕ
	σ = 50 kPa	σ = 100 kPa	σ = 150 kPa	σ = 200 kPa		
Daytona Beach Sand	27.82	50.29	78.10	101.50	0.51	27^0
Circular Particles	15.07	33.89	45.91	59.89	0.31	17.2^0

The coefficients of internal shearing resistance ($\tan\phi$) are evaluated by plotting the shear stress values against normal stresses in Figure 7.8. The angles of internal friction for Daytona Beach sand sample and circular particles are 27^0 and 17.2^0 respectively. It is evident that the Daytona Beach sand sample possesses higher value of internal friction coefficient which can be explained by the angularity of the grains.

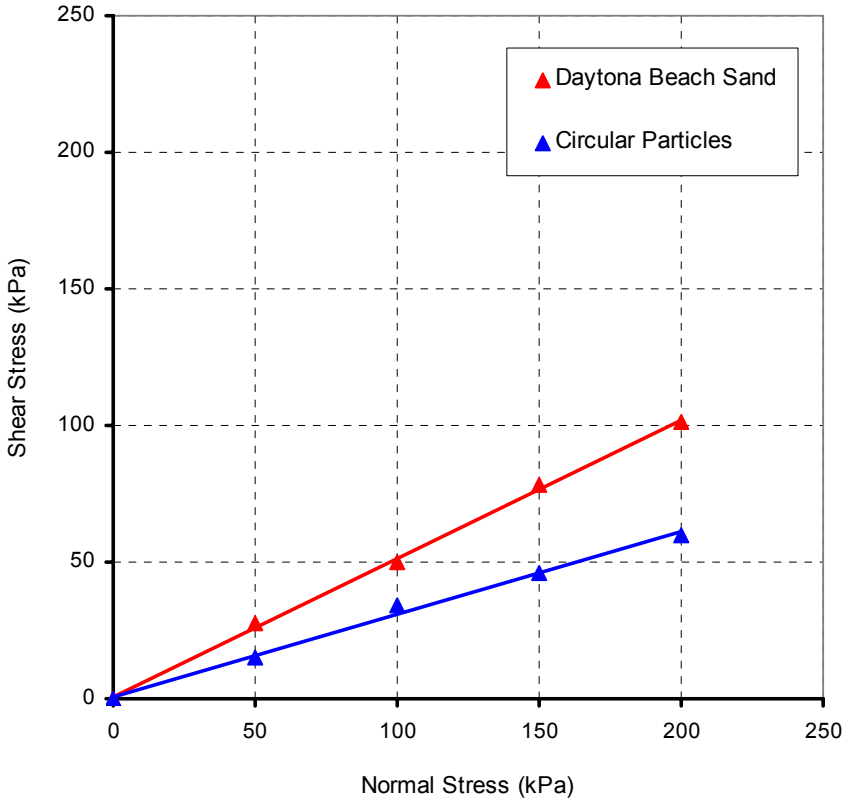

Figure 7.8 Variation of Shear Stress with Normal Stress (Two-Dimensional Simulation)

7.3 Three-Dimensional Discrete Element Simulation

From quantitative standpoint, three-dimensional discrete simulation is necessary to compare the test results with the experiments. Therefore, three-dimensional numerical simulation of direct shear test was performed to understand the real micromechanical behavior of granular media. The same materials are used for three-dimensional simulation as were used for two-dimensional simulation except the circular particles are replaced by spherical ones for three-dimensional simulation. To implement the particle shape within 3-D DEM simulation, discrete spherical particles are first generated within the desired range of grain sizes (as shown in Figure 7.9) using discrete element modeling code PFC^{3D} (Itasca, 1999). The shape conversion algorithm (described in Chapter 2) is then invoked to transform each spherical particle into its angular equivalent (as shown in Figure 7.10) following the same procedure as used for two-dimensional simulation.

7.3.1 Model Set-Up

The size of direct shear box is chosen as 2 mm in height, 4 mm in length and 4 mm in width. The grain size distribution and particle density are kept constant in all simulations, with a mean grain size of 0.375 mm. The inter-particle friction coefficient is taken as 0.5. The shear and normal stiffness of the wall forming the box are set to 1×10^3 N/m. Total 800 spherical particles are generated within the box with a void ratio of 0.45. The density, shear and normal stiffness of the particles are set to 2500 kg/m^3, 1×10^3 N/m respectively. Figure 7.9 and Figure 7.10 show the simulated model of direct shear box with spherical particles generated in PFC^{3D} and corresponding equivalent angular particles of Daytona Beach sand sample respectively.

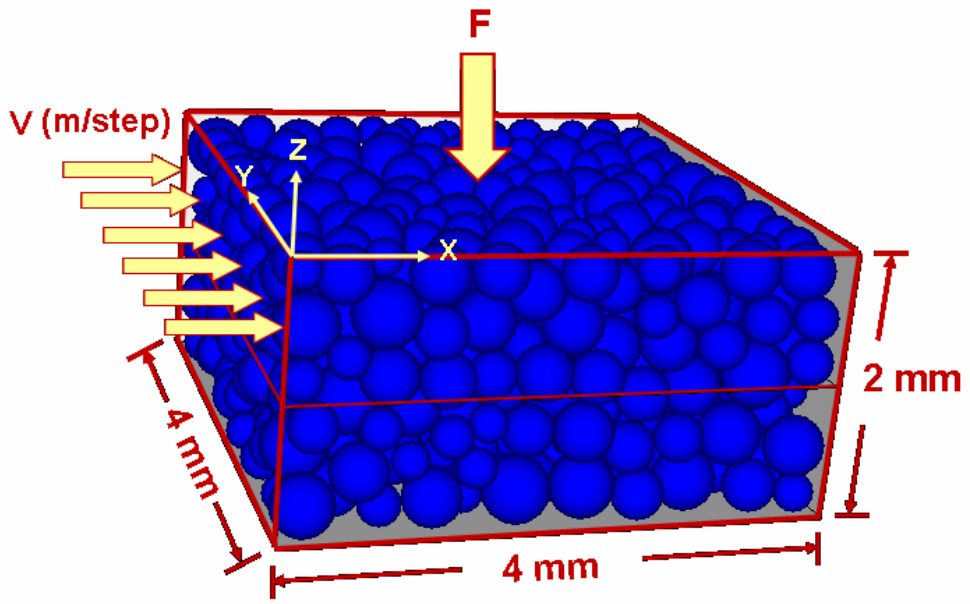

Figure 7.9 Three-Dimensional Direct Shear Test Simulation with Spherical Particles

7.3.2 Numerical Simulation

After generating the assembly of particles in PFC^{3D}, a vertical load (F) is applied on the top wall of the shear box and the force is kept constant throughout the simulation. After the vertical stress (σ) reaches a constant value, shearing stage is started by moving the upper half of the shear box to the right with a constant velocity of 5×10^{-3} m/step. The test

is continued until the horizontal displacements are equal to 2.1 mm for Daytona Beach sand sample and 1.6 mm for the materials with spherical particles (sample #2).

The variation of shear stress and vertical displacement with shear displacement are shown in Figure 7.11 through Figure 7.14 for Daytona Beach sand sample (σ = 250 kPa) and spherical particles (σ = 200 kPa) with different particle arrangements. The simulations are performed for three different particle assemblies. No significant variation is observed in stress-displacement and volumetric behaviors of spherical particles for different particle orientations whereas small variation is observed for Daytona Beach sand due to difference in fabric, coordination numbers and contact force chain generated for each assembly. From the stress-displacement plots, it is observed that the Daytona Beach sand (sample #1) possesses highest shear strength compared to the spherical particles. The same trend is observed in volumetric behavior for both the samples as was observed in two-dimensional simulation. After initial contraction, the Daytona Beach sand dilates due to angularity of the grains whereas the spherical particles contracts due to the roundness of the particles. The test is performed for three different normal stresses and the corresponding peak shear stresses are obtained. Table 7.2 presents the values of peak shear stresses and internal friction angles of Daytona Beach sand and spherical particles with three different particle assembly.

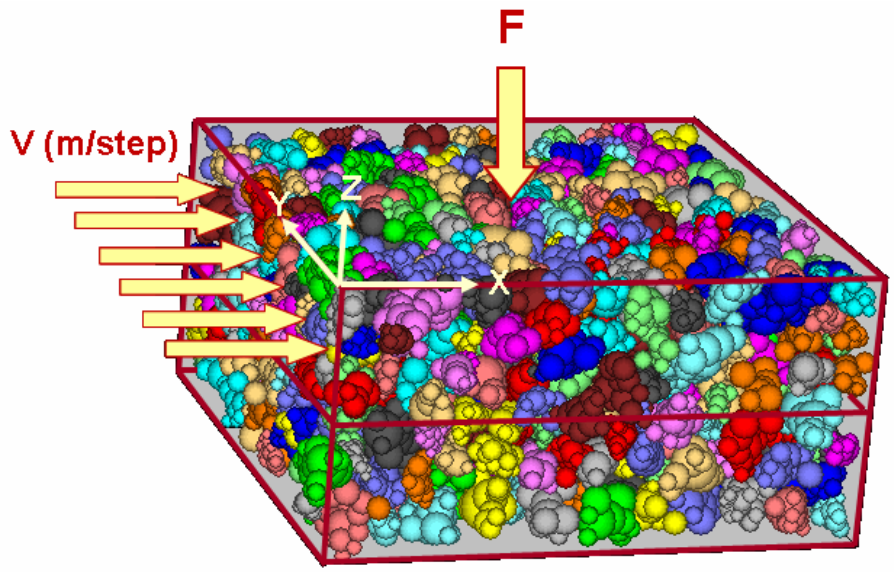

Figure 7.10 Three-Dimensional Direct Shear Test Simulation with Daytona Beach Sand Sample

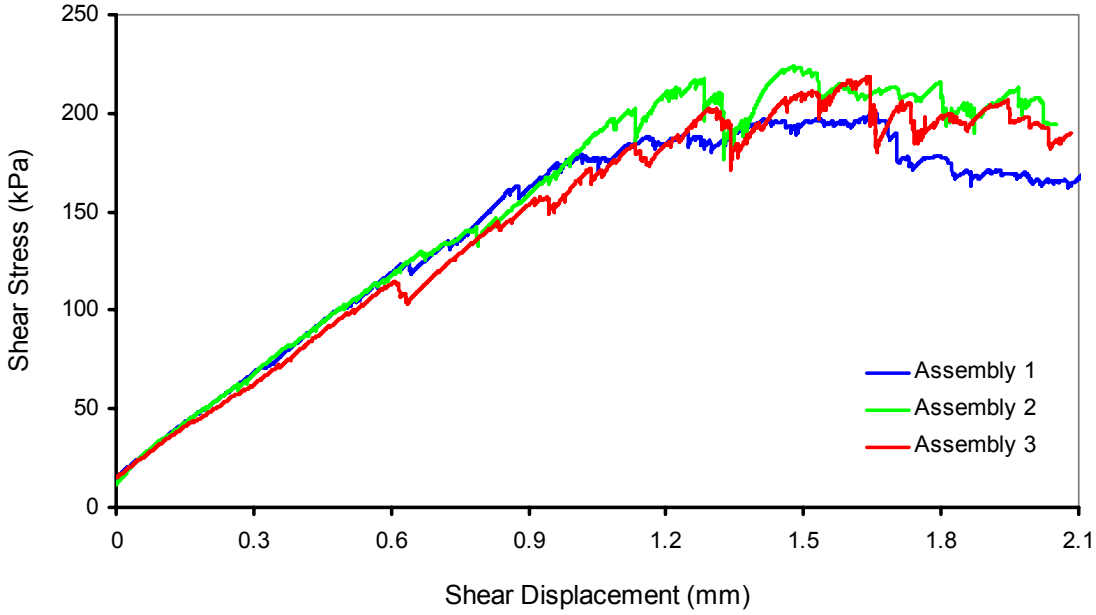

Figure 7.11 Variation of Shear Stress with Shear Displacement for Daytona Beach Sand Sample (Three-Dimensional Simulation)

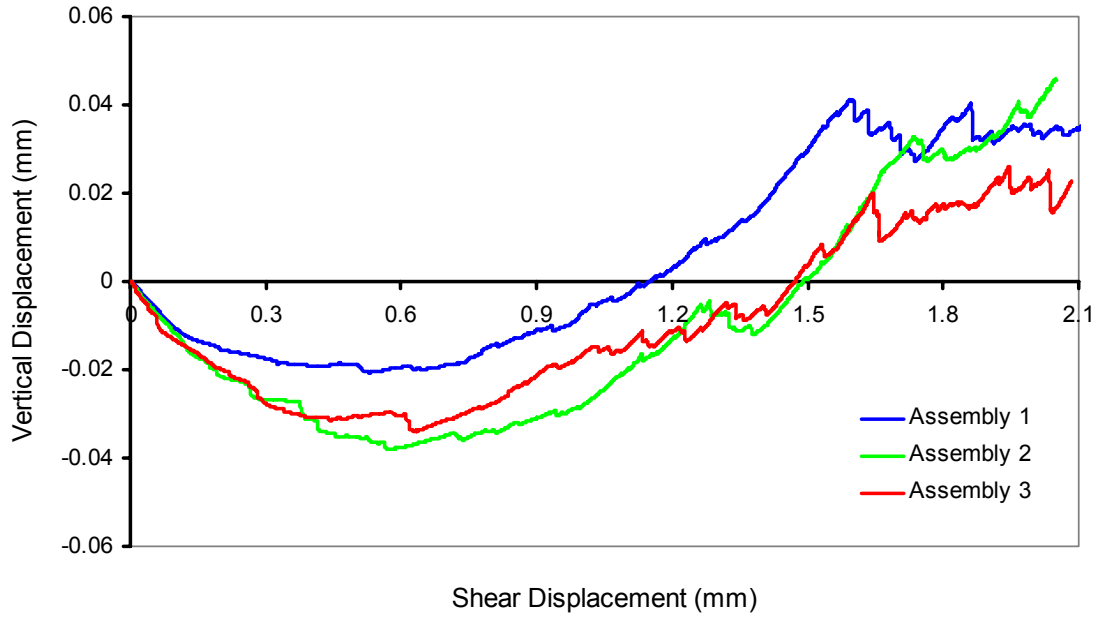

Figure 7.12 Variation of Vertical Displacement with Shear Displacement for Daytona Beach Sand Sample (Three-Dimensional Simulation)

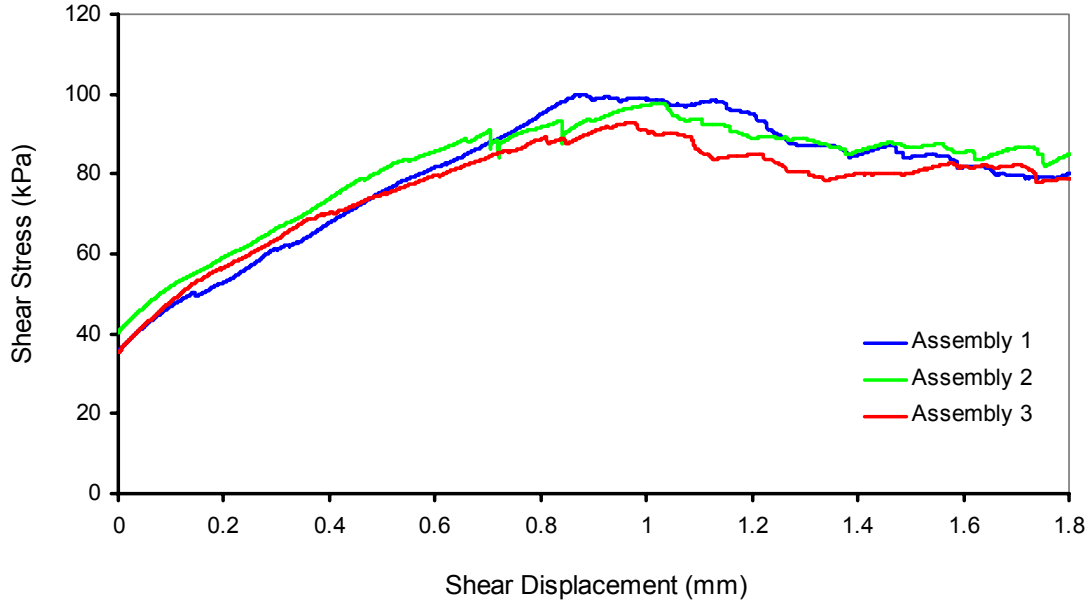

Figure 7.13 Variation of Shear Stress with Shear Displacement for Spherical Particles (Three-Dimensional Simulation)

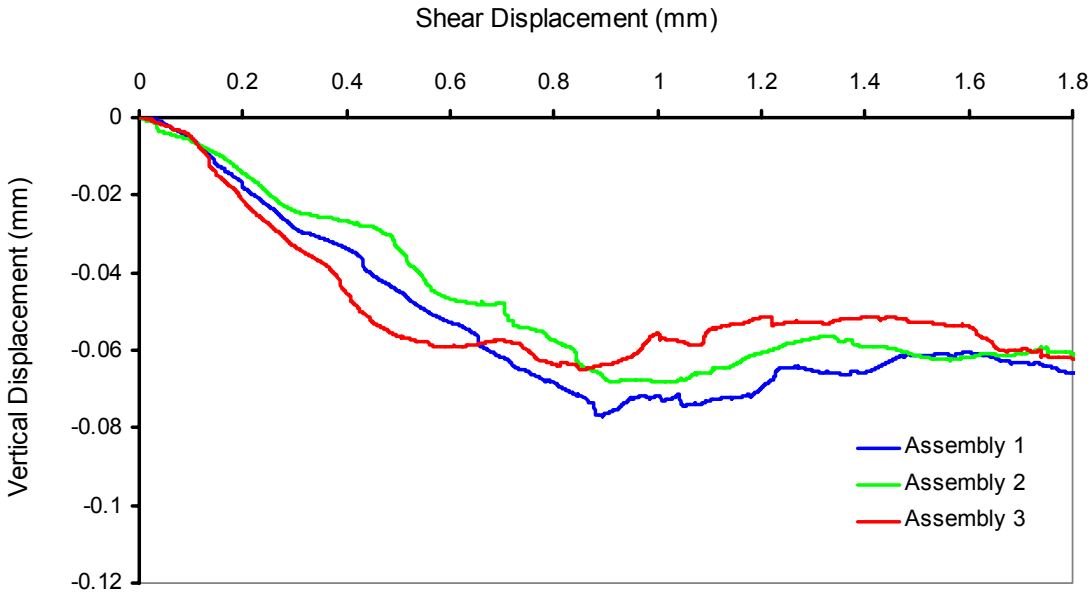

Figure 7.14 Variation of Vertical Displacement with Shear Displacement for Spherical Particles (Three-Dimensional Simulation)

Table 7.2 Values of Maximum Shear Stresses and Internal Friction Angles for Different Particle Arrangements (Three-Dimensional Simulation)

Materials	Particle Orientation	Maximum Shear Stress (kPa)			$\tan\phi$	ϕ
		σ = 150 kPa	σ = 200 kPa	σ = 250 kPa		
Daytona Beach Sand	Assembly 1	118.04	166.60	199.93	0.813	39.1^0
	Assembly 2	138.80	197.10	223.80	0.929	42.9^0
	Assembly 3	139.00	168.20	218.70	0.875	41.2^0
Spherical Particles	Assembly 1	82.95	100.04	111.80	0.50	26.6^0
	Assembly 2	82.09	97.76	104.40	0.474	25.3^0
	Assembly 3	79.35	92.86	107.90	0.467	25.0^0

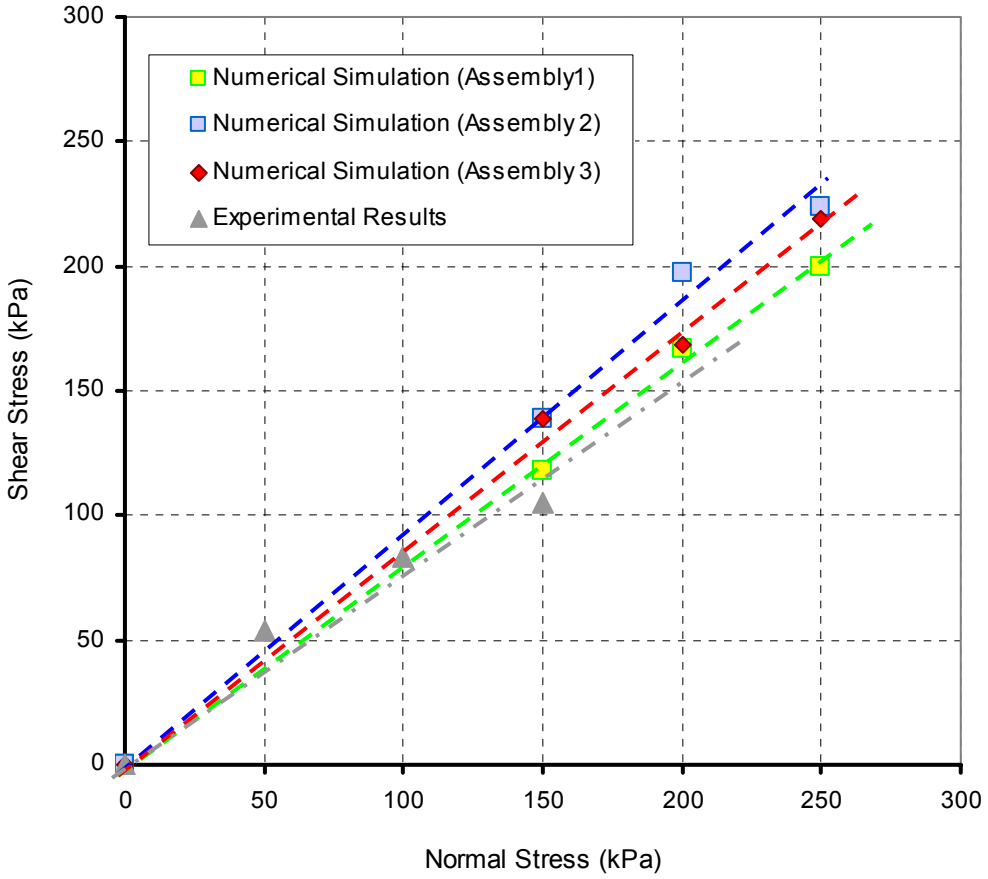

Figure 7.15 Variation of Shear Stress with Normal Stress for Daytona Beach Sand (Three-Dimensional Simulation)

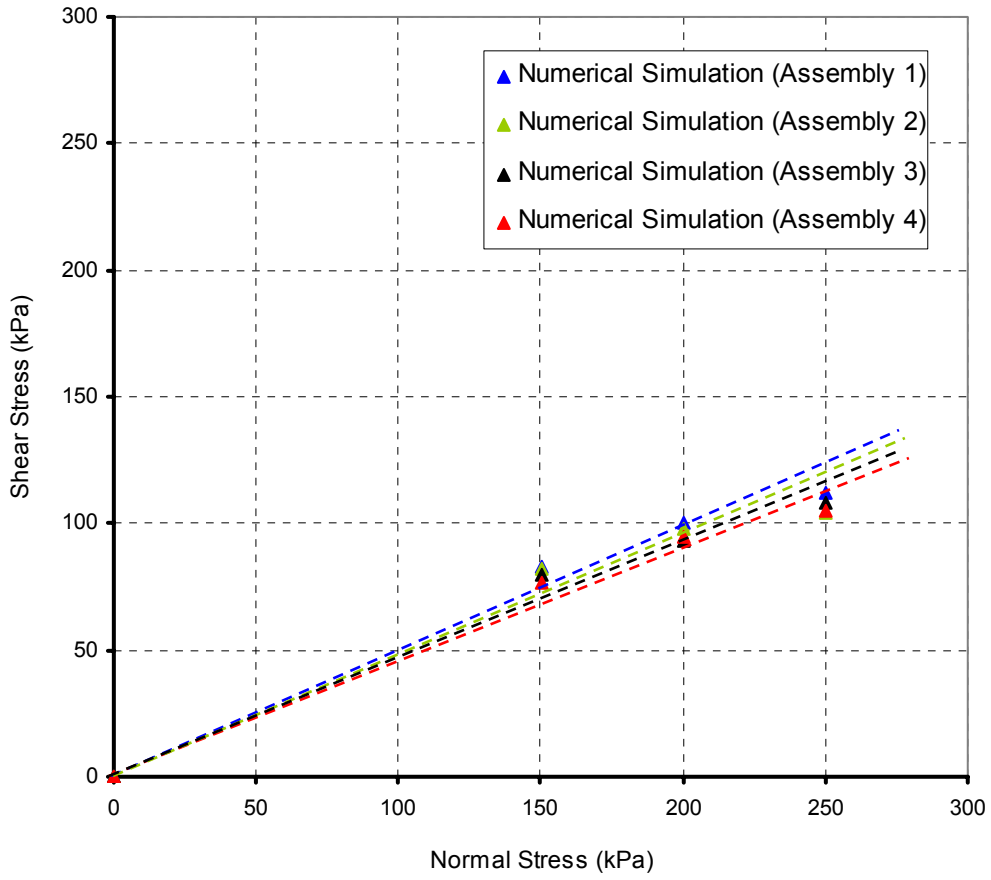

Figure 7.16 Variation of Shear Stress with Normal Stress for Spherical Particles (Three-Dimensional Simulation)

Table 7.3 Comparison of Internal Friction Angles Obtained from 2-D and 3-D Simulations

Material	2-D Simulation	3-D Simulation	Experiments
Daytona Beach Sand	27.0^0	$39.1^0 – 42.9^0$	37.4^0
Rounded Particles	17.2^0	$25^0 – 26.6^0$	$24.4^0 – 27^0$

Figure 7.15 and Figure 7.16 present the variation of shear stress with normal stress for different particle assemblies of Daytona Beach sand and spherical particles respectively. For comparison purpose, experimental data of direct shear test are collected from Rowan University (NJ) and plotted in Figure 7.15 for Daytona Beach sand sample

with normal stresses of 50 kPa, 100 kPa and 150 kPa. Even though three different numerical simulations produced significantly different particle arrangements, the angle of shearing resistance obtained from different particle assemblage are very close to each other for both materials. It is evident from the figures that the Daytona Beach sand sample possesses higher value of internal shearing resistance than the spherical particles due to particles angularity.

Table 7.3 summarizes the values of internal friction angle obtained from two-dimensional and three-dimensional simulations. By comparing experimental results with numerical simulations, it is found that the two-dimensional simulations underestimate the results for both materials. The angle of shearing resistance (ϕ) of Daytona Beach sand obtained from three-dimensional simulations varies from of $39.1^0 – 42.9^0$ which is close to the experimental value (37.4^0) whereas for rounded materials, the angle of shearing resistance varies from 25^0 - 26.6^0 which is within the range of internal friction angle of $24.4^0 – 27^0$ reported in literature (O'Sullivan et al., 2004, Phillips et al., 2006). Although two-dimensional simulation allows simplistic ways to capture and reconstruct particle images, three-dimensional simulation still remains more practical from quantitative standpoint.

7.4 Particle Shape Library

A particle shape library is developed in MS Excel format and will be made available online to the geotechnical community. The database is comprised of a wide variety of natural and processed sands, their morphological characteristics, size distributions, shape descriptors and other shape parameters. The database includes (1) general information on geomaterials regarding geographic location, particle size distribution, sample size; (2) pixel and voxel coordinate data of each particle; (3) quantitative descriptors such as Fourier Descriptors and (4) centers and radii of circular and spherical discrete elements used to reconstruct the angular particles. The geomaterial database is summarized in Table 7.4 and the Two-dimensional projection images of the sand samples are presented in Appendix A.

Table 7.4 Geomaterial Database

Type of Sand	Gradation			Location	Shape Descriptors				Sample Size
	D_{50} (mm)	D_{10} (mm)	C_u		Aspect Ratio	Elongation	Triangularity	Squareness	
Daytona	0.13	0.08	1.87	Florida	1.423	0.168487	0.078809	0.052109	130
Toyoura	0.20	0.17	1.24	Japan	1.333	0.139724	0.100307	0.0518	90
Michigan	0.34	0.26	1.39	Michigan	1.341	0.140109	0.063223	0.04587	100
Tecate	0.95	0.76	1.32	Mexico	1.421	0.168221	0.082782	0.057527	150
#1 Dry	0.27	0.13	2.46	New Jersey	1.420	0.167989	0.088005	0.054268	150
Kahala	0.70	0.50	1.52	Hawaii	1.426	0.167344	0.080716	0.048941	170
Hostun	0.58	0.41	1.66	France	1.377	-	-	-	110
Oxnard	0.8	0.53	1.60	California	1.401	-	-	-	120
Ala Wai	1.05	1.01	1.05	Hawaii	1.500	-	-	-	200
Std. Melt	0.28	0.14	2.29	New Jersey	1.501	-	-	-	200
Loire	0.73	0.52	1.5	France	1.403	-	-	-	130
Rincon	0.68	0.46	1.61	Puerto Rico	1.369	-	-	-	110
Long Beach	0.25	0.17	1.56	California	1.444	-	-	-	130
Fontainebleau	0.20	0.11	1.91	France	1.386	-	-	-	110
Arroyo Alamar	0.90	0.60	1.55	Tijuana	1.438	-	-	-	140
Clearwater	0.18	0.10	1.95	Florida	1.460	-	-	-	150
Rhode Island	0.25	0.19	1.42	Rhode Island	1.474	-	-	-	150
Boca Grande	0.20	0.16	1.31	Columbia	1.425	-	-	-	230
Red Sea	0.44	0.28	1.79	Egypt	1.369	-	-	-	90
Panama Malibu	0.25	0.18	1.47	Panama	1.289	-	-	-	70

Table 7.5 and 7.6 present the centers and radii of circular discrete elements of four particles for Daytona Beach and Michigan Dune sand samples and these data were used to reconstruct the assemblies of two-dimensional angular particles for discrete element modeling. The whole dataset cannot be shown in its entirety due to its large volume. Only a portion of the database is presented here. However, comprehensive information about the database will be compiled in the form of an online particle shape library.

Table 7.5 ODEC Data (2-D) for Daytona Beach Sand Grains (98% Area Coverage)

Type of Sand	Particle Index #	Disc #	X_c	Y_c	Radius
Daytona Beach Sand	1	1	0.044911	0.071133	0.837580
		2	-0.11790	-0.476535	0.666082
		3	-0.029098	0.603999	0.554822
		4	0.163326	-0.713364	0.384278
		5	-0.029098	0.367170	0.710642
		6	-0.014296	0.826027	0.397726
		7	0.533372	-0.121291	0.380554
		8	0.548174	0.248755	0.370046
		9	-0.088305	-0.269309	0.740092
		10	0.000506	0.011926	0.828109
		11	-.043900	0.485585	0.632335
	2	1	-0.042798	0.049540	0.765721
		2	0.005206	-0.366491	0.744529
		3	-0.026796	0.417568	0.734140
		4	0.389235	-0.638512	0.416031
		5	0.181219	0.737592	0.448034
		6	-0.154806	-0.622511	0.519238
		7	-0.202810	0.561578	0.534066
		8	0.213222	-0.510502	0.576043
	3	1	0.086271	0.140719	0.781997
		2	-0.632913	-0.379744	0.511787
		3	0.777067	0.055552	0.461458
		4	-0.244932	-0.162096	0.649161
		5	-0.793783	-0.493299	0.420223
		6	-0.074599	0.689570	0.336966
		7	0.341771	0.140719	0.674795
		8	1.051492	0.197496	0.243292
		9	0.956863	-0.143170	0.243292
		10	-0.093525	-0.020152	0.719433
		11	-0.973579	-0.682558	0.199621
	4	1	0.137521	0.140768	0.782373
		2	-0.336156	-0.486854	0.550490
		3	0.137521	0.543393	0.595991
		4	-0.691413	-0.996056	0.221225
		5	0.587513	0.081558	0.444979
		6	0.137521	1.005227	0.272364
		7	0.042785	-0.072387	0.720121
		8	-0.478259	-0.664482	0.442133
		9	-0.265104	-0.392118	0.598456
		10	0.090153	0.211819	0.746040
		11	-0.786149	-1.102633	0.153945
		12	0.8954036	0.06971	0.192772
		13	0.5993559	0.27102	0.364800
		14	-0.383524	0.318396	0.285191

Table 7.6 ODEC Data (2-D) for Michigan Dune Sand Grains (98% Area Coverage)

Type of Sand	Particle Index #	Disc #	X_c	Y_c	Radius
Michigan Dune Sand	1	1	0.069201	0.134643	0.805323
		2	-0.189597	-0.522703	0.623633
		3	0.131312	0.357210	0.778547
		4	-0.329348	-0.926428	0.331019
		5	-0.163717	-0.326017	0.705470
		6	0.457398	0.403793	0.492369
		7	-0.065374	-0.118979	0.748154
		8	0.012265	0.538368	0.580169
	2	1	-0.111929	-0.006224	0.846130
		2	0.227153	0.117078	0.798189
		3	-0.370865	-0.345307	0.625967
		4	0.498419	0.283537	0.565885
		5	-0.611306	-0.499436	0.411543
		6	0.603227	-0.148023	0.409878
		7	0.264144	0.708932	0.265960
		8	-0.438682	0.437666	0.344642
		9	-0.284553	-0.332977	0.642625
		10	0.036034	0.055427	0.838187
		11	0.812842	0.394510	0.270846
		12	-0.216737	0.006106	0.754115
	3	1	0.062274	0.366943	0.747018
		2	-0.075913	-0.349117	0.662960
		3	-0.031944	-1.096583	0.319109
		4	0.062274	0.775223	0.506954
		5	-0.057069	-0.079024	0.720619
		6	-0.069632	-0.694585	0.497448
		7	0.018306	-1.291302	0.212543
		8	0.074837	0.429756	0.737771
		9	0.018306	0.247600	0.745458
		10	0.049712	0.530255	0.679564
	4	1	0.259312	-0.047216	0.708469
		2	-0.789453	0.098815	0.498936
		3	0.591200	-0.080404	0.652664
		4	-0.278346	0.098815	0.638468
		5	-0.988585	0.085539	0.449215
		6	1.049205	-0.491945	0.209589
		7	0.033629	0.025800	0.697090
		8	0.777057	-0.219797	0.493386
		9	0.982827	0.112090	0.267576
		10	-0.497392	0.112090	0.577332
		11	-1.161167	-0.000751	0.283565

In the similar fashion, three-dimensional data for sand samples are complied in the database and these include the coordinates (X_c, Y_c, Z_c) of the center and radii of the spheres needed to capture the shape. Table 7.7 and Table 7.8 summarize the information about spherical discrete elements used to model a three-dimensional grain of Michigan Dune sand and Daytona Beach sand for 85% volume coverage which corresponds to 32 and 39 spheres for those two sand grains respectively.

Table 7.7 ODEC Data (3-D) for Michigan Dune Sand Grain (85% Volume Coverage)

Material	Particle Index #	Disc #	X_c	Y_c	Z_c	Radius
Michigan Dune Sand	1	1	0	-0.177794	0.400037	0.594681
		2	-0.222243	0.133346	0	0.556939
		3	0.133346	0.62228	-0.400037	0.440018
		4	-0.177794	-0.577832	0.577832	0.464057
		5	0.31114	0.400037	0.177794	0.400037
		6	0	0.355589	-0.533383	0.440018
		7	0.177794	-0.177794	-1.066766	0.28461
		8	-0.088897	-0.31114	-0.488934	0.291469
		9	0.355589	0.755626	-0.222243	0.384936
		10	-0.266691	-0.444486	0.93342	0.341416
		11	0.177794	-0.044449	0.400037	0.537074
		12	-0.133346	-0.222243	0.400037	0.581241
		13	0.088897	-0.266691	-0.222243	0.314299
		14	0	-0.400037	-0.844523	0.239363
		15	0.133346	0.444486	-0.711177	0.358356
		16	0.31114	1.066766	-0.222243	0.273999
		17	-0.355589	-0.177794	-0.044449	0.39756
		18	-0.177794	0.62228	-0.400037	0.332623
		19	0.133346	0.088897	-0.93342	0.255338
		20	0.222243	0.044449	0.62228	0.400037
		21	-0.355589	0	0.444486	0.39756
		22	-0.177794	-0.711177	0.62228	0.400037
		23	-0.400037	-0.666729	1.022317	0.239363
		24	0.31114	-0.444486	0.355589	0.314299
		25	0.400037	0.666729	0.222243	0.27037
		26	-0.133346	-0.31114	0.666729	0.480785
		27	0.266691	0.577832	-0.666729	0.323591
		28	-0.044449	0.93342	-0.400037	0.239363
		29	-0.355589	-0.444486	0.177794	0.332623
		30	-0.533383	0.177794	-0.044449	0.332623
		31	0	-0.400037	-1.155663	0.183266
		32	0.266691	-0.044449	-1.200112	0.208482

Table 7.8 ODEC Data (3-D) for Daytona Beach Sand Grain (85% Volume Coverage)

Material	Particle Index #	Disc #	X_c	Y_c	Z_c	Radius
Daytona Beach Sand	1	1	0.371605	0.222963	0.371605	0.532057
		2	-0.07432	-0.03716	-0.22296	0.501323
		3	-0.11148	0.074321	0.891852	0.442819
		4	0.557408	0.297284	-0.07432	0.445926
		5	-0.29728	-0.26012	0.334445	0.395022
		6	-0.26012	-0.07432	-0.66889	0.400231
		7	0.222963	0.297284	0.780371	0.450547
		8	0.520247	0.111482	-0.59457	0.308678
		9	-0.44593	-0.44593	-0.14864	0.317499
		10	-0.37161	-0.1858	0.74321	0.378964
		11	0	-0.14864	0.408766	0.462645
		12	-0.33445	-0.33445	-1.07766	0.262764
		13	0.780371	0.334445	0.222963	0.360284
		14	-0.52025	-0.48309	-0.66889	0.252035
		15	0.185803	0.074321	-0.11148	0.49856
		16	0.74321	0.334445	-0.26012	0.340582
		17	-0.14864	-0.03716	1.151976	0.319667
		18	0.074321	0	-0.70605	0.290233
		19	-0.55741	-0.52025	0.074321	0.260124
		20	0.148642	0.594568	0.631729	0.283006
		21	-0.66889	-0.44593	0.594568	0.200115
		22	-0.37161	0	-0.96617	0.24928
		23	0.222963	0.222963	1.114815	0.270533
		24	0.891852	0.334445	0.037161	0.315317
		25	0.260124	0.557408	0.260124	0.292602
		26	-0.44593	-0.22296	1.040494	0.240828
		27	-0.37161	-0.29728	-0.29728	0.365989
		28	0.445926	0.371605	0.74321	0.350571
		29	-0.33445	-0.40877	-1.26346	0.213471
		30	-0.59457	-0.63173	-0.33445	0.200115
		31	-0.22296	-0.22296	0.037161	0.430164
		32	0.408766	0.074321	-0.85469	0.203536
		33	0.631729	0.148642	-0.70605	0.24928
		34	0.222963	0.520247	-0.03716	0.260124
		35	-0.26012	0.260124	-0.33445	0.24928
		36	-0.59457	-0.33445	0.780371	0.246495
		37	-0.48309	-0.59457	-0.92901	0.161979
		38	0	0.408766	0.817531	0.315317
		39	0.260124	0.074321	0.445926	0.48877

CHAPTER 8
SUMMARY AND CONCLUSIONS

This chapter provides a summary and draws conclusions of the research effort presented in the previous chapters. A comprehensive research has been conducted on three-dimensional characterization of particle morphology and discrete element modeling to understand the effect of particle shape on the behavior of geomaterials.

8.1 Summary and Conclusions

A wide variety of sand samples having different angularity and roundness were collected for the purpose of the current study. Two-dimensional images of the sand grains were acquired using the microscope system and image analysis software and the acquired images were processed through successive steps of erosion, dilation and contrast enhancement techniques to obtain the final binary images of the particles. In three dimensions, particle shapes were characterized using X-ray CT, which generated stacks of two-dimensional images. These image stacks were then combined together to reconstruct three-dimensional shape of the particles and to obtain three-dimensional surface points in voxel format.

After shape characterization, particle shape quantification was performed in order to design an optimum sample size and to investigate the relationship between grain size and shape. The grain shapes were quantified using Fourier shape descriptors and the first four Fourier descriptors were used to investigate the relationship between grain size and shape.

Considering the importance of optimum sample size selection to any experimental design, a suitable methodology was established to obtain sample size for various sand samples. The optimum sample size of a particular sand sample was determined based on

the variability in size and shape of particles within that sample. In the current study, sample size was found to vary from 70 (for Panama Malibu Beach sand) to 230 (for Boca Grande Beach sand). Selection of an optimum sample size is important to increase accuracy of numerical simulation and it can save significant amount of resources.

The study verified any existing relationship between grain size and grain shape using six different natural and processed sand samples. Though in the previous literature strong relationships were documented, the current research verified that there is no relationship between grain size and grain shape in terms of circularity, elongation, triangularity and squareness for the sand samples analyzed. It should be noted that the grain shapes are highly variable in nature and they are likely to be influenced by the origin and mineralogical compositions, distance of transport, mechanical and chemical processes, velocity of the transporting medium and the depositional environment (aeolian, fluvial, glacial). Considering all these factors, it is unlikely to identify a universal relationship between grain size and grain shape for all sands. Even though the sands in the current study came from different sources and underwent considerably different depositional processes, no relationship was found between shape and size. As such, discrete element models of angular particle assemblies were constructed by selecting the shapes belonging to a particular sand sample randomly from its particle shape library, irrespective of size. However, all the sand samples used in the study to evaluate the size-shape relationship were uniformly-graded. Therefore, it is suggested to perform the analysis on well-graded sand samples to confirm the veracity of the above statement.

This research presented a detailed particle shape modeling procedure in two and three dimensions using the ODEC technique. A skeletonization algorithm was developed to automate the ODEC technique and the algorithm is capable of generating skeleton of any irregular shape. The ODEC2D and ODEC3D algorithms were found to model irregular particle shape accurately in two and three dimensions respectively. It was observed that 8 to 16 discs are sufficient to capture the shape accurately in two dimensions, resulting an uncovered area of 2% (error). However, based on the analysis, an area coverage of 95% was considered as a reasonable threshold for this experimental

design and the corresponding number of discs varied from 4 to 8 for Daytona Beach sand sample. Three-dimensional shapes were modeled using ODEC3D algorithm with an error of 5% in grain volume which corresponds to 123-133 spherical elements for Daytona Beach sand and 98-126 spherical elements for Michigan Dune sand. No specific value of error threshold could be established for volume coverage, because very limited number of particles were modeled using the ODEC technique in three dimensions due to large volume of data sets. After modeling particle shape using the ODEC technique, shapes were then implemented within discrete element modeling software, PFC^{2D} and PFC^{3D} by using shape conversion algorithm.

Numerical Simulation of direct shear test was performed to study the effect of grain shape on shear strength characteristics of granular soil. Daytona Beach Sand was chosen to study the effect of particle shape on the shear strength behavior of the granular soils. To compare the behavior of angular Daytona Beach sand with rounded materials, circular and spherical particles were used in the study for two-dimensional and three-dimensional simulations respectively. It was observed that the stress-strain and volumetric behavior of simulated materials followed typical soil behavior of angular and rounded particles. Angularity of grains and interlocking effect contributed more shearing resistance and higher shear strength in Daytona Beach sand in comparison with spherical particles. The three-dimensional simulation was repeated three times to generate three different particle assemblies and to study the effect of particle orientation on the shear strength response of granular soil. No significant variation was observed between spherical assemblies whereas small variation was observed between assemblies of Daytona Beach sand sample due to the difference in coordination numbers of the three assemblies. A very small-size model with limited number of particles was generated in PFC to reduce the computation time. The increase in the dimension of shear box, total number of particles within the assembly and number of spheres within each particle can increase the accuracy of the model estimation results. Angle of shearing resistance was computed from numerical simulation and the results obtained from three-dimensional simulations are in good agreement with the values reported in literature and obtained through experiments. A direct comparison was made between two-dimensional and three-

dimensional peak angle of internal friction (ϕ) and higher value of ϕ and hence higher shear strength were obtained from three-dimensional simulation. From practical standpoint it would not be appropriate to compare the results between two and three-dimensional simulations because only two different types of shapes of Daytona Beach sand sample were characterized due to large number of surface data points and the number of spherical discrete elements within each clump was limited to 15 to reduce the computation time in three-dimensional simulation, still three-dimensional characterization and modeling is more practical in order to simulate soil behavior accurately from computational standpoint.

8.2 Methodological Contributions

The automation of ODEC2D algorithm and development of ODEC3D algorithm in the current study can be considered as a valuable contribution in the field of geotechnical engineering, particularly in three-dimensional discrete element modeling. This method would allow modeling any number of particles of arbitrary shape with a desired level of accuracy. Grain shape can be modeled more realistically using the ODEC method compared to other ellipsoid or polyhedron based approach (Lin and Ng, 1997; Ghaboussi and Barbosa, 1990) and the percent error in grain volume was found to be less than that obtained from another sphere-based approach proposed by Matsushima (2004). The main contribution of this research effort is to automate the entire multi-phase procedure starting from image capturing, reconstruction to three-dimensional particle shape modeling and finally linking the process to discrete element modeling framework by implementing three-dimensional particle shape into DEM environment which will allow researchers to simulate particulate behavior of cohesionless soil numerically.

The relationship between grain size and shape was explored and documented in the literature, but the concept has never been applied in the area of discrete element modeling. For example, size-shape relationship is important for generating and reconstructing particle assemblies in DEM environment. If any such relationship exists, then it would be necessary to divide the particle size into different bins in order to generate representative assemblies of angular particles for discrete element modeling

simulation. In other situations, where there is no relationship between grain size and shape such as in case of poorly-graded sand samples as evidenced from the present study, shapes belonging to a particular sand sample can be selected randomly from its particle shape library irrespective of size for DEM simulation. Therefore, understanding such relationship would certainly improve the accuracy of numerical simulation.

The study also develops a methodology to select an optimum sample size for each sand sample. The idea of using optimum sample size has never been taken into account in early research efforts in micromechanical modeling. The study explicitly considers that the behavior of a soil mass is greatly influenced by the variability of the particle shapes (sample size) within the sample. The use of small sample size may lead to inaccurate results while too large sample size can result inefficient use of resources.

8.3 Practical Contributions

The development of an online particle shape library will be an extremely valuable contribution for future research on granular particle morphology. In this study, a particle shape library was developed in excel format and the images of different natural and processed sand samples, their locations, grain size distributions, sample size, quantitative shape descriptors, pixel and voxel coordinates of each particle, centers and radii of circular and spherical discrete elements used to reconstruct the two-dimensional and three-dimensional angular particles were compiled in the database. It would be the most diverse particle shape library in the field of discrete element modeling. This database will be made available online and would provide researchers an instant access to a diverse range of particle morphology data to simulate different aspects of micromechanical behaviors of granular soil and such arrangement would potentially reduce the sample collection, image capturing and reconstruction effort.

The research methodology presented in this study can have significant contribution to many areas in the field of geotechnical engineering. For example, this research can be applied to pavement engineering to study the strength and deformations characteristics of base, sub-base layers of granular substructures. The study can also be applied in numerical simulation of stress-strain relationship and stress-paths to

understand the dilative/contractive behavior and deformation characteristics of granular material. Another potential application of the current research could be to study the influence of particle shape on liquefaction behavior of cohesionless soil in earthquake-prone regions.

Other practical applications of this research could be studying the effect of grain shape on the flow rate of materials flowing from hopper, modeling dynamic behavior of debris during rockfall which is important for cliff stabilization, designing geotechnical interfaces, selecting suitable materials for constructions, studying surface roughness of sand grains, soil-structure interaction and others.

8.4 Future Recommendations

This section addresses some future recommendations and shed light on some potential future research problems for further extension of the current research effort.

Applications of advanced mathematical techniques are rapidly emerging in the field of micromechanical modeling. Such techniques have been contributing in gaining computational efficiency and solving many unsolved complex problems in geotechnical engineering. The application of spherical harmonics in quantitative characterization of particle surface by means of three-dimensional shape descriptors is one of the finest examples that hold enormous promise in the future of three-dimensional quantification of particle morphology. The spherical harmonic series algorithm can be used to obtain surface information in terms of three-dimensional shape descriptors and to reconstruct the particle surface accurately.

It was concluded from the current study that there is no relationship between grain size and shape for the sand samples analyzed. However, it is necessary to perform the analysis on well-graded sand samples to verify the relationship. Use of three-dimensional shape descriptors to explore the size-shape relationship would be an interesting future research topic.

As previously mentioned, the three-dimensional modeling was performed on very limited number of different particle shapes, which may be considered as a limitation of the present analysis. Therefore, it is suggested that sufficient number of different

particle shapes as much as the optimum sample size should be used to perform the three-dimensional simulation to closely capture the actual behavior of soil. Very small size of specimen was used in the study which warrants a bigger specimen size with more number of sand particles for numerical simulation to compare it with experimental results. Evaluating the effect of three-dimensional grain shape on the liquefaction susceptibility of granular soil by using the ODEC technique will be a worth while extension of the current research effort and a valuable contribution in the field of geotechnical engineering.

This research methodology can also be extended to study the surface roughness of particles, grain crushing during shear, the influence of three-dimensional particle shape on the flow rate of granular materials flowing from hoppers. The behavior of the interface between two materials (soil-foundation or soil-geosynthetic interface) can also be investigated.

REFERENCES

Alarcon-Guzman, A., Leonards, G.A., and Chameau, J.L. (1988). Undrained monotonic and cyclic strength of sands. Journal of Geotechnical Engineering, 114(10), 1089-1109.

Alshibi, K.A., and Alsaleh, M.I. (2004). Characterizing surface roughness and shape of sands using digital microscopy. Journal of Computing in Civil Engineering, 18(1), 36-45.

Anderson, G.E. (1926). Experiments on the rates of wear of sand grains. Journal of Geology, 34, 144-158.

Arulanandan, K., Seed, H. B., Yogachandran, C., Muraleetharan, K. K., and Seed, R. B. (1993). Centrifuge study on volume changes and dynamic stability of earth dams. Journal of Geotechnical Engineering, 119(11), 1717-1731.

Ashmawy, A.K., Sukumaran, B., and Hoang, A.V. (2003). Evaluating the influence of particle shape on liquefaction behavior using Discrete Element Method. Proceedings of the thirteenth international offshore and polar engineering conference (ISOPE 2003), Honolulu, Hawaii, May 2003.

Balazs, R.J., and Klein, G.D. (1972). Roundness-mineralogical relations of some intertidal sands. Journal of Sedimentary Petrology, 42(2), 425-433.

Banerjee, I. (1964). Size-roundness relation in the Barakar sandstones of the south Karanpur Coalfield, India. Sedimentology, 3, 22-28.

Barbosa, R., and Ghaboussi, J. (1992). Discrete finite element method. Engineering Computations, 9, 253-266.

Barret, P.J. (1980). The shape of rock particles, a critical review. Sedimentology, 27, 291-303.

Bathurst, R.J., and Rothenburg, L. (1989). Investigation of micromechanical features of idealized granular assemblies using DEM. Proceedings of the 1st US Conference on Discrete Element Methods, CSM, Golden, CO (1989); Engineering Computations, 9, 199-210 (1992).

Been, K., and Jefferies, M. G. (1985). A state parameter for sands. Geotechnique, 35(2), 99-112.

Been, K., Jefferies, M. G., and Hachey, J. (1991). The critical state of sands. Geotechnique, 41(3), 365-381.

Bolton, M.D. (1986). The strength and dilatancy of sands. Geotechnique, 36(2), 65-78.

Borgefors, G., Nyström, I., and Baja, G.S.D. (1999). Computing skeletons in three dimensions. Pattern Recognition, 32(7), 1225-1236.

Bowman, E.T., Soga, K., and Drummond, W. (2001). Particle shape characterization using Fourier descriptor analysis. Geotechnique, 51(6), 545-554.

Chen, J.W., Lin, C.Y., and Lee, W.F. (2003). Dilative Behavior of Granular Materials. International Journal of Offshore and Polar Engineering, 13(4).

Cho, G., Dodds, J, and Santamarina, J.C. (2006). Particle shape effects on packing density, stiffness, and strength: natural and crushed sands. Journal of Geotechnical and Geoenvironmental Engineering, 132(5), 591-602.

Chu, J., and Lo, S. C. R. (1993). On the measurement of critical state parameters of dense granular soils. Geotechnical Testing Journal, 16(1), 27-35.

Chuang, J.-H., Tsai, C.-H., and Ko, M.-C (2000). Skeletonization of three-dimensional object using generalized potential field. IEEE Transactions on Pattern Analysis and Machine Intelligence, 22(11), 1241-1251.

Clark, M.W. (1981). Quantitative shape analysis: a review. Mathematical Geology, Vol. 13(4), 303-320.

Cleary, P.W. (2000). DEM simulation of industrial particle flows: case studies of dragline excavators, mixing in tumblers and centrifugal mills. Powder Technology, 109(1), 83-104.

Conolly, J.R. (1965). The occurrence of polycrystallinity and undulatory extinction in quartz in sandstones. Journal of Sedimentary Petrology, 35, 116-135.

Cubrinovski, M., and Ishihara, K. (2002). Maximum and minimum void ratio characteristics of sands. Soils and Foundations, 42(6), 65-78.

Cundall, P. A. (1971). A computer model for simulating progressive large scale movements in block rock systems. Proceedings of the Symposium of the International Society of Rock Mechanics, Nancy, II, Article 8.

Cundall, P. A., and Strack O. D. L. (1979). A discrete numerical model for granular Assemblies. Geotechnique, 29, 47-65.

Cundall, P. A., and Strack O. D. L. (1979). The distinct element method as a tool for research in granular media, Part II. Report to NSF, Department of Civil and Mineral engineering, University of Minnesota. Minneapolis, MN.

Das, N. and Ashmawy, A.K. (2007). Relationship between grain size and shape of natural and crushed sand. Geo-Denver 2006 Conference, Denver, CO.

Diepenbroek, M., Bartholoma, A., and Ibbeken, H. (1992). How round is round? A new approach to the topic 'roundness' by Fourier grain shape analysis. Sedimentology, 39, 411-422.

Dinesh, S.V., and Sitharam, T.G. (2003). discrete element simulation of liquefaction behavior of granular soils under cyclic loading. CPFTEGE.

Dodds, J. (2003). Particle shape and stiffness - effects on soil behavior. M.S.C.E. Thesis, Georgia Institute of Technology, GA.

Dowdeswell, J.A. (1982). Scanning electron micrographs of quartz sands from cold environments examined using Fourier Shape Analysis. J. Sediment. Petrol., 52(4), 1315-1323.

Dyskin, A. V., Estrin, Y., Kanel-Belov, A. J., and Pasternak, E. (2001). Toughening by fragmentation - How topology helps. Adv. Eng. Mater., 3(1), 885-888.

Ehrlich, R., Brown, J., Yarus, J. M., and Przygocki, R. S. (1980). The origin of shape frequency distributions and the relationship between size and shape. J. Sediment. Petrol., 50(2), 475-484.

Ehrlich, R., and Weinberg, B. (1970). An exact method for characterization of grain shape. J. Sediment. Petrol., 40(1), 205-212.

Favier, J., Abbaspour-Fard, M, Kremmer, M., and Raji, A. (1999). Shape representation of axi-symmetrical, non-spherical particles in discrete element simulation using multi-element model particles. Engineering Computations, 16, 467-480.

Flook, A.G. (1979). The characterization of textural and structural profiles by the automated measurement of their fractal dimensions. 2nd European Symposium on Particle Characterization, 591-599.

Folk, R.L. (1978). Angularity and silica coatings of Simpson Desert sand grains, Northern Territory Australia. Journal of Sedimentary Petrology, 48, 611-624.

Fraser, H. J. (1935). Experimental study of the porosity and permeability of elastic sediments. Journal of Geology, 13(8), 910-1010.

Garboczi, E.J. (2002). Three-dimensional Mathematical Analysis of Particle Shape using x-ray Tomography and Spherical Harmonics: Application to Aggregates used in Concrete. Cement and Concrete Research, 32(10), 1621-1638.

Ghaboussi, J., and Barbosa, R. (1990). Three-dimensional discrete element method for granular materials. International Journal for Numerical and Analytical Methods in Geomechanics, 14, 451-472.

Gonzalez, R.C., and Woods, R.E. (2003). Digital image processing. Prentice Hall.

Goudie, A.S., and Watson, A. (1981). The shape of desert sand grains. Journal of Arid Environment, 4, 185-190.

Holtz, R.D., and Kovacs, W.D. (1981). An Introduction to Geotechnical Engineering. Prentice-Hall, Inc., Englewood, Cliffs, NJ.

Houlsby, G.T. (1991). How the dilatancy of soils affects their behavior. European Conference on Soil Mechanics and Foundation Engineering, 4, 1189-1202.

Hunt, A.R. (1887). The evidence of the Skerries Shoal on the wearing of fine sand by waves. Devonshire Association for the Advancement of Science, Literature and Art, Report and Transactions, 19, 498-515.

Inman, D.L. (1953). Areal and seasonal variations in beach and nearshore sediments at LaJolla, California. U.S. Army Corp. of Engineers, Beach Erosion Board, Tech. Memo 39, 134.

Inman, D.L., Ewing, G.C., and Corliss, J.B. (1966). Coastal sand dunes of Guerrero Negro, Baja, California, Mexico. Geological Society of America Bulletin, 77, 787-802.

Ishihara, K. (1985). Stability of natural deposits during earthquakes. Proc. 11th Int. Conf. Soil Mechanics and Foundation Engineering, San Francisco, CA, 1, 321-376.

Itasca Consulting Group (1999). Particle Flow Code in Two Dimensions. Software Version 3.1.

Itasca Consulting Group (1999). Particle Flow Code in Three Dimensions. Software Version 3.1.

Iyer, N., Jayanti, S., Lou, K., Kalyanaraman, Y., and Ramani, K. (2005). Three-dimensional shape searching: state-of-the-art review and future trends. Computer-Aided Design, 37, 509–530.

Janoo, V. (1998). Quantification of shape, angularity, and surface texture of base course materials. Special Report 98-1, Cold Regions Research & Engineering Laboratory, US Army Corps of Engineers.

Jensen, R., Bosscher, P., Plesha, M., and Edil, T. (1999). DEM simulation of granular media-structure interface: effect of surface roughness and particle shape. International Journal for Numerical and Analytical Methods in Geomechanics, 23, 531-547.

Jensen, R.P., Edil, T.B., Bosscher, P.J., Plesha, M.E., and Ben Kahla, N. B. (2001). Effect of particle shape on interface behavior of DEM-simulated granular materials. The International Journal of Geomechanics, 1(1), 1-19.

Jia, X., and Williams, R. A. (2001). A packing algorithm for particles of arbitrary shapes. Powder Technology, 120, 175-186.

Kaye, B.H. (1978). Specification of the ruggedness and/or texture of a fine particle profile by its fractal dimension. Powder Technology, 21, 207-213.

Kazhdan, M., Funkhouser, T. and Rusinkiewicz, S. (2003). Rotation invariant spherical harmonic representation of 3D shape descriptors. Eurographics Symposium on Geometry Processing.

Kennedy, S.K., and Lin, W.H. (1986). FRACT-a FORTRAN subroutine to calculate the variables necessary to determine the fractal dimension of closed forms. Computers and Geoscience, 12, 705-727.

Kennedy, S.K., and Lin, W.H. (1992). A comparison of Fourier and fractal techniques in the analysis of closed forms. Journal of sedimentary petrology, 62(5), 842-848.

Khalaf, F.I., and Gharib, I.M. (1985). Roundness parameters of quartz grains of recent aeolian sand deposits in Kuwait. Sedimentary Geology, 45, 147-158.

Koerner, R.M. (1970). Effects of Particle Characteristics on Soil Strength. Journal of Soil Mechanics and Foundation Div., ASCE, 96(4), 1221-1233.

Kolar, J. (2004). Global indexing of 3-D vector geographic features. In Proceedings of International Society for Photogrammetry and Remote Sensing, 20th Congress, 4, 669-672.

Konrad, J. M., and Watts, B. D. (1995). Undrained shear strength for liquefaction flow failure analysis. Canadian Geotechnical Journal, 32, 783-794.

Krumbein, W.C. (1941). Measurement and geological significance of shape and roundness of sedimentary particles. Journal of Sedimentary Petrology, 11(2), 64-72.

Kuenen, P.H. (1960). Experimental abrasion, 4. Aeolian action on sand. Journal of Geology, 68, 427-449.

Lambe, T.W. and Whitman, R.V. (1969). Soil Mechanics, John Wiley & Sons, Inc., NY, USA.

Lanius, C. (1997). Fractal Dimension. http://math.rice.edu/~lanius/fractals/dim.html, (Last accessed: 04/24/2007).

Lees, G. (1964). The measurement of particle shape and its influence in engineering materials. Journal of the British Granite and Whinestone Federation, London, 1-22.

Li, J. (2002). Three-dimensional shape modeling: segmentation, reconstruction and registration. Ph.D. Thesis, Electrical Engineering, University of Michigan.

Lien, J.-M., and Amato, N.M. (2005). Simultaneous Shape Decomposition and Skeletonization Using Approximate Convex Decomposition. Technical Report, TR05-004, Parasol Lab. Department of Computer Science, Texas A&M University.

Lin, X., and NG, T.T. (1997). A three-dimensional discrete element model using arrays of ellipsoids. Geotechnique, 47(2), 319-329.

Lipson, H., and Shpitalni, M. (2002). Correlation-based reconstruction of a 3D object from a single freehand sketch. Proceedings of AAAI Spring Symposium Series - Sketch understanding, 99-104, http://citeseer.ist.psu.edu/509787.html.

Loy, J. (2002). The Koch Curve. http://www.jimloy.com/fractals/koch.htm, (Last accessed: 04/24/2007).

Luaña, V. (1996). The Spherical Harmonics gallery page, Universidad de Oviedo, Oviedo, Spain. http://web.uniovi.es/qcg/harmonics/harmonics.html, (Last accessed: 04/24/2007).

MacCarthy, G.R. (1933). The rounding of beach sands. American Journal of Science, 25, 205-224.

Mandelbrot, B. B. (1967). How long is the coast of Britain? Statistical self-similarity and fractal dimension. Science, 156(3775), 636-638.

Mandelbrot, B. B. (1977). Fractals: Forms, chance and Dimensions. W. H. Freeman, San Francisco, 361.

Manzari, M.T., and Nour, M.A. (2000). Significance of soil dilatancy in slope stability analysis. Journal of Geotechnical and Geoenvironmental Engineering, 126(1), 75-80.

Masad, E., and Button, J. W. (2000). Unified imaging approach for measuring aggregate angularity. The International Journal of Computer-Aided Civil and Infrastructure Engineering, 15(4), 273-280.

Masad, E., Saadeh, S., Al-Rousan, T., Garboczi, E., and Little, D. (2005). Computations of particle surface characteristics using optical and X-ray CT images. Computational Materials Science, 34, 406-424.

Matsushima, T. (2004). 3-D image-based discrete element modeling for irregularly-shaped grains. Numerical Modeling in Micromechanics via Particle Methods – 2004 – Shimizu, Hart & Cundall (eds.), 2004 Taylor & Francis Group, London, 421-427.

Matuttis, H.G., Luding, S., and Herrmann, H.J. (2000). Discrete element simulations of dense packings and heaps made of spherical and non-spherical particles. Powder Technology, 109(1), 278-292.

Mazzullo, J., Alexander, A., Tieh, T., and Menglin, D. (1992). The effects of wind transport on the shapes of quartz silt grains. Journal of Sedimentary Petrology, 62(6), 961-971.

Mazzullo, J., Sims, D., and Cunningham, D. (1986). The effect of aeolian sorting and abrasion upon the shapes of fine quartz sand grains. Journal of Sedimentary Petrology, 56(1), 45-56.

Meloy, T.P. (1977). Fast Fourier transform applied to shape analysis of particle silhouettes to obtain morphological data. Powder Technology, 17, 27-35.

Miura, K., Maeda, K., Furukawa, M., and Toki, S. (1998). Mechanical characteristics of sands with different primary properties. Soils and Foundations, 38, 159-172.

Montgomery, D.C., and Runger, G.C. (2003). Applied statistics and probability for engineers. John Wiley & Sons, Inc., USA.

Morse, P.M., and Feschbach, H. (1953). Methods of theoretical physics. McGraw Hill, New York, NY, 1978.

Mustoe, G.G.W., Henriksen, M., and Huttelmaier, H.P. (1989). Proceedings of the 1st US Conference on Discrete Element Methods, CSM, Golden, CO.

Nakata, Y., Kato, Y., Hyodo, M., Hyde, A. F. L., and Murata, H. (2001). One-dimensional compression behavior of uniformly graded sand related to single particle crushing strength. Soils and Foundations, 41(2), 39-51.

Ng, T.T. (1989). Numerical simulation of granular soils under monotonic and cyclic loading: A particulate mechanics approach. Ph.D. Dissertation, Rensselaer Polytechnic Institute, Troy, NY.

Ng, T.T. (1994). Numerical simulations of granular soil using elliptical particles. Computers and Geotechnics, 16(2), 153-169.

Ng, T.T., and Dobry, R. (1991). CONBAL – Simulated granular material using quartz spheres with the Discrete Element Method. Report to NSF, Rensselaer Polytechnic Institute, Troy, NY.

Norris, G. (1976). The effect of particle size and the natural variation in particle shape and surface roughness on the stress-strain and strength behavior of uniform quartz sands. Ph.D. thesis, University of California, Berkeley, CA.

Orford, J.D., and Whalley, W.B. (1983). The use of fractal dimension to quantify the morphology of irregular-shaped particles. Sedimentology, 30, 655-668.

O'Sullivan, C., Cui, L., and Bray, J.D. (2004). Three-dimensional discrete element simulations of direct shear test. Numerical Modeling in Micromechanics via Particulate Methods – 2004 – Shimizu, Hart and Cundall (eds.), 2004 Taylor and Francis Group, London.

Pettijohn, F.J. (1957). Sedimentary Rocks. Harper & Bros, New York, NY, 718.

Pettijohn, F.J., and Lundahl, A.C. (1934). Shape and roundness of Lake Erie beach sand. Journal of Sedimentary Petrology, 14, 69-78.

Phillips, J.C., Hogg, A.J., Kerswell, R.R., and Thomas, N.H. (2006). Enhanced mobility of granular mixtures of fine and coarse particles. Earth and Planetary Science Letters, 246, 466–480.

Plumley, W.J. (1948). Black hills terrace gravels: a study in sediment transport. Journal of Geology, 56, 526-577.

Podczeck, F. (1997). A shape factor to asses the shape of particles using image analysis. Powder Technology, 93, 47-53.

Pollack, J.M. (1961). Significance of compositional and textural properties of South Canadian River Channel sands, New Mexico, Texas and Oklahoma. Journal of Sedimentary Petrology, 31, 15-37.

Potapov, A., and Campbell, C. (1998). A fast model for the simulation of non-round particles. Granular Matter, 1, 9-14.

Powers, M.C. (1953). A new roundness scale for sedimentary particles. Journal of Sedimentary Petrology, 23, 117-119.

Ramez, M.R., and Mosalamy, F.H. (1969). The deformed nature of various size fractions in some clastic sands. Journal of Sedimentary Petrology, 39, 1182-1187.

Rao, C., Tutumluer, E., and Kim, I. T. (2002). Quantification of coarse aggregate angularity based on image analysis. Transportation Research Record, 1787, Transportation Research Board, National Research Council, Washington DC.

Riester, D.D., Shipp, R.C., and Ehrlich, R. (1982). Patterns of quartz sand grain shape variation, Long Island Littoral and shelf. J. Sediment. Petrol., 52(4), 1307-1314.

Rivas, J.A. (2005). Three-dimensional digital image processing and reconstruction of granular particles. M.S.C.E. Thesis, University of South Florida, Tampa, FL.

Russell, R.D. (1939). Recent marine sediments. Society of Economic Paleontologists and Mineralogists Special Publication, 4, 736.

Russell, R.D., and Taylor, R.E. (1937). Roundness and shape of Mississippi River sands. Journal of Geology, 45, 225-267.

Sallam, A.M. (2004). Studies on Modeling Angular Soil Particles Using the Discrete Element Method. Ph.D. Thesis, University of South Florida, Tampa, FL.

Santamarina, J.C., and Cascante, G. (1998). Effect of surface roughness on wave propagation parameters. Geotechnique, 48(1), 129-136.

Santamarina, J. C., and Cho, G. C. (2001). Determination of critical state parameters in sandy soils-simple procedure. Geotechnical Testing Journal, 24(2), 185-192.

Santamarina, J.C., and Cho, G.C. (2004). Soil Behavior: The Role of Particle Shape. Proc. Skempton Conf., March, London.

Sasitharan, S., Robertson, P. K., Sego, D. C., and Morgenstern, N. R. (1994). State-boundary surface for very loose sand and its practical implications. Canadian Geotechnical Journal, 31, 321-334.

Schanz, T., and Vermeer, P.A. (1996). Angle of friction and dilatancy of sand. Geotechnique, 46(1), 145-151.

Schwarcz, H.P., and Shane, K.C. (1969). Measurement of particle shape by Fourier analysis. Sedimentology, 13, 179-212.

Schwarz, H.B., and Exner, H.E. (1980). The implementation of the concept of fractal dimension in a semi-automatic image analyzer. Powder Technology, 27, 207-213.

Shimobe, S., and Moroto, N. (1995). A new classification chart for sand liquefaction. Earthquake geotechnical engineering, K. Ishihara, ed., Balkema, Rotterdam, The Netherlands, 315-320.

Shinohara, K., Oida, M., and Golman, B. (2000). Effect of particle shape on angle of internal friction by triaxial compression test. Powder Technology, 107, 131-136.

Sorby, H.C. (1877). The application of the microscope to geology. Monthly Microscopical Journal, 17, 113-136.

Strack O. D. L. and Cundall, P. A. (1978). The distinct element method as a tool for research in granular media, Part I. Report to NSF, Department of Civil and Mineral engineering, University of Minnesota. Minneapolis, MN.

Sukumaran, B. (1996). Study of the effect of particle characteristics on the flow behavior and strength properties of particulate materials. Ph.D. Thesis, Purdue University, West Lafayette, IN.

Sukumaran, B., and Ashmawy, A.K. (2001). Quantitative characterization of the geometry of discrete particles. Geotechnique, 51(7), 619-627.

Sukumaran, B., and Ashmawy, A.K. (2001). Influence of inherent particle characteristics on the strength properties of Particulate materials. Annual International Society of Offshore and Polar Engineering Conference, Oslo, Norway.

Taylor, D.W. (1948). Fundamentals of soil mechanics. John Wiley and Sons, New York.

Taylor, L.M., and Preece, D.S. (1989). Simulation of blasting induced rock motions using spherical element models. Proceedings of the 1st US Conference on Discrete Element Methods, CSM, Golden, CO.

Thomas, D.S.G. (1987). The roundness of aeolian quartz sand grains. Sedimentary Geology, 52, 149-153.

Thomas, M.C., Wiltshire, R.J., and Williams, A.T. (1995). The use of Fourier descriptors in the classification of particle shape. Sedimentology, 42, 635-645.

Thomas, P.A., and Bray, J.D. (1999). Capturing nonspherical shape of granular media with disk clusters. Journal of Geotechnical and Geoenvironmental Engineering, 125(3), 169-178.

Ting, J., Khawaja, M., Meachum, L., and Rowell, J. (1993). An ellipse-based discrete element model for granular materials. International Journal for Numerical and Analytical Methods in Geomechanics, 17, 603-623.

Ting, J.M., Corkum, B.T., Kauffman, C.R., and Greco, C. (1989). Discrete numerical model for soil mechanics. Journal of Geotechnical Engineering, ASCE, (3), 379-398.

Twenhofel, W.H. (1946). Beach and river sands on the coastal region of southwest Oregon with particular reference to black sands. American Journal of Science, 244, 114-139, 200-214.

Twenhofel, W.H. (1950). Principles of sedimentation. McGraw-Hill Book Co. Inc., New York, 302-311.

Uthus, L, Hoff, I., and Horvli, I. (2005). Evaluation of grain shape characterization methods for unbound aggregates. 7th International Conference on the bearing capacity of roads, railways and airfields 2005, BCRA. Trondheim, Norway.

Wadell, H. (1932). Volume, shape & roundness of rock particles. J. of Geology, 40, 443-451.

Wadell, H. (1933). Sphericity and roundness of rock particles. J. of Geology, 41, 310-331.

Wadell, H. (1935). Volume, shape & roundness of quartz particles. Journal of Geology, 43, 250-286.

Williams, J., and Mustoe, G.G.W. (1993). Proceedings of the International Conference on the Discrete Element Methods, MIT, Cambridge, MA.

Williams, J.R., and Pentland, A.P. (1992). Superquadrics and modal dynamics for discrete elements in interactive design. Engineering Computations, 9(2), 115-127.

Wu, F.-C., Ma, W.-C., Liou, P.-C., Laing, R.-H. and Ouhyoung, M. (2003). Skeleton extraction of 3d objects with visible repulsive force. In Computer Graphics Workshop 2003, Hua-Lien, Taiwan.

Yang, J., and Li, X.S. (2004). State-Dependent Strength of Sands from the Perspective of Unified Modeling. J. Geotech. and Geoenvir. Eng., 130(2), 186-198.

Youd, T.L. (1973). Factors controlling maximum and minimum densities of sands, evaluation of relative density and its role in geotechnical projects involving cohesionless soils, ASTM STP 523, 98-112.

Yudhbir and Abedinzadeh, R. (1991). Quantification of particle shape and angularity using image analyzer. Geotechnical Testing Journal, 14(3), 296-308.

Zahn, C.T., and Roskies, R.Z. (1972). Fourier descriptors for plane closed curves. IEEE Transactions on Computers, C-21(3), 269-282.

Zelasko, J.S., Krizek, R.J., and Edil, T.B. (1975). Shear Behavior of Sands as a Function of Grain Characteristics. Istanbul Conference on Soil Mech. Found. Eng., 1, 55-64.

Zwillinger, D. (1995). Spherical coordinates in space, §4.9.3 in CRC standard mathematical tables and formulae. Boca Raton, FL: CRC Press, 297-298.

APPENDICES

Appendix A: Data Sets

Total 26 types of different sand samples were collected from various locations. Their two-dimensional projection images are shown below.

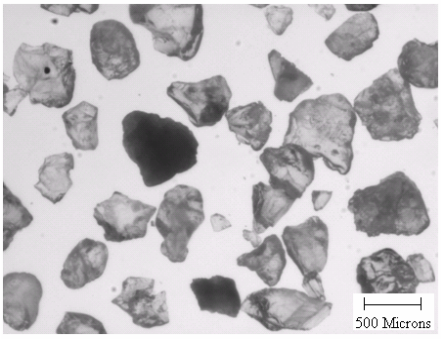

US Silica #1 Dry

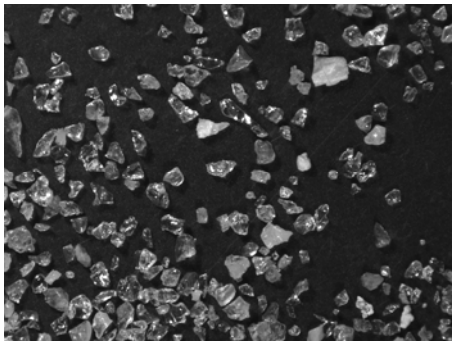

US Silica Std.Melt

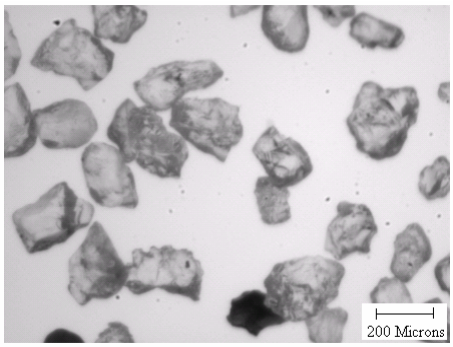

Daytona Beach Sand

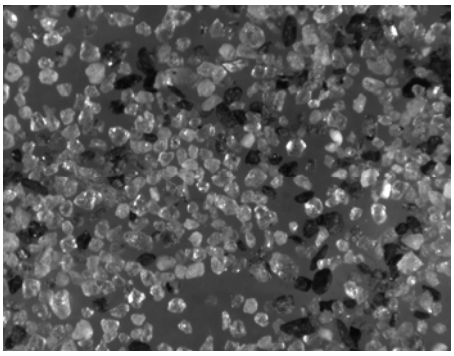

Rhode Island Sand

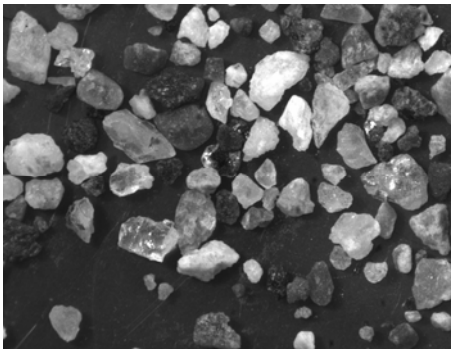

Nice Sand

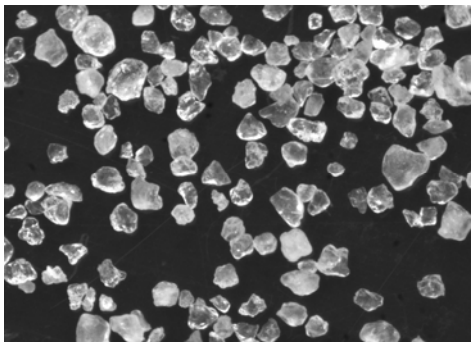

Fontainebleau Sand

Figure A.1 Sand Samples Collected for the Present Study

Appendix A: (Continued)

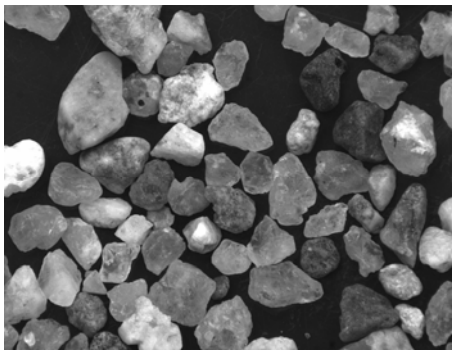

Loire River Sand

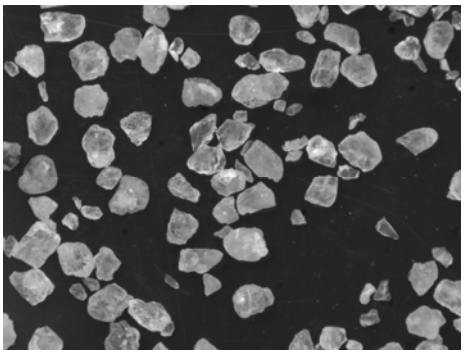

Hostun Sand

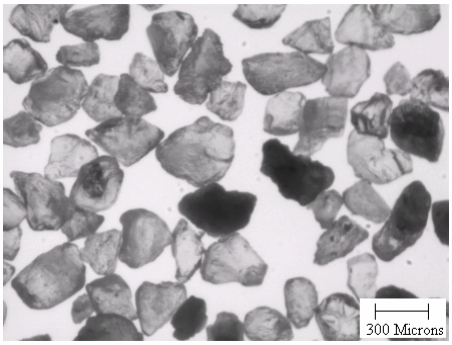

Toyoura Sand

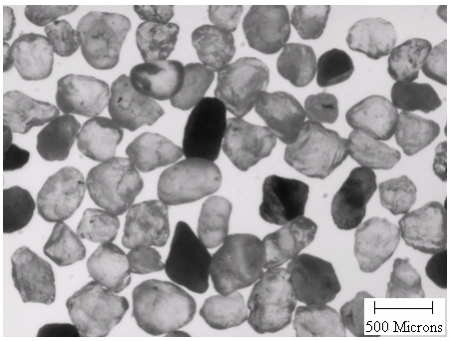

Michigan Dune Sand

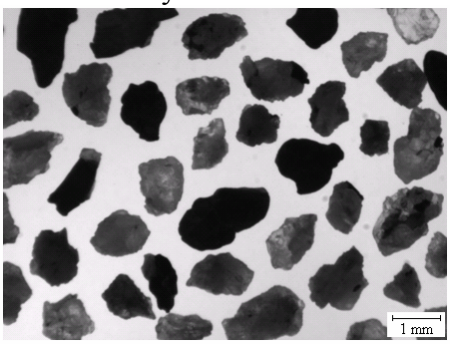

Tecate River Sand

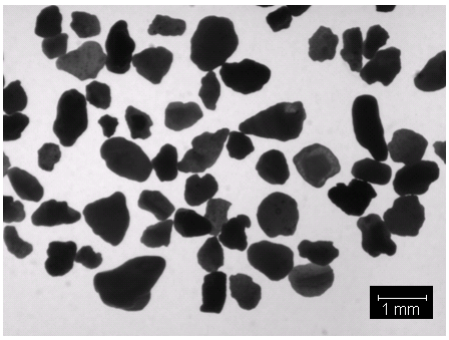

Kahala Beach Sand

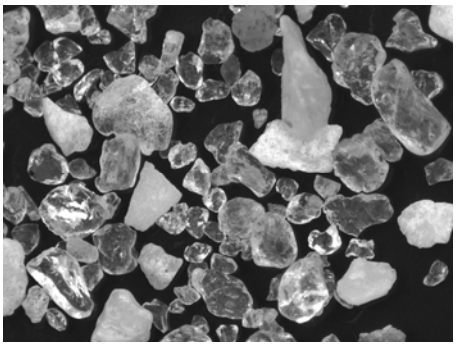

Indian Rocks Beach Sand

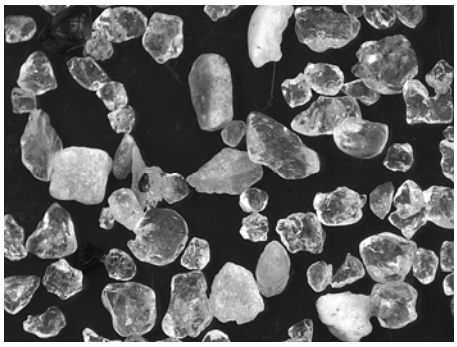

Belle Air Beach Sand

Figure A.1 (Continued)

Appendix A: (Continued)

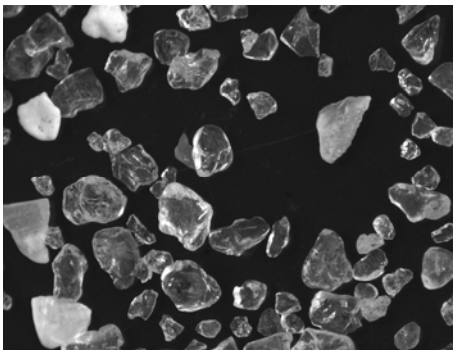

Clearwater Beach Sand

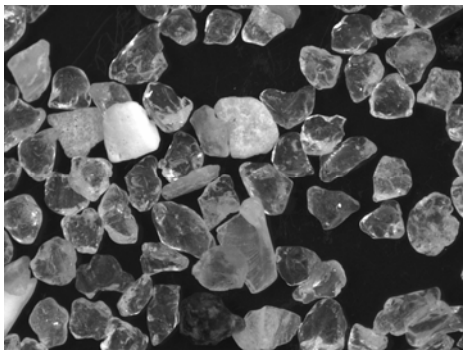

Gulf Beach Sand

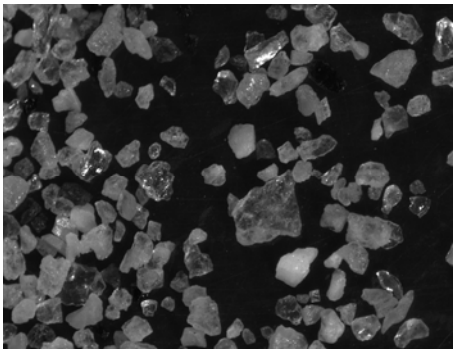

Long Beach Sand

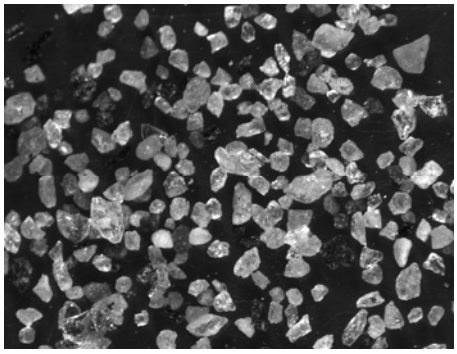

Boca Grande Beach Sand

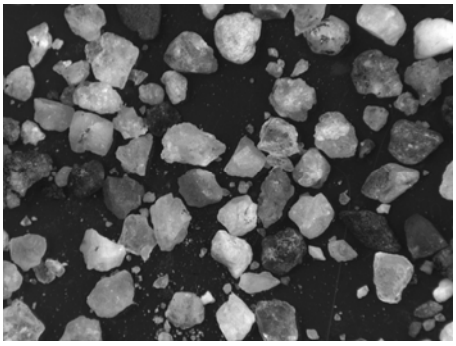

Oxnard Beach Sand

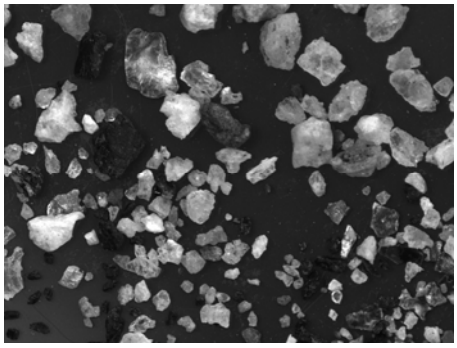

Arroyo Alamar River Sand

Figure A.1 (Continued)

Appendix A: (Continued)

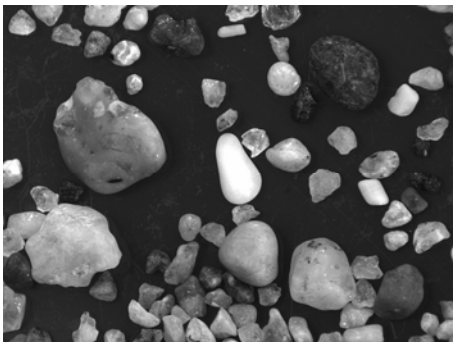

Rincon Beach Sand

Panama Malibu Beach Sand

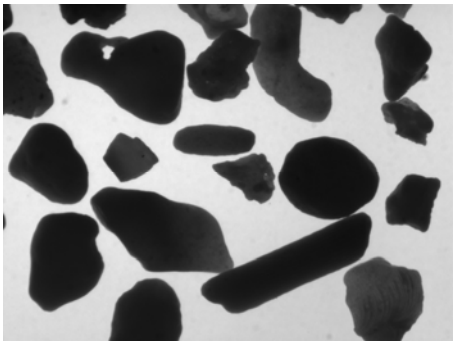

Ala Wai Beach Sand

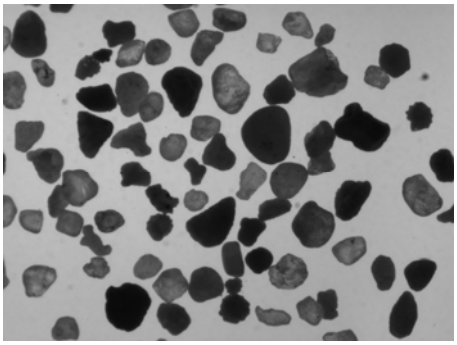

Red Sea Dune Sand

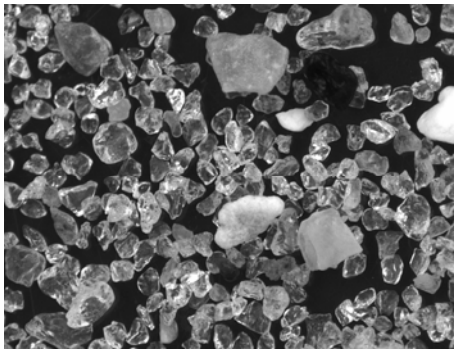

Madeira Beach Sand

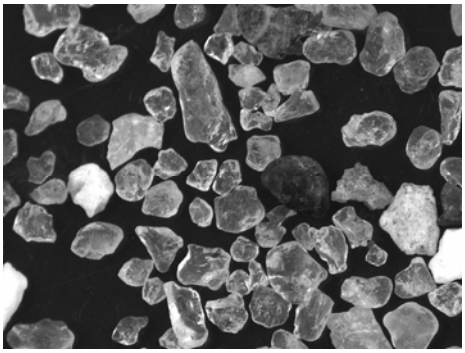

Redington Shores Sand

Figure A.1 (Continued)

ABOUT THE AUTHOR

Ms. Nivedita Das received a bachelor's Degree in Civil Engineering from Jadavpur University, India in 2000 and Master's Degree in Geotechnical Engineering from Bengal Engineering College, India in 2002. She started working with an engineering consultancy firm until she joined the Ph.D. program in Geotechnical Engineering in the department of Civil and Environmental Engineering at the University of South Florida in 2003 under the supervision of Dr. Alaa Ashmawy. Her primary areas of doctoral research include three-dimensional characterization particle morphology and discrete element modeling. She served as a secretary/treasurer for the USF Geotechnical Society Student Chapter. She coauthored two conference publications and three of her research papers are under review in referred journals.